Sorption of Palladium onto Bentonite, Illite and Shale Under High Ionic Strength Conditions

SORPTION OF PALLADIUM ONTO BENTONITE, ILLITE AND SHALE UNDER HIGH IONIC STRENGTH CONDITIONS

BY

JUSTIN RIDDOCH, BA Sc.

A THESIS

SUBMITTED TO THE DEPARTMENT OF ENGINEERING PHYSICS

AND THE SCHOOL OF GRADUATE STUDIES

OF MCMASTER UNIVERSITY

IN PARTIAL FULFILMENT OF THE REQUIREMENTS

FOR THE DEGREE OF

MASTER OF APPLIED SCIENCE

Master of Applied Science (2016) McMaster University

(Engineering Physics) Hamilton, Ontario, Canada

TITLE:	Sorption of Palladium onto Bentonite, Illite and Shale Under High Ionic Strength Conditions
AUTHOR:	Justin Riddoch BASc, (Engineering Physics) Queen's University, Kingston, Canada
SUPERVISOR:	Dr. Shinya Nagasaki
NUMBER OF PAGES:	xxii, 138

For the Gunz

Abstract

Both crystalline and sedimentary rocks are being considered as potential host rocks for a deep geological repository in Canada. Deep-seated sedimentary rocks in the Michigan Basin, Ontario, Canada contain highly saline ground and pore waters. The relatively high I of these waters may influence speciation and rock matrix sorption properties. To this end, laboratory sorption experiments were conducted to examine sorption of Pd(II) on sodium bentonite, illite and Ordovician age shale as a function of pH and solution I and initial concentration of Pd. Solutions with pH values in the range of 5 to 9, I ranging from 0.1 to 4 M and initial concentration of Pd ranging from 5×10^{-8} to 1×10^{-6} M were considered. A sorption time of 14 days was used and the separation method was by centrifuge. Experiments were performed under aerobic conditions at 25 °CC, and the Eh value of the solution ranged from 300 to 600 mV. The data from sorption experiments were used to validate surface complexation models developed in PHREEQC with the JAEA TDB. The sorption of Pd on bentonite, shale and illite all showed strong dependence on I and pH. The dependence on initial concentration of Pd was used to plot sorption isotherms. The slope of the isotherms showed that Pd was forming inner- and outer- sphere complexes inside the stern layer for sorption onto bentonite and illite. It also showed however that shale was most likely undergoing cooperative sorption. Strong fit was found between the single layer surface complexation model for montmorillonite (the major constituent clay mineral of sodium bentonite) and experimental data, but not for illite (the major constituent clay mineral of shale).

Acknowledgements

I would like to thank my supervisor, Dr. Shinya Nagasaki, for all of his help through out my time at McMaster. I would also like to thank my colleagues for their guidance and support through out my research and the writing of this thesis.

Abbreviations

ACC American Colloid Company. 47

ACS American Chemistry Society. 47

ANDRA French National Radioactive Waste Management Agency. 26

CMS Clay Mineral Society. 47

CPS counts per second. 38, 137

DGR deep geological repository. 2, 4, 5

EFPY effective full power years. 1

HCl hydrochloric acid. 38, 39, 44, 45, 58, 59

HNO_3 nitric acid. 9, 47

ICP-MS inductively coupled plasma mass spectroscopy. 37, 38, 41, 47, 57, 58, 84, 85, 87

IUPAC International Union of Pure and Applied Chemistry. 13, 29

JAEA Japan Atomic Energy Agency. 6, 7, 11, 26, 29, 75, 131

NaOH sodium hydroxide. 38, 44, 45, 47, 58, 59

NWMO Nuclear Waste Management Organization. 5, 7, 47

PHREEQC PH REdox EQuilibrium in C. iv, xi, xii, 6, 24–26, 29, 31, 34, 49, 52, 71, 89, 96, 107

ppb parts per billion. 7

SDB sorption data base. 7, 88

SHE standard hydrogen electrode. 6, 63, 64, 68

SIT theory specific ion interaction theory. 7, 24–26, 31, 50

t-HM tonnes of heavy metal. 1

TDB thermodynamic data base. 6, 11, 26, 29, 75, 131

Nomenclature

C_b concentration in the blank solution, measured in mol/l. 22

C_{eq} equilibrium concentration in the sample solution, measured in mol/l. 22, 84

C_i inital concentration in the sample solution, measured in mol/l. 22, 84

C_s sorbed concentration, measured in mol/l. 23

I ionic strength, a measure of the concentration of ions in solution, measured in mol/l. iv, xv, xvi, xviii–xxi, 4–9, 11, 16, 18, 26, 34, 35, 38, 42–46, 48, 50, 59–61, 63–65, 67, 70–72, 77–83, 86, 88–92, 94–96, 98, 99, 101, 102, 104–108, 116–130, 133

K_d Distribution coefficient, used to describe the sorption behavior of a substance, measured in m^3/kg. 8, 10, 22, 23, 42–45, 47, 61, 63–65, 67, 68, 75, 84, 87–96, 99–101, 105, 106, 108, 117–126

$\frac{L}{S}$ liqud to solid ratio, measured in m^3/kg. 22, 84

$[\mathbf{Pd}]_f$ equilibrium concentration of the element inside the square brackets, in this case palldium, in mol/l. 11, 70

$[\mathbf{Pd}]_i$ initial concentration of the element inside the square brackets, in this case palldium, in mol/l. 11, 70

Ar argon. 85, 86, 104

Bi bismuth. 57

Ca calcium. xiv, 16, 39, 42–46, 48, 91, 92, 133

$\mathbf{CaCl_2}$ calcium chlorine. 48, 99

$\mathbf{CaCl_2\ 2{\times}H_2O}$ calcium chlorine dihydrate. 47, 48

Cd cadmium. 41

Cl chlorine. xiv, 39, 42–46, 48, 133

Cu copper. 85, 86, 104, 137

Eh redox potential, measured in mV. 6, 60, 61, 63, 64, 67, 68, 70

Na sodium. xiv, 16, 39, 42–46, 48, 91, 92, 133

NaCl sodium chlorid. 47, 48, 99

Pb lead. 5, 108

Pd palladium. iv, xv, xviii, 4–7, 9, 11, 12, 16, 20–22, 26, 27, 37–39, 41–47, 49, 52, 55–58, 60, 62–64, 68, 70, 71, 84–87, 90–96, 102, 104–108, 117–130, 136, 137

$\mathbf{pH}_c$ the actual pH of solution, corresponds to the concentration of hydrogen ions in solution. 38, 39, 58–61, 63, 65, 67, 70, 86, 89, 90, 117–130

$pH_{measured}$ the pH measured using a pH probe, corresponds to the hydrogen ion activity in solution. 38, 60, 86

Zn Zinc. 85, 86, 104, 137

Contents

List of Tables

List of Figures

Chapter 1

Introduction

1.1 Background

As of June 30th 2015 in Canada there are approximately 2.6 million used CANDU fuel bundles containing some 52,000 tonnes of heavy metal (t-HM) stored at reactor sites. At the end of life of all reactors currently operating in Canada, assuming 25 effective full power years (EFPY) of operation, the total amount of used CANDU fuel bundles will rise to 3.4 million. If we consider the case that many reactors in Canada are set to be refurbished before they reach their end of life, the number of used CANDU fuel bundles has the potential to rise to, assuming an additional 25 EFPY of operation, 5.2 million. There is also the possibility of new reactors being constructed in Canada. If we also consider the case that all reactors that have already initiated formal licensing are eventually constructed the total amount of used fuel could increase further to 6.8 million CANDU fuel bundles or by an additional 10,800 PWR fuel assemblies (Garamszeghy, 2015).

The current inventory of used CANDU fuel bundles is stored at reactor sites in spent fuel pools and dry cask storage containers. These storage facilities are temporary, fuel is stored in the spent fuel pool for approximately 6 years (Allan and Dormuth, 2001), after which is it moved to dry cask storage. The fuel can be stored in dry cask containers for 50 years (Candu Energy Inc., 2014). Currently there are no long term storage facilities in Canada, however we are in the process of determining a permanent solution. One such solution is the deep geological repository (DGR). A DGR is nuclear waste repository excavated deep within a stable geological environment, typically below 300 m. Once stored in the DGR the nuclear waste can safely decay down to background levels.

A DGR consists of several barriers; confinement matrix, engineering barrier and geological barrier, which help to prevent or retard the transport of radionuclides. The confinement matrix, typically glass (through vitrification) or concrete, is what the nuclear waste is sealed in. The confinement matrix is then separated from the host rock (geological barrier) by an engineered barrier, see Figure 1.1. This multi layer approach helps separate nuclear waste from the biosphere.

Both crystalline and sedimentary rocks are being considered as potential host rocks for a DGR in Canada. The two sedimentary rock types of particular interest are argillaceous limestone (as host rock) and shale (as natural barriers). Figure 1.2 shows a geological cross section of a prospective site on the Bruce Peninsula near Kincardine, Ontario. At the design depth, in this figure approximately 500 m, the DGR is embedded in argillaceous limestone with a shale cap. The engineered barriers, or

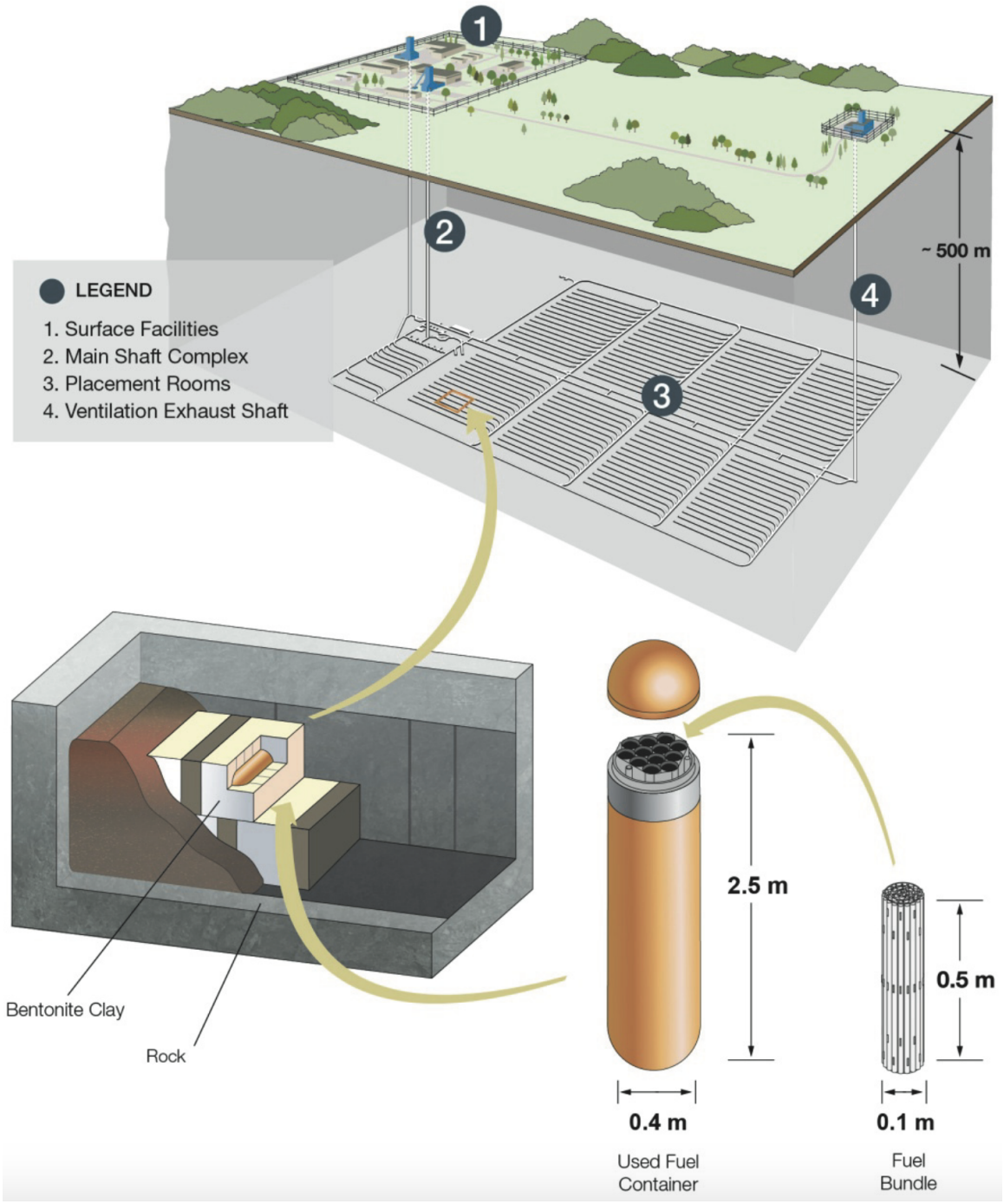

Figure 1.1: Proposed design of the Canadian DGR (Crowe *et al.*, 2015).

seal materials are bentonite, and bentonite-sand mixtures. Deep-seated sedimentary rocks in the Michigan Basin, Ontario, Canada contain highly saline ground and pore waters, the relatively high ionic strength (I) of which may influence speciation and rock matrix sorption properties Vilks (2016).

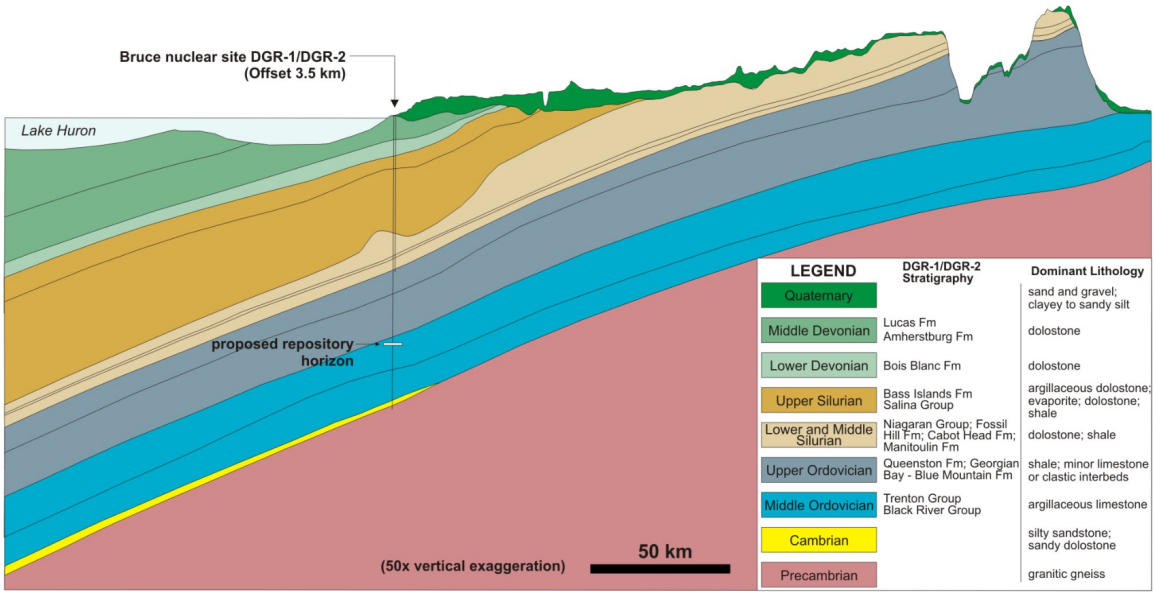

Figure 1.2: Geological cross section at site showing the possible location of the DGR. In this cross section the design depth is 500 m (Ontario Power Generation, 2011).

The safety assessment for a DGR is very challenging as the safety of a possible solution cannot be demonstrated directly, waste will remain in these facilities for millions of years, as a result we must rely on data gathered from experiments to conduct the safety assessment.

Sorption data has been compiled for several elements of interest, by Vilks (2016), however data gaps still exist between sorption data and various experimental conditions, such as high I. Palladium (Pd) is one such element of interest. It has been

identified as an element of interest by the Nuclear Waste Management Organization (NWMO) because isotopes of Pd are present in high-level radioactive waste (Wasywich, 1993). Specifically Pd-107 which has a half-life of 6.5×10^6 years (Tachi *et al.*, 1999). Figure 1.3 shows the weight percentage of radionuclides in used CANDU fuel after 1×10^6 years, at which point in time the weight percentage of Pd is close to 1%.

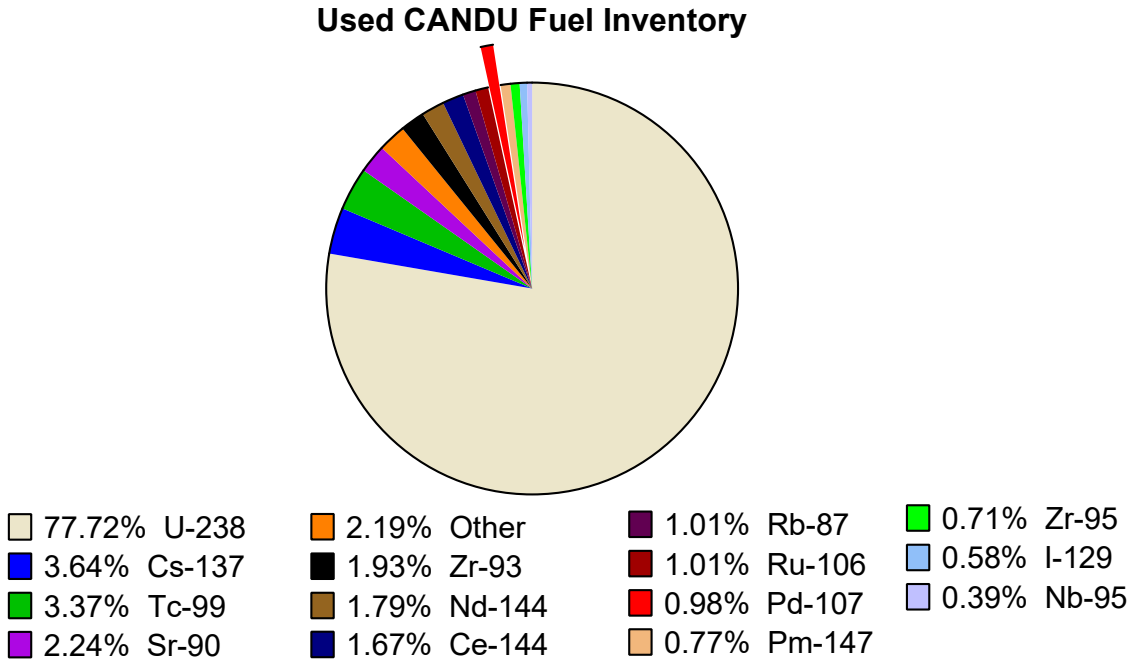

Figure 1.3: Inventory of used CANDU fuel, by weight percentage, after 1×10^6 years (Tait *et al.*, 1989). Inventories were calculated using ORIGEN-S code for used fuel at a burnup of 685 GJ/kg U. Any isotope with weight percentage of less than 0.25% was grouped into 'Other'.

Currently lead (Pb) is being used as a chemical analogue for of Pd because sorption data for Pd is only available for sorption onto bentonite, when considering materials of interest for a DGR in Canada, and only at low, < 0.1 M, I (Tachi *et al.*, 1999). The goal of this thesis is to investigate the effects I has on the sorption of Pd onto

sodium bentonite, illite and Ordovician age shale, as well as the effect it has on the speciation of Pd.

Laboratory sorption experiments have recently conducted Pd on sodium bentonite, illite and Ordovician age shale as a function of pH, solution I and initial concentration of Pd. pH values in the range of 5 to 9 were considered as well as I of 0.1 M, 0.5 M, 1 M, 2 M, 3 M and 4 M. The initial concentration of Pd for the pH and I dependence experiments was 1×10^{-7} M, however for the isotherm experiments initial concentrations of Pd of 1×10^{-8} M, 5×10^{-8} M, 2.5×10^{-7} M and 5×10^{-7} M were also considered. The initial concentration of Pd was confirmed to be below the solubility limit by experiment. The experiments were carried out under aerobic conditions at 25 °C. In aqueous solution Pd only occurs in a single redox state, Pd(II), so redox conditions were not used (Vilks, 2016). The Eh value of the solutions were measured during experiment and ranged from 300 to 600 mV vs. standard hydrogen electrode (SHE).

In order to understand the process by which Pd is sorbed onto the surface it is necessary to conduct modeling. The sorption mechanism is very complicated, however by developing a model that is able to replicate the results from experiment we can assume that the sorption mechanism occurring in experiment is that which was used in the model. The model we developed for Pd sorption and speciation was constructed in the geochemical code PHREEQC. PHREEQC calculations depend on thermodynamic data, we have selected to use the Japan Atomic Energy Agency (JAEA) thermodynamic data base (TDB) as our source. The JAEA TDB includes

specific ion interaction theory (SIT theory) parameters for calculating single ion activity coefficients. SIT theory theory has been proved adequate for solutions with I up to 3 to 4 M (Grenthe and Plyasunov, 1997). Debye-Hückel approach was used to correct activity coefficients for species with no SIT theory parameter specified in the database, and the Davies equation was used to correct activity coefficients for species with no Debye-Hückel parameters in the database (Parkhurst and Appelo, 1999).

1.2 Literature Review

1.2.1 Review of Available Sorption Data

As mentioned previously, there is very limited sorption data available for Pd. Figure 1.4 shows the number of data points listed for elements, being studied by NWMO, included in the JAEA sorption data base (SDB). There are 106 data points available for Pd which were collected from five different papers. The majority of the data points, 82, come from a single paper Tachi *et al.* (1999). If we consider how the data included in the JAEA SDB compares to the experimental conditions outlined by the NWMO, that is, sorption onto bentonite, illite or shale, we find that only 24 of the data appoints are relevant, all of which are from Tachi *et al.* (1999). These 24 data points are for the sorption of Pd onto bentonite at I of 0.01 M and 0.1 M for pH values of 5, 8 and 11. These values are shown in Table 1.1. The sorption experiments conducted by Tachi *et al.* (1999) were carried out under aerobic conditions at room temperature. Sorption time was 30 days, the separation method was by filtration and the initial concentration of Pd was 50 ppb (approximately 5×10^{-7} M).

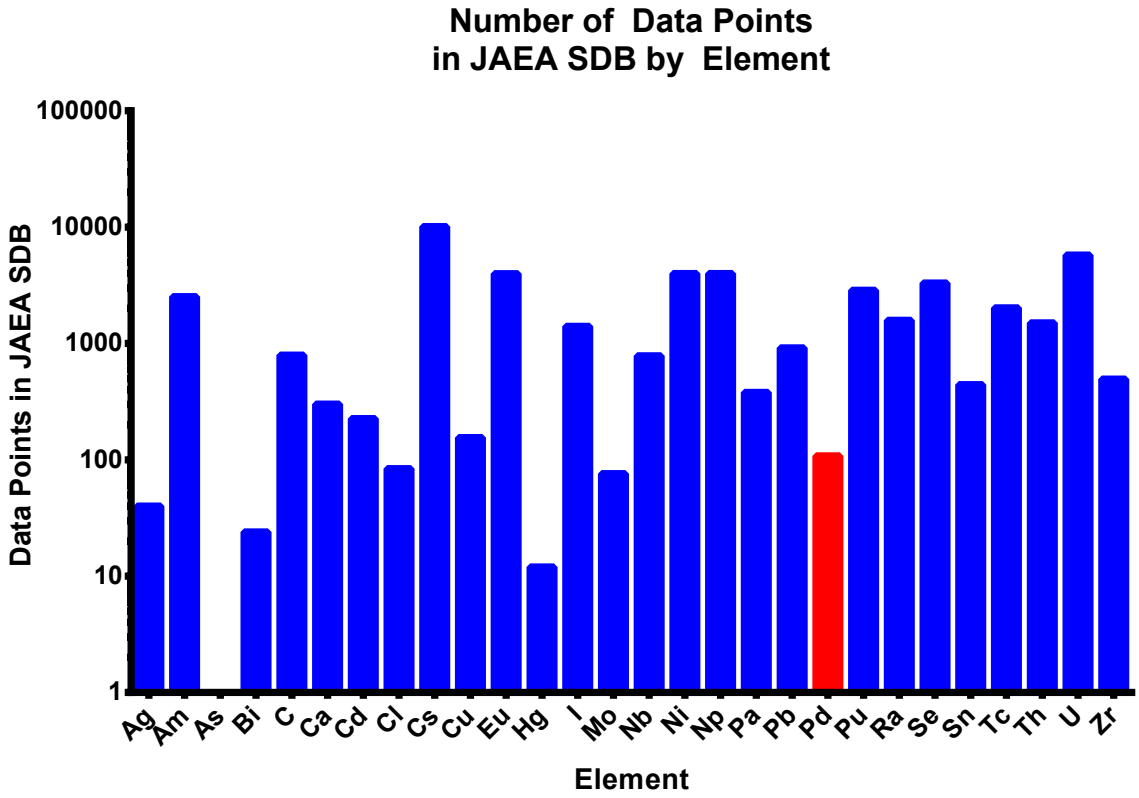

Figure 1.4: The number of data points for elements, currently being studied by NWMO, included in the JAEA SDB (Suyama and Tachi, 2012).

To summarize the results of Tachi *et al.* (1999), shown in Table 1.1, at pH 5 the K_d value was in the range of 17 to >250 m^3/kg, at pH 8 it was in the range of 0.67 to 28 m^3/kg and at pH 11 it was in the range of 0.35 to 25 m^3/kg. The results of Tachi *et al.* (1999) show that there is both a dependence of K_d on pH and on liquid to solid ratio. As pH increased from 5 to 11 the value of K_d decreased. K_d values increased with increasing solid to liquid ratio, between a liquid to solid ratio of 0.1 m^3/kg and 1 m^3/kg. Tachi *et al.* (1999) also concluded that there was little dependence of K_d on I, between I of 0.01 M and 0.1 M.

Tachi *et al.* (1999) conducted blank sorption experiments, sorption experiments where no solid is present so that all sorption is onto the vessel wall, in parallel with their batch sorption experiments. In addition to this, he measured vessel wall sorption in the batch experiments by bathing the vessels, after experiment completion, in nitric acid (HNO_3). The HNO_3 would cause all Pd sorbed onto the walls to desorb into solution. When comparing the wall sorption in the blank to the wall sorption in the batch sorption experiments he found that in all conditions Pd sorption on the vessel wall in the blank sorption experiments was much greater that sorption on the vessel wall in batch sorption experiments. From this Tachi *et al.* (1999) concluded that in the presence of a solid, sorption onto the vessel wall is insignificant.

Tachi *et al.* (1999) also conducted solubility experiments for Pd under various conditions. The results of which are shown in Table 1.2. They found that solubility was at it's lowest at pH 8, solubility increased when shifting pH in either direction, however it was much higher at pH 5 then at pH 11. There was also very little change in solubility between I of 0.01 M and 0.1 M.

Selecting an initial concentration of Pd of 4.7×10^{-7} M might have led to the production of precipitate at pH 8. Tachi *et al.* (1999) mentioned this possibility however they concluded since sorption would have occurred more quickly then precipitation it would have had little to no effect on the results.

Table 1.1: Relevant sorption data for Pd taken from the JAEA SDB.

Solution	**pH**	**S/L** ($\mathbf{m^3/kg}$)	K_d ($\mathbf{m^3/kg}$)
0.01M NaCl	5	0.1	>25.0
0.01M NaCl	5	0.1	>25.0
0.01M NaCl	5	1.0	82.3
0.01M NaCl	5	1.0	>250
0.01M NaCl	8	0.1	0.964
0.01M NaCl	8	0.1	7.04
0.01M NaCl	8	1.0	16.9
0.01M NaCl	8	1.0	2.85
0.01M NaCl	11	0.1	2.84
0.01M NaCl	11	0.1	1.09
0.01M NaCl	11	1.0	25.3
0.01M NaCl	11	1.0	10.9
0.1M NaCl	5	0.1	16.6
0.1M NaCl	5	0.1	>25.0
0.1M NaCl	5	1.0	61.5
0.1M NaCl	5	1.0	>250
0.1M NaCl	8	0.1	0.669
0.1M NaCl	8	0.1	5.46
0.1M NaCl	8	1.0	28.4
0.1M NaCl	8	1.0	3.55
0.1M NaCl	11	0.1	0.614
0.1M NaCl	11	0.1	0.355
0.1M NaCl	11	1.0	10.6
0.1M NaCl	11	1.0	16.2

Table 1.2: Solubility data for Pd in 0.01 M and 0.1 M Na-Cl solutions at pH 5, 8 and 11 (Tachi *et al.*, 1999).

Solution	**pH**	$[\mathbf{Pd}]_i$ **(M)**	$[\mathbf{Pd}]_f$ **(M)**
0.01M NaCl	5	4.7×10^{-6}	5.0 to 5.1×10^{-6}
0.01M NaCl	8	4.7×10^{-6}	3.9 to 4.4×10^{-7}
0.01M NaCl	11	4.7×10^{-6}	5.5 to 17×10^{-7}
0.1M NaCl	5	4.7×10^{-6}	1.7 to 3.9×10^{-6}
0.1M NaCl	8	4.7×10^{-6}	1.4 to 3.8×10^{-7}
0.1M NaCl	11	4.7×10^{-6}	7.4 to 19×10^{-7}

1.2.2 Review of Sorption Modeling

Thermodynamic data for Pd and Pd species has been collected in the JAEA TDB as well as others, such as NAGRA ThermoChemie. This thermodynamic data has been used to model speciation and solubility however since there is limited sorption data available for Pd, sorption for Pd has not been modeled extensively.

1.3 Purpose

The purpose of this thesis is the fill the data gaps between sorption data of Pd and various experimental conditions. The dependence of the distribution coefficient on I, pH and initial concentration will be measured for the sorption of Pd onto bentonite, shale and illite. The experimental conditions are I in the range of 0.1 M to 4 M I, pH in the range of pH 5 to 9 and initial concentration of Pd in solution in the range of 5×10^{-8} M to 1×10^{-6} M. In order to conduct the I, pH and initial concentration of Pd dependence experiments it was first necessary to determine, experimentally, several factors. First it was necessary to determine the initial concentration of Pd

by measuring the detection limit of Pd by ICP-MS. Once the initial concentration of Pd was determined, we had to determine how long it would take for Pd to reach a steady dissolved state and we had to verify that the initial concentration of Pd would be below the solubility limit of Pd. Lastly we had to measure the sorption kinetics of Pd in order to determine how long it takes to reach sorption equilibrium for sorption onto bentonite, illite and shale.

In addition to the experiments, we would also like to model the both the speciation and sorption of Pd under the same experimental conditions. The purpose is to model both the surface site and aqueous speciation of Pd in order to give insight into sorption behaviors measured in experiment. Also by modeling the sorption we may be able to determine the sorption mechanism for sorption of Pd onto bentonite, illite and shale. If there is strong agreement between sorption data and the sorption model then we can assume that the sorption mechanisms included in the model are the same that are occurring in experiment.

Chapter 2

Theory

2.1 Sorption

Sorption is the term used to describe the process by which one substance becomes attached to another without considering a specific mechanism (Tinsley, 2004). There are two different processes involved in sorption, they are the physical and chemical processes of absorption and adsorption. Absorption is the process by which atoms, ions and molecules enter the bulk phase of a substance (McMurry and Fay, 2003). If the phase of the substance is solid it can absorb atoms, ions and molecules in both liquid and gas phases, where as if the phase of the substance is a liquid only atoms, ions and molecules in the gaseous phase can be absorbed. Absorption is characterized by uptake into the volume of a substance. Converse to this is adsorption, where the uptake is characterized by the surface of a substance. This is because, as defined by the International Union of Pure and Applied Chemistry (IUPAC), a substance is considered to be adsorbed when there is an increase in the concentration of a dissolved substance at the boundary of a solid and a liquid phase (IUPAC, 1987). There is an

increase in the concentration of a dissolved substance at the surface when atoms, ions or molecules are bound to the surface. The atoms, ions or molecules can be gases, liquids, or dissolved solids.

2.1.1 Sorption Mechanisms

Sorption mechanisms are the mechanisms by which absorption and adsorption occur. The main sorption mechanisms are Non-specific Columbic sorption and specific chemical sorption. There are additional minor sorption mechanisms such as structural penetration, isotopic exchange and physical sorption.

Non-specific Columbic Sorption

As the name suggests, non-specific Columbic sorption is dependent on charge. Mineral surfaces can acquire a charge from one of two ways, the first such was is a permanent charge balance inherent in the structure of the mineral. The permanent charge imbalance at the surface is caused by lattice imperfections at the solid surface and isomorphous replacements in the lattice. Isomorphous replacements are substitutions of atoms on the surface with other atoms with different charge (Stumm and Morgan, 1996). For example, in the tetrahedral layer of a clay mineral the replacement of Si^{+4} with Al^{+3} occurs and in the octahedral layer of a clay mineral the replacement of Al^{+3} with Mg^{+2} occurs (Vilks, 2016). The second such way a charge can arise at the surface is from chemical reactions at the surface (Stumm and Morgan, 1996). The edges of clay crystals contain broken bonds resulting form the interruption of the gibbsite and silica sheets. The broken bonds generate exposed metal ions in the

surface layer which behave as Lewis acids because they have a reduced coordination number (Stumm and Morgan, 1996). The exposed metal ions, $-S^+$, will coordinate with water molecules to form a neutral surface site, S$-$OH. This reaction is shown in equation (2.1).

$$-S^+ + H_2O \Longleftrightarrow S{-}OH + H^+ \tag{2.1}$$

The protonation reaction, shown by equation (2.2), and the deprotonation, shown by equation (2.3), of the neutral surface site, S$-$OH, leads to the formation of the positive surface site, $S{-}OH_2^+$, and the negative surface site, $S{-}O^-$ respectively.

$$S{-}OH + H^+ \Longleftrightarrow S{-}OH_2^+ \tag{2.2}$$

$$S{-}OH \Longleftrightarrow S{-}O^- + H^+ \tag{2.3}$$

The values of the protolysis constants associated with equations (2.2) and (2.3) is dependent on the mineral and the exposed metal ion which makes up the surface site (Vilks, 2016). The charge at the surface site due to these chemical reactions is dependent on pH. At low pH the surface charge is positive as the $S{-}OH_2^+$ surface site is dominant. As pH increases, the S$-$OH site becomes more dominant, and eventually at high pH the $S{-}O^-$ site becomes dominant, and the surface charge becomes negative. This relationship is shown in Figure 2.1. When the surface charge is negative, cation ions in solution located near the surface experience opposing forces. There is Columbic attraction between the cation and the negatively charged surface but there is also pull due to the kinetic energy of the cations which tries to pull the cations away from the surface. The result of these opposing forces is the formation of a diffuse layer. Inside the diffuse layer the concentration of cations is higher than

the concentration of cations in the bulk solution, with the highest concentration being adjacent to the surface and the concentration decreasing with distance from the surface according to the Boltzman function (Vilks, 2016). The charge of the diffuse layer counteracts the charge of the surface. Stern (1924) proposed that there was a monolayer on the surface, now called the Stern layer, in which ions adsorb. Unlike the diffuse layer where the amount of adsorbed ions is restricted by charge, in the Stern layer the amount of adsorb ions is restricted by their size and the surface area. A portion of the surface charge is therefore neutralized by the Stern layer, and the charge which the diffuse layer must counteract is decreased (Vilks, 2016).

Non-specific Columbic sorption is fast and reversible. Fast because the rate limiting step is diffusion, and reversible because no bonds need to be broken in order for desorption to occur. As I increases, cations from the salts (*e.g.* Na^+ and Ca^{2+}) will displace other cations due to the mass action of the salt (Vilks, 2016). This means, first, that non-specific Columbic sorption is dependent on I and second, that it is only the dominant sorption mechanism at low I. Non-specific Columbic sorption is modeled using cation exchange reactions. Cation exchange is not considered for elements whose speciation is dominated by anionic and neutral species at low I (Vilks, 2016). Pd speciation is dominated by anionic chloride complexes at low pH and neutral hydroxide complexes at high pH for all I (see Figures 5.8(b) to 5.8(d)) and therefore cation exchange is not included in the sorption model.

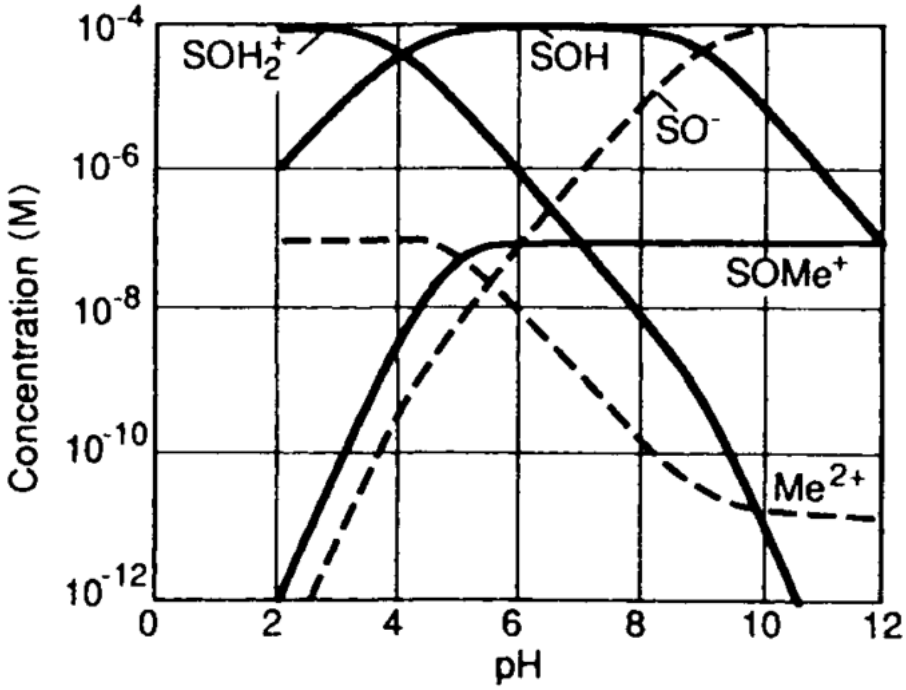

Figure 2.1: Example of sorption by metal binding complexation as a function of pH. As pH increases the dominant surface site species changes. At low pH the $S-OH_2^+$ site is dominant and the overall surface charge is positive. As pH increases S−OH site becomes dominant and the surface charge reduces to zero, eventually the $S-O^-$ site becomes dominant and the surface charge is negative. As the $S-OH_2^+$ surface site becomes less dominant, the formation of metal bound surface complexes, $S-OMe^+$, increases. Figure is taken from Stumm and Morgan (1996).

Specific Chemical Sorption

Specific chemical sorption is not dependent on charge. In fact, it is used to explain non-charge dependent sorption peaks. For a given surface the surface site speciation is dependent on pH and independent of solution composition, *i.e.* what metal ion is in solution. Therefore the pH at which the negative surface site, $S-O^-$, becomes dominant and hence the pH at which the overall charge of the surface becomes negative is the same when considering the sorption of different metals onto the same surface. If sorption was only dependent on charge then we would expect to see the

sorption of all metal cations to increase at the pH where the surface charge becomes negative. However, this effect is not observed in experiment, as is shown in Figure 2.2.

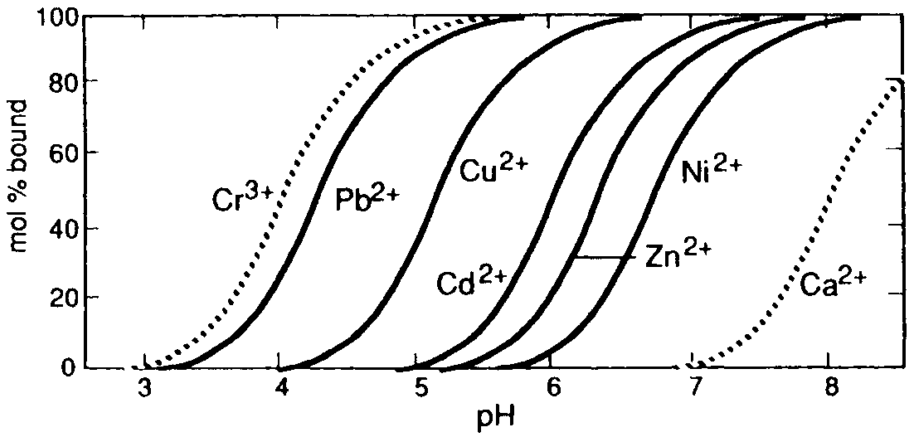

Figure 2.2: Sorption onto hydrous ferric oxide as a function of pH for various metals, taken from Stumm and Morgan (1996). Original figure is created using data from Dzombak and Morel (1990).

Specific chemical sorption is most commonly explained with surface complexation (Vilks, 2016). Surface complexation is the formation of metal complexes with surface sites through metal binding, or ternary complex formation. Metal binding involves the coordination of metal ions with the oxygen donor atoms on the surface and the release of a proton, H^+, from the surface (Stumm and Morgan, 1996). Similarly, ternary complex formation involves the coordination, and subsequent release of a proton from the surface, of a oxygen donor atom and a metal ion however additional ligands are also included the complex. Surface complexation is dependent on pH, solution I, and solution composition *i.e.* what elements are present in solution. A cation can associate with a surface as a inner-sphere complex or as an outer-sphere complex, depending on whether a direct chemical bond is formed between the cation

and the surface or if the cation approaches the surface to a critical distance after which it is held to the surface by Columbic forces. The former is an inner-sphere complex and the latter is an outer-sphere complex. Outer-sphere complexes have one or more water molecule separating the cation from the surface (Stumm and Morgan, 1996). Inner- and outer-sphere complexes are depicted in Figure 2.3.

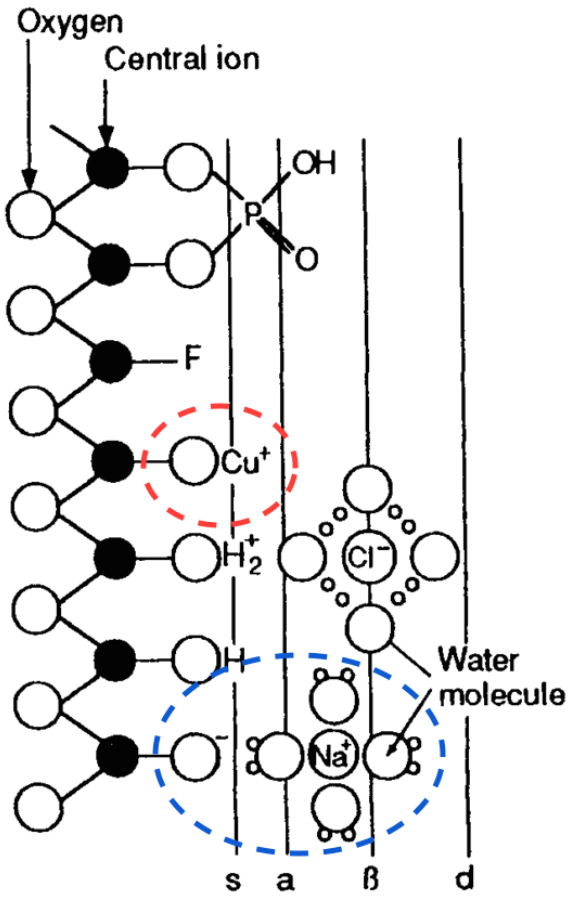

Figure 2.3: Comparison of inner- and outer-sphere complexes, taken from Stumm and Morgan (1996). $S{-}OCu^{+}$ (circled in red) is an example of an inner-sphere complex, where as $S{-}O^{-} - H_2O - Na^{+}$ (circled in blue) is an example of an outer-sphere complex.

Other Sorption Mechanisms

Structural penetration occurs when a dehydrated cation is small enough to penetrate the holes in the tetrahedral layer of a clay, and when rehydrated, become stuck. Cations that are smaller still might pass through the tetrahedral layer and occupy empty sites in the octahedral layer where they will remain fixed after water is added to the system (Vilks, 2016). Vilks (2016) commented that atoms with ionic radii greater than 74 pm would most likely not sorb by structural penetration. Pd(II) has an effective ionic radius of 86 pm, and a crystal ionic radius of 100 pm (Shannon, 1976). Shannon (1976) stated that he felt that crystal radii correspond more closely to the physical size of ions in a solid. Therefore Pd most likely will not sorb by structural penetration and it is not necessary to include it in the model.

Isotopic exchange is a sorption mechanism by which a radionuclide exchanges with it's stable, naturally occurring isotope in the mineral structure or a inner-sphere complex (Vilks, 2016). Natural Pd is made up of six stable isotopes, ^{102}Pd, ^{104}Pd, ^{105}Pd, ^{106}Pd, ^{109}Pd and ^{110}Pd. The natural abundance, in terms of atom percentage, of these isotopes are 1.02%, 11.14%, 22.33%, 27.33%, 26.46% and 11.72% respectively (Coplen *et al.*, 2002). Therefore it is possibly that isotopic exchange will occur for Pd. Pd sorption experiments in this thesis were completed using non-radioactive, naturally occurring Pd, with concentrations being determined from the amount of ^{105}Pd in solution. It is not necessary to consider isotopic exchange in the sorption model as we can assume that there will be an equal distribution of Pd isotopes on or in the surface and an equal distribution of Pd isotopes in solution and therefore that ^{105}Pd sorption is representative of all Pd sorption.

Physical Sorption is caused by electric interactions at surfaces, *e.g.* vad der Waals, which extend over longer distances then chemical forces, however they are typically much weaker (Stumm and Morgan, 1996). Physical sorption can be used to explain the sorption of neutral metal hydrolysis complexes onto neutral surface sites (S−OH).

2.1.2 Measuring Sorption Experimentally

There are currently two experimental methods being used to measure sorption; batch sorption experiments and diffusion experiments. Batch sorption experiments, see Figure 2.4(a), place both the sorbate, *i.e.* Pd, and the solid, *i.e.* bentonite, illite or shale, being studied in a vessel together. The sorbate sorbs directly onto to the solid and the sorption is measured by determining the amount of sorbate left in solution after equilibrium has been achieved.

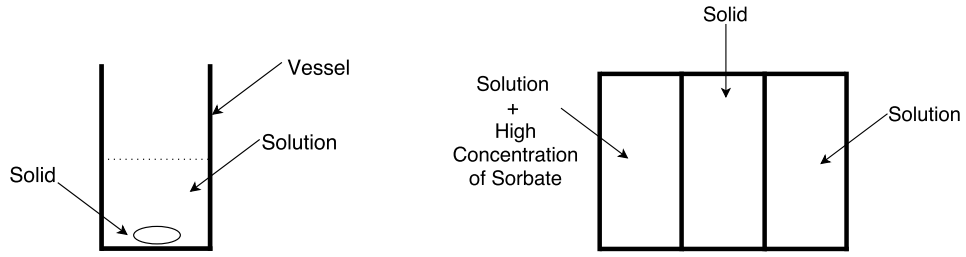

(a)Batch Sorption Experiment (b)Diffusion Experiment

Figure 2.4: Comparison of batch sorption and diffusion type experiments.

In diffusion experiments, see Figure 2.4(b), the solid is not placed in solution with the sorbate. The solid is placed between two reservoirs filled with solution. One of the reservoirs contains a high concentration of sorbate. Sorption occurs as the sorbate

diffuses from the high concentration reservoir to the low concentration reservoir. Similar to batch sorption experiments, sorption is measured by determining the amount of sorbate left in solution after equilibrium has been achieved.

Calculating K_d Values

Sorption is usually quantified by distribution coefficients or more simply, K_d values. It is defined as the ratio of sorbate concentration in the solid to sorbate concentration in the liquid. It is difficult to directly measure the sorbate concentration in the solid so a difference is used to calculate it. Traditionally K_d, is calculated using equation (2.4).

$$K_d = \frac{C_b - C_{eq}}{C_{eq}} \times \frac{L}{S} \tag{2.4}$$

Where C_b is the final concentration of Pd in the blank solution, C_{eq} is the final concentration of Pd in the sample solution and $\frac{L}{S}$ is the liquid to solid ratio used in the sample. Therefore the sorbate concentration is the difference between C_b and C_{eq}. However according to Tachi *et al.* (1999) Pd sorption onto the wall of the experimental vessel is only significant in blank solutions, and only a small amount of Pd appears to sorb onto the vessel walls when a solid is present. Tachi *et al.* (1999) concluded that is inappropriate to use the final concentration in the blank solution to calculate K_d and that it is more appropriate to use C_i, the initial concentration of Pd in the sample. Therefore K_d values in this report will be calculated using equation (2.5) where the concentration of sorbate in the solid is the difference between C_i and C_{eq}.

$$K_d = \frac{C_i - C_{eq}}{C_{eq}} \times \frac{L}{S} \tag{2.5}$$

2.1.3 Sorption Isotherms

A sorption isotherm is a plot of sorbed concentration of an element against the amount of element still remaining in solution at sorption equilibrium. In this thesis the sorbed concentration is assumed to be the difference between the initial concentration and the equilibrium concentration, as discussed in section 2.1.2. A sorption isotherm can be described using Freundlich isotherms, shown by equation (2.6).

$$C_s = C_i - C_{eq} = m \times C_{eq}^n \tag{2.6}$$

Where C_s is the sorbed concentration, m is the Freundlich constant and n is the measure of the non linearity involved (Stumm and Morgan, 1996). It is common to plot isotherms on log $-$ log plots, in which case the Freundlich equations becomes equation (2.7).

$$log(C_s) = n \times log(C_{eq}) + log(m) \tag{2.7}$$

This equation is of the form of the equation of a line, *i.e.* $y = mx + b$. Therefore the Freundlich constant can be derived from the y-intercept, and n can be derived from the slope. The slope of the isotherm can be used to explain the sorption behavior. For example, if we consider the case where the slope (n) is one, then equation (2.6) becomes equation (2.8).

$$C_s = m \times C_{eq} \tag{2.8}$$

From this it is clear that m is K_d. Therefore K_d is independent of the initial concentration in solution (Dada *et al.*, 2012). Additionally, a slope of one indicates that sorption is occurring between adsorbate molecules and surface sites, *i.e.* formation of inner- and outer- sphere complexes inside the Stern layer. A slope less than one

indicates that cooperative sorption is most likely occurring. Cooperative sorption is interactions between sorbates, or between sorbates and sorbents and is explained using a multilayer approach (Liu, 2015).

2.1.4 Modeling Sorption

The sorption mechanisms under which sorption occurs are very complex and difficult to predict. In order to determine which sorption mechanisms are occurring, sorption modeling is used. Various mechanisms (*e.g.* specific chemical sorption) are modeled (*e.g.* through surface complexation) and then compared to experimental data. If a good fit between experiment and the model is achieved, the mechanisms which were included in the model can be assumed to be the mechanism under which sorption is occurring. Sorption can be modeled using a variety of different codes; PHREEQC (**PH RE**dox **EQ**uilibrium in **C**) (Parkhurst and Appelo, 2013), MINTEQA2 (a portmanteau of MINEQL (Westall *et al.*, 1976) and WATEQ3 (Ball *et al.*, 1981), the two computer codes which were combined to create the original MINTEQ (Felmy *et al.*, 1984)) (Allison *et al.*, 1991), MINSORB (Bradbury and Baeyens, 1997) and others. The key difference between these codes is the mathematical formulation in which they determine activity coefficients. Activity coefficients can be calculated using various methods; the Debye-Hückel equation (2.9) (Debye and Huckel, 1923), the Davies equation (2.10) (Davies, 1962), the extended (or WATEQ) Debye-Hückel equation (2.11) (Truesdell and Jones, 1974) and specific ion interaction theory (SIT theory) (2.12) (Grenthe and Plyasunov, 1997).

$$log\gamma_i = -Az_i^2\sqrt{\mu} \tag{2.9}$$

$$log\gamma_i = -Az_i^2 \left(\frac{\sqrt{\mu}}{1+\sqrt{\mu}} - 0.3\mu \right) \tag{2.10}$$

$$log\gamma_i = -\frac{Az_i^2\sqrt{\mu}}{1+Ba_i^0\sqrt{\mu}} + b_i\mu \tag{2.11}$$

$$log\gamma_i = -\frac{Az_i^2\sqrt{\mu}}{1+1.5\sqrt{\mu}} + \sum_k \epsilon_{ik} m_k \tag{2.12}$$

In these equations γ_i is the activity coefficient of aqueous species i, μ is the ionic strength, z_i is the ionic charge of aqueous species i and A and B are temperature dependent constants. Equation (2.11) is referred to as the extended Debye-Hückel equation if b_i is zero and the WATEQ Debye-Hückel Equation if b_i is not zero. In the Extended Debye-Hückel Equation a_i^0 is the ion size parameter. In the WATEQ Debye-Hückel Equation a_i^0 and b_i are ion-specific parameters fitted from mean-salt activity coefficient data (Parkhurst and Appelo, 1999). Lastly, the summation $\sum_k$ is over all species, inside the summation ϵ_{ik} is the interaction coefficient between species i and k and m_k is the molality of species k.

The MINSORB code uses the Davies Equation (2.10) to solve for activity coefficients (Bradbury and Baeyens, 1997). When the relevant parameters (a_i and b_i) are available in the database MINTEQA2 will use the Extended/WATEQ Debye-Hückel Equation (2.11), however if not all relevant parameters are in the database, MINTEQA2 will use the Davies Equation (2.10) (Allison *et al.*, 1991). The same applies for Visual MINTEQ (Gustafsson, 2009), the most recent revision of MINTEQ which was developed using MINTEQA2. PHREEQC, by default, uses the same method as MINTEQA2 and Visual MINTEQ (Parkhurst and Appelo, 1999), however, with a supporting database it has the ability to use SIT theory.

Due to the high I conditions being considered in this thesis it was necessary to chose a code which would be accurate up to I of 4 M. SIT theory has been shown to be effective up to I of 4 M (Grenthe and Plyasunov, 1997), where as the other methods have not, therefore it was necessary to use PHREEQC with a SIT theory capable database for modeling sorption.

PHREEQC comes packaged with several databases, one of which is SIT theory specific, however we elected to go with a database provided by the JAEA. The JAEA TDB (Kitamura *et al.*, 2014) has more accurate data on formation reactions for Pd species, as well as additional epsilon values for Pd to be used in SIT theory calculations. The JAEA TDB is more accurate and has more epsilon values because, with regard to Pd, the JAEA TDB has been more recently updated. For example, the JAEA TDB uses a log k of zero for the formation reaction of $PdOH^+$ as discussed by Rai *et al.* (2012) however the database provided with PHREEQC, the ThermoChimie TDB developed by French National Radioactive Waste Management Agency (ANDRA), still uses a value of -1.86 for log k from Navibantes and Kalabina (1970). The formation reaction constants for all palladium-hydroxide and palladium-chloride species were updated by Rai *et al.* (2012) where as all the palladium-hydroxide and palladium-chloride species in the ThermoChimie database still use formation reaction constants taken from Navibantes and Kalabina (1970) and Lothenbach *et al.* (1999).

Surface Complexation Modeling

Surface complexation modeling is used to model specific chemical sorption. It is the only sorption mechanism being considered for the sorption of Pd onto montmoillonite and illite. This is because anionic Pd species are dominant at low pH, and neutral Pd species are dominant at high pH and therefore cation exchange is not considered.

As discussed previously in section 2.1.1, solids have a variety of surface sites; $S-OH$, $S-OH_2^+$ and $S-O^-$. The surface sites are generally referred to as surface hydroxl groups. Surface hydroxl groups have similar donor properties to their corresponding counter parts in dissolved solutes (Stumm and Morgan, 1996) as is shown by equations (2.13) and (2.14) below.

$$H_2O + Me^{2+} \Longleftrightarrow Me(OH)^+ + H^+ \tag{2.13}$$

$$S-OH + Me^{2+} \Longleftrightarrow S-OMe^+ + H^+ \tag{2.14}$$

Equation (2.13) is the formation reaction for the aqueous species $Me(OH)^+$, where as equation (2.14) is the formation reaction for the surface complex $S-OMe^+$. In both reactions we see an oxygen atom donating a hydrogen to a make a bond. Therefore surface complex formation, or surface complexation, can be interpreted as competitive complex formation and modeled using equilibria. There are several types of equilibria to be considered in surface complexation; acid-base equilibria, metal binding, ligand exchange and ternary surface complex formation (see section 2.1.1).

Acid-Base Equilibria

$$\mathrm{S{-}OH} + \mathrm{H^+} \Longleftrightarrow \mathrm{S{-}OH_2^+} \tag{2.15}$$

$$\mathrm{S{-}OH} \Longleftrightarrow \mathrm{S{-}O^-} + \mathrm{H^+} \tag{2.16}$$

Metal Binding

$$\mathrm{S{-}OH} + \mathrm{Me^{z+}} \Longleftrightarrow \mathrm{S{-}OMe^{(z-1)+}} + \mathrm{H^+} \tag{2.17}$$

$$\mathrm{S{-}OH} + \mathrm{Me^{z+}} + \mathrm{H_2O} \Longleftrightarrow \mathrm{S{-}OMeOH^{(z-2)+}} + 2\mathrm{H^+} \tag{2.18}$$

$$\mathrm{S{-}OH} + \mathrm{Me^{z+}} + 2\mathrm{H_2O} \Longleftrightarrow -\mathrm{SOMe(OH)_2^{(z-3)+}} + 3\mathrm{H^+} \tag{2.19}$$

Ligand Exchange

$$\mathrm{S{-}OH} + \mathrm{L^-} \Longleftrightarrow \mathrm{SL} + \mathrm{OH^-} \tag{2.20}$$

Ternary Surface Complex Formation

$$\mathrm{S{-}OH} + L^- + \mathrm{Me^{z+}} \Longleftrightarrow \mathrm{S{-}OMeL^{(z-2)+}} + \mathrm{H^+} \tag{2.21}$$

$$\mathrm{S{-}OH} + 2L^- + \mathrm{Me^{z+}} \Longleftrightarrow \mathrm{S{-}OMeL_2^{(z-3)+}} + \mathrm{H^+} \tag{2.22}$$

$$\mathrm{S{-}OH} + 3L^- + \mathrm{Me^{z+}} \Longleftrightarrow \mathrm{S{-}OMeL_3^{(z-4)+}} + \mathrm{H^+} \tag{2.23}$$

Equations (2.15) to (2.23) show examples of the varies types of equilibria considered in a surface complexation model for a fictitious metal Me(II). The acid-base equilibria reactions were originally shown in section 2.1.1, and repeated here for completeness. They describe the pH dependence of surface charge.

2.2 Speciation

Speciation is defined by IUPAC as the distribution of an element amongst it's defined chemical species (Nordberg *et al.*, 2004). Where a chemical species is a specific form of a chemical element defined as its molecular or complex structure, or oxidation state (Michalke, 2003). For example, if we consider the fictitious metal Me(II), chemical species can be of the form Me^{2+}, $Me(OH)^{+}$, $MeCl_3^{-}$, etc.

2.2.1 Modeling Speciation

Speciation is modeled using the same software and database as sorption *i.e.* PHREEQC in conjunction with the JAEA TDB. Determining speciation is actually an integral part to modeling sorption, as the speciation model determines the aqueous concentration of all chemical species. This is necessary to model sorption as the formation of surface complexes depends on the presence of it's corresponding aqueous complex. For example, if we consider Me(II) again, $Me(OH)^{+}$ is the corresponding aqueous complex to the $S{-}OMe^{+}$ surface complex and the surface complex can only form if the aqueous complex is present.

2.3 PHREEQC

In PHREEQC every element (or element valence state) in the database has a single master species associated with it, in the case of the fictitious metal Me(II) the master aqueous species would be Me^{2+}. If there was also a Me(III) valence state, then it would have a separate master aqueous species then Me(II), namely Me^{3+}. The formation reactions of all subsequent species will contain master aqueous species.

If we consider the aqueous species $Me(OH)_3^-$, it's corresponding formation reaction would be as shown in equation (2.24) (Parkhurst and Appelo, 1999).

$$Me^{2+} + 3H_2O \Longleftrightarrow Me(OH)_3^- + 3H^+ \tag{2.24}$$

Me^{2+} and H^+ are master aqueous species, and H_2O would be defined by its own formation reaction consisting of master aqueous species. The purpose of the master aqueous species is to reduce the number of unknowns associated with the number of species down to the number of unknowns associated with the number of master aqueous species. The unknowns for a given master aqueous species i are the activity a_i, the activity coefficient γ_i, the molality m_i and the moles in solution n_i (Parkhurst and Appelo, 1999). These unknowns can be related using equations (2.25) and (2.26), where W_{aq} is the amount of water. These equations can be combined to yield equation (2.27).

$$a_i = \gamma_i m_i \tag{2.25}$$

$$n_i = m_i W_{aq} \tag{2.26}$$

$$n_i = W_{aq} \frac{a_i}{\gamma_i} \tag{2.27}$$

All species are assumed to be in equilibrium which requires that all mass action equations for aqueous species are satisfied (Parkhurst and Appelo, 1999).

$$K_i = a_i \prod_m^{M_{aq}} a_m^{-c_{m,i}} \tag{2.28}$$

In the mass action equation for aqueous species i (2.28), K_i is a temperature dependent equilibrium constant (found in the database), $c_{m,i}$ is the stoichiometric coefficient of master species m and M_{aq} is the total number of aqueous master species. If we consider again the formation reaction shown by equation (2.24), the corresponding mass action equation would be as follows.

$$K_{Me(OH)_3^-} = \frac{(a_{Me(OH)_3^-})(a_{H+}^3)}{(a_{Me^{+2}})(a_{H_2O}^3)} \tag{2.29}$$

The activities of Me^{2+} and H_2O appear on the denominator because the convention of PHREEQC is that terms on the left hand side of the formation reaction have negative coefficients and the terms on the right hand side have positive coefficients (Parkhurst and Appelo, 1999). Equation (2.28) can be used to determine the total moles of an aqueous species by combining it with equation (2.27).

$$n_i = K_i W_{aq} \frac{\prod_m^{M_{eq}} a_m^{c_{m,i}}}{\gamma_i} \tag{2.30}$$

In equation (2.30) W_{aq} is a known value specified in the input file, $c_{m,i}$ is defined in the formation reaction and K_i is specified in the database for each formation reaction. The unknowns, as specified earlier, are the activity a_i, the activity coefficient γ_i, and the moles in solution n_i. The activity coefficient is solved for using the methods discussed earlier in section 2.1.4, namely SIT theory (2.12) if the database contains the relevant SIT parameters, or the Extended Debye-Hc̈kel Equation (2.11) if it's relevant parameters are available in the database, and lastly, if no relevant parameters are available, the Davies Equation (2.10). The remaining unknowns are solved using the Netwon-Raphson method which will be discussed in section 2.3.1 (Parkhurst and

Appelo, 1999).

The same method in which the total moles of an aqueous species can be determined can be applied to determine the total moles of a surface species, among other things (*e.g.* total moles of exchange species, gaseous species, etc.). The mass action equation for a surface species (2.32) can be combined with equation (2.31) to yield the equation for total moles of a surface species (2.33).

$$n_{i_{s_k}} = a_{i_{s_k}} \frac{T_{s_k}}{b_{i_{s_k}}} \tag{2.31}$$

$$K^{int}_{i_{s_k}} = a_{i_{s_k}} \prod_{m}^{M} a_m^{-c_{m,i_{s_k}}} \tag{2.32}$$

$$n_{i_{s_k}} = K^{int}_{i_{s_k}} \frac{T_{s_k}}{b_{i_{s_k}}} \prod_{m}^{M} a_m^{c_{m,i_{s_k}}} \tag{2.33}$$

The notation i_{s_k} is used to describe species i attached to surface s at a surface site of type k. There are additional terms in equation (2.33) when compared to it's aqueous counterpart, equation (2.30). The additional terms are the total number of surface sites for surface s, type k $T_{i_{s_k}}$, and the number of surface sites bounded to the species $b_{i_{s_k}}$. Additionally, instead of the product extending over all master aqueous species, as is the case with equation (2.30), it extends over all master species (*i.e.* master surface and aqueous species). Another difference between the aqueous and surface species calculations is that for the aqueous calculation, the mass action equation is based off of the formation reactions specified in the databases, where as the mass action equation for surface species is based off of the surface complexation reactions specified in the model. If we consider the surface complexation reaction (2.19) the

corresponding mass action equation would be as follows.

$$K^{int}_{SOMe(OH)^-_2} = \frac{(a_{SOMe(OH)^-_2})(a_{H+})^3}{(a_{Me^{+2}})(a_{H_2O})^3(a_{S-OH})} \tag{2.34}$$

2.3.1 Newton-Raphson Method

Newton-Raphson method is a method for iteratively solving for the roots of a real valued function. Newton-Raphson method in one dimension, for a function f and root x (*i.e.* $f(x) = 0$), is shown by equations (2.35) and (2.36). The first approximation of the root, x_1, can be determined from an initial guess of the root, x_0, as is shown by equation (2.35). This process can be repeated until a suitable value of the root is found, that is, $f(x_n) < \epsilon$ where ϵ is the convergence criterion.

$$x_1 = x_0 - \frac{f(x_0)}{f'(x_0)} \tag{2.35}$$

$$\vdots$$

$$x_{n+1} = x_n - \frac{f(x_n)}{f'(x_n)} \tag{2.36}$$

Newton-Raphson method can be applied to solve non linear systems of equation, such as those used in PHREEQC. In stead of dividing by $f'(x_0)$ in equation (2.35) we can left multiply by the inverse of the Jacobian matrix (Remani, 2013).

$$\mathbf{x_1} = \mathbf{x_0} - \mathbf{J}(x)^{-1}\mathbf{F}(x_0) \tag{2.37}$$

Instead of solving the equation $f(x) = 0$ we are now solving the system of equations $\mathbf{F}(\mathbf{x}) = 0$. If we make the substitution shown by equation (2.38) then equation (2.37)

becomes equation (2.39).

$$\mathbf{y}(\mathbf{x_0}) = \mathbf{J}(\mathbf{x_0})^{-1}\mathbf{F}(\mathbf{x_0}) \tag{2.38}$$

$$\mathbf{x_1} = \mathbf{x_0} - \mathbf{y}(\mathbf{x_0}) \tag{2.39}$$

Instead of solving for the inverse of the Jacobian matrix it is possible to solve the system of linear equations shown by equation (2.40), which was simply a rearrange of the substitution equation (2.38) (Remani, 2013).

$$\mathbf{J}(\mathbf{x_0})\mathbf{y}(\mathbf{x_0}) = -\mathbf{F}(\mathbf{x_0}) \tag{2.40}$$

Solving equation (2.40) will give a solution to $\mathbf{y}(\mathbf{x_0})$ which can be substituted into (2.39) to solve for $\mathbf{x_1}$. As earlier the process can be repeated until suitable values of the roots ($\mathbf{x}$) are found, that is, $\mathbf{F}(\mathbf{x}) < \epsilon$.

Application to PHREEQC

In PHREEQC there are a series of functions used to describe equilibrium. These functions can be derived by substituting the equations for moles of species, which were in turn derived from mass action equations, into mole- and charge-balances. In addition to these, we have functions for determining the I and activity of water. By definition, when equilibrium is satisfied, all functions are equal to zero (Parkhurst

and Appelo, 1999). Therefore we have a system of equations of the form $\mathbf{F}(x) = 0$.

$$\mathbf{F}(\mathbf{x}) = \begin{bmatrix} f_{H_2O}(a_{H_2O}, \mu, m_{ss}, m, \ldots, z_{aq}) \\ f_{\mu}(a_{H_2O}, \mu, m_{ss}, m, \ldots, z_{aq}) \\ f_{m,ss}(a_{H_2O}, \mu, m_{ss}, m, \ldots, z_{aq}) \\ f_{m}(a_{H_2O}, \mu, m_{ss}, m, \ldots, z_{aq}) \\ \vdots \\ f_{z,aq}(a_{H_2O}, \mu, m_{ss}, m, \ldots, z_{aq}) \end{bmatrix} \tag{2.41}$$

Where f_{H_2O} is the function for calculating the activity of water, f_{μ} is the function for calculating I, $f_{m,ss}$ is the function derived from the mole balance of surface sites, f_m is the function derived from the mole balance of elements and $f_{z,aq}$ is the equation derived from the aqueous charge balance. PHREEQC considers many other functions, a full list of which are derived and listed in Parkhurst and Appelo (1999). The Jacobian matrix is derived from differentiating these functions with respect to the unknowns; the activity of water (a_{H_2O}), I (μ), moles of each species(m_{ss}, m), charge of aqueous solution (z_{aq}), etc.

$$\mathbf{x} = \begin{bmatrix} a_{H_2O} \\ \mu \\ m_{ss} \\ m \\ \vdots \\ z_{aq} \end{bmatrix} \tag{2.42}$$

$$\mathbf{J}(x) = \begin{bmatrix} \frac{\partial f_{H_2O}}{\partial a_{H_2O}} & \cdots & \frac{\partial f_{H_2O}}{\partial z_{aq}} \\ \frac{\partial f_{\mu}}{\partial a_{H_2O}} & \cdots & \frac{\partial f_{\mu}}{\partial z_{aq}} \\ \frac{\partial f_{m,ss}}{\partial a_{H_2O}} & \cdots & \frac{\partial f_{m,ss}}{\partial z_{aq}} \\ \frac{\partial f_{m}}{\partial a_{H_2O}} & \cdots & \frac{\partial f_{m}}{\partial z_{aq}} \\ \vdots & & \vdots \\ \frac{\partial f_{z,aq}}{\partial a_{H_2O}} & \cdots & \frac{\partial f_{z,aq}}{\partial z_{aq}} \end{bmatrix} \tag{2.43}$$

Iteratively solving successive sets of linear equations will yield a solution to the non linear equations.

Chapter 3

Experimental Methods

3.1 Detection Limit of Palladium by ICP-MS

The detection limit of Pd by inductively coupled plasma mass spectroscopy (ICP-MS) was determined by experiment. The detection limit of Pd by ICP-MS determines how high the initial concentration of Pd in solution needs to be. Pd stock solution with concentration of 1μg/ml was added to deionized water such that the concentration of Pd ranged from 1×10^{-7} M to 1×10^{-10} M by one order of magnitude. Table 3.1 shows the volume of Pd stock solution required to prepare 10 ml solutions of the desired Pd concentrations.

Table 3.1: Preparation of Pd detection limit samples. The volume of stock solution added replaced an equal volume of deionized water. The total volume of each solution was 10ml.

Volume of Pd Stock Solution Added (μl)	**Resulting Pd Concentration**
1064.0	1×10^{-7} M
106.4	1×10^{-8} M
10.6	1×10^{-9} M
1.1	1×10^{-10} M

The ICP-MS was calibrated using these four solutions of known concentration and a fifth blank solution, deionized water. The detection limit was determined by the difference between the counts per second (CPS) of ^{105}Pd in the blank solution and the CPS of ^{105}Pd in the Pd solutions. If the CPS of ^{105}Pd in the Pd solutions was the same or below the CPS of ^{105}Pd in the blank solution then it was considered to be below the detection limit.

3.2 pH Probe Calibration Using Titration

In order to ensure that pH measurements by pH probe, $\mathrm{pH}_{measured}$, are accurate we conducted acid-base titrations and compared the measured pH to the actual pH calculated from the concentration of hydrogen ions, *i.e.* $\mathrm{pH}_c = -log[\mathrm{H}^+]$. A metrohm titrator was used for the experiment. 100 ml solutions with 0.1 M, 1 M and 4 M I solutions were placed in 350 ml beakers. The solutions had a hydrogen ion concentration of 0.001 M from adding 10 ml of 0.1 M hydrochloric acid (HCl) to the solutions. Therefore the initial pH was exactly 2. The titrator then added 0.1 M sodium hydroxide (NaOH) in increments ranging from 4 μl to 200 μl until the measured pH reached

12. The volume added depended on (1) how close to the stop value the solution was and (2) how slowly the pH was changing. If the pH was changing slowly, or it was close to the stop value the amount of volume added was reduced. When the measured pH reached 12 the process was reversed; 0.1 M HCl was added until the measured pH reached 4. The titrator records the amount of volume added at each step, as well as the total volume added and measured pH. The amount of acid or base added can be used to calculate pH_c.

3.3 Palladium Solubility and Stability Experiment

A solubility experiment was conducted to ensure that the Pd concentration used during experiments was below the solubility limit and to see how long Pd takes to reach a steady dissolved state when added to a Na-Ca-Cl solution. Na-Ca-Cl solutions with I of 0.1 M, 1 M and 4 M were used. Pd was added to the solutions such that the initial concentration of Pd in solution was 1×10^{-6} M. Over a period of 14 days, measurements of palladium concentration in solution were measured. Measurements were taken after 1 hour, 1 day, 2 days, 5 days, 7 days, and 14 days, using the procedure outlined in section 3.4.1.

3.4 Sorption Methodology

Batch sorption experiments were carried out in this paper. The sorption experiments were carried out under aerobic conditions at 25 °C. Triplicates were used for each experimental condition to ensure experimental accuracy. Figure 3.1 shows the general procedure used for the experiments.

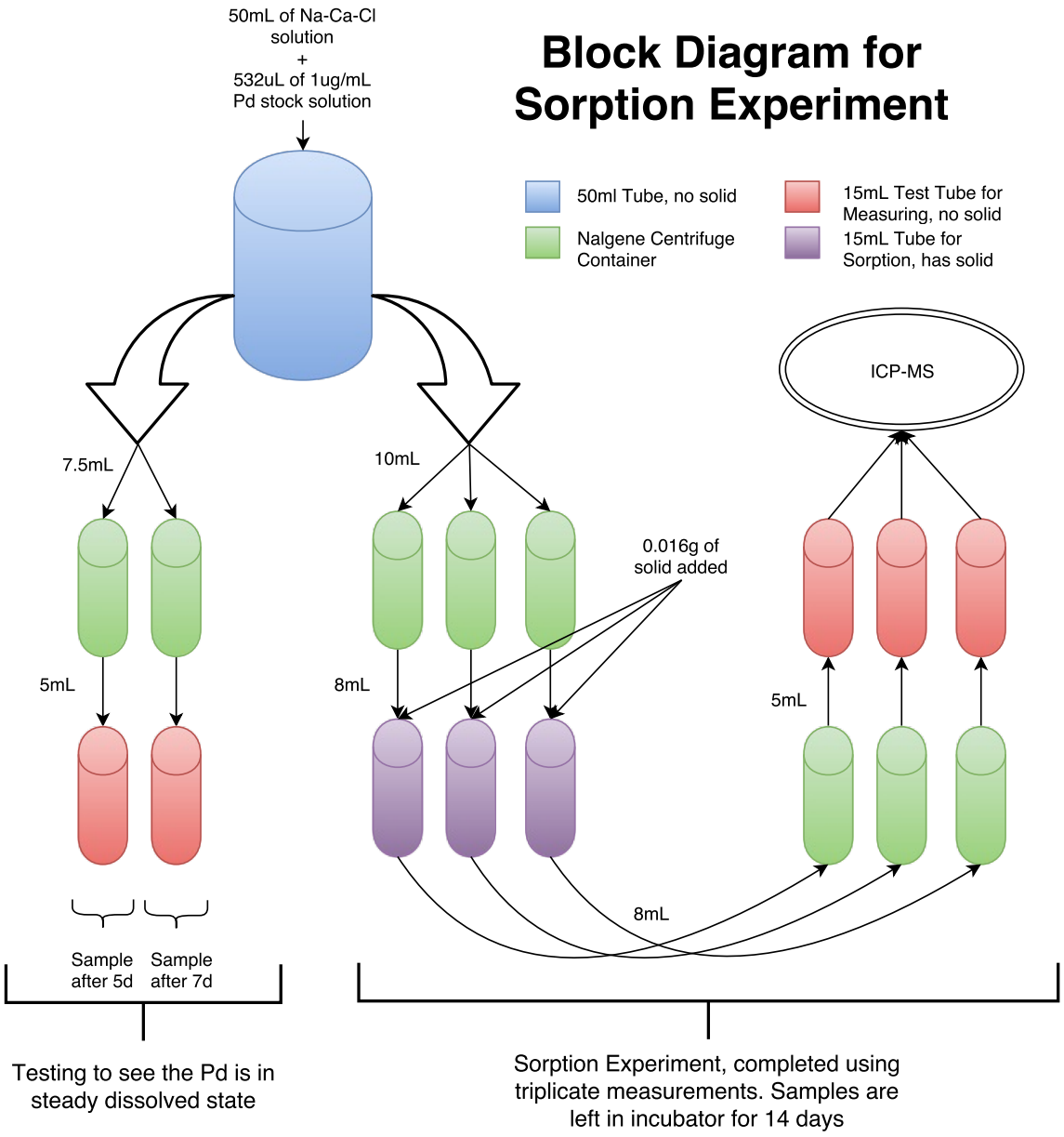

Figure 3.1: Block diagram showing the general procedure for batch sorption experiments.

3.4.1 Separation and Measurement Procedure

When a sorption measurement was taken, a volume of solution was removed and placed in a Nalgene centrifuge container and centrifuged for 30 minutes at 18,000 rpm. The volume removed depends on the measurement being taken, the values for the different measurement types are listed in Table 3.2. After centrifuging, a smaller volume of solution was removed, the volume removed can be also be found in Table 3.2. A smaller volume was used after centrifuging to ensure that any Pd precipitate or other solid separated during centrifuging was not transferred to the new vessels.

After centrifuging the concentration of ^{105}Pd in solution was measured by ICP-MS. However the ICP-MS was designed to handle ionic strengths up to approximately 0.75 M (Agilent Technologies, 2013), therefore it was necessary to dilute the high ionic strengths before analyzing them. 1 M solutions were diluted by a factor of two, 2 M solutions by a factor of three, 3 M solutions by a factor of four and 4 M solutions by a factor of six. ^{105}Pd and ^{106}Pd are the two most commonly chosen isotopes of Pd measured using ICP-MS because they have the largest percent abundance, 22.33% and 27.33% respectively in natural Pd (Coplen *et al.*, 2002). Even though the percent abundance of ^{105}Pd is lower than ^{106}Pd, it was chosen because there are no other isotopes with the same mass. ^{106}Pd and ^{106}Cd have similar masses and would be indistinguishable to the mass spectrometer. The isobar ^{106}Cd concentration may be low as no Cd should be present in solution so ^{106}Pd can be used as backup for ^{105}Pd in the event that the ^{105}Pd has high background.

Table 3.2: Centrifuging and sampling volumes by measurement type.

Measurement	**Volume Removed before Centrifuge (ml)**	**Volume Removed after Centrifuge (ml)**
Initial Conc. of Pd	7.5	5
Contacting solid	10	8
Equilibrium Conc. of Pd	8	5

3.4.2 Sorption Kinetics Experiment

A sorption kinetics experiment was conducted in order to determine the amount of time it takes for Pd sorption to reach equilibrium. The three different solid samples, bentonite MX-80, Queenston shale and illite were contacted with 8 ml of Na-Ca-Cl solutions of ionic strengths 0.1 M, 1 M and 4 M in polypropylene test tubes. Before contact, the solutions were centrifuged for 30 minutes at 18,000 rpm. A liquid to solid ratio of 2.0 μg/l was used for the bentonite, shale and illite. A 1 μg/l Pd solution was added to the solutions such that the final concentration of Pd in the samples was 1×10^{-7} M. The samples were stored in an incubator at 20 rpm and 25 °C up until it was time to take measurements. The concentration of Pd in solution was measured after 1 hour, 1 day, 2 days, 5 days, 7 days, and 14 days using the procedure outlined in section 3.4.1.

3.5 Ionic Strength Dependence of K_d Experiment

A sorption experiment was conducted in order to determine the dependence of K_d on I. Three different solid samples were used, bentonite MX-80, Queenston shale and

illite. A liquid to solid ratio of 2.0 μg/l was used for the bentonite, shale and illite. 50 ml solution of Na-Ca-Cl with I of 0.1 M, 0.5 M, 1 M, 2 M, 3 M and 4 M were prepared in polypropylene test tubes. 532 μl of Na-Ca-Cl solution was replaced by 1μg/ml Pd stock solution so that the initial concentration of Pd in solution was 1×10^{-7} M. The solutions were placed in an incubator for 7 days at 20 rpm and 25 °C, as determined by the solubility and stability experiment (see Section 5.3.) Pd concentration in solution was measured after 5 and 7 days, according to the procedure outlined in section 3.4.1, to ensure that the initial concentration of Pd was stable and below the solubility limit. If the concentration of Pd in solution after 5 and 7 days was equal it was assumed to be stable and below the solubility limit. After verifying stability and solubility, 0.016g of solid was measured using a mass balance and placed into new polypropylene test tubes and contacted with 8ml of Na-Ca-Cl solution. Before contact, the solutions were centrifuged for 30 minutes at 18,000 rpm. This step of the experiment was completed in triplicate, that is, for each initial solution with I of either 0.1 M, 0.5 M, 1 M, 2 M, 3 M or 4 M, three samples of the same solid were contacted. The samples were left in an incubator for 14 days at 20 rpm and 25 °C, as determined by the sorption kinetics experiment (see Section 5.4.) Measurements of Pd concentration in solution were made after the 14 days of sorption time according to the procedure outline in Section 3.4.1. K_d was calculated using the concentration of Pd in solution 7 days after it was added as the initial concentration, and the concentration in solution after 14 days of contact with the solid as the final concentration.

3.6 pH Dependence of K_d Experiment

A sorption experiment was conducted in order to determine the dependence of K_d on pH. The values of pH being studied were, 5, 6, 7, 8 and 9. Three different solid samples were used, bentonite MX-80, Queenston shale and illite. A liquid to solid ratio of 2.0 μg/l was used for the bentonite, shale and illite. 50 ml solution of Na-Ca-Cl with I of 0.1 M, 1 M and 4 M were prepared in polypropylene test tubes. 532 μl of Na-Ca-Cl solution was replaced by 1μg/ml Pd stock solution so that the initial concentration of Pd in solution was 1×10^{-7} M. The solutions were placed in an incubator at 20 rpm and 25 °C for 7 days, as determined by the solubility and stability experiment (see Section 5.3.) pH was adjusted daily to one of the pH values of interest; 5, 6, 7, 8 or 9. pH adjustment was done manually, the initial pH of the solution was measured and either 0.1 M HCl or 0.1 M NaOH was added according to which direction the pH had to be adjusted. The amount of HCl or NaOH added was heavily dependent on; I and difference between initial pH and target pH, and was determined experimentally. Initial pH, HCl added, NaOH added, solution I and final pH were recorded for each adjustment and used for determining the amount of HCl or NaOH to add in future adjustments. pH was adjusted to within $\pm$ 0.1 of the desired value. Pd concentration in solution was measured after 5 and 7 days, according to the procedure outlined in section 3.4.1, to ensure that the initial concentration of Pd was stable and below the solubility limit. If the concentration of Pd in solution after 5 and 7 days was equal it was assumed to be stable and below the solubility limit. After verifying stability and solubility, 0.016g of solid was measured using a mass balance and placed into new polypropylene test tubes and contacted with 8ml of Na-Ca-Cl solution. Before contact, the solutions were centrifuged for 30 minutes

at 18,000 rpm. This step of the experiment was completed in triplicate, that is, for each initial solution with I of either 0.1 M, 1 M or 4 M and pH of either 5, 6, 7, 8 or 9, three samples of the same solid were contacted. The samples were left in an incubator at 20 rpm and 25 °C for 14 days, as determined by the sorption kinetics experiment (see Section 5.4,) during which the pH continued to be adjusted daily. The same procedure as earlier was used however it was found that in addition to being dependent on I and difference between initial pH and target pH, the amount of HCl and NaOH which needed to be added was also dependent on the solid. Therefore solid, initial pH, HCl added, NaOH added, solution I and final pH were recorded for each adjustment and was used for determining the amount of HCl or NaOH to add in future adjustments. Measurements of Pd concentration in solution were made after the 14 days of sorption time according to the procedure outline in Section 3.4.1. K_d was calculated using the concentration of Pd in solution 7 days after it was added as the initial concentration, and the concentration in solution after 14 days of contact with the solid as the final concentration.

3.7 Measurement of Sorption Isotherms of Pd

A sorption experiment was conducted in order to determine the dependence of K_d on initial concentration of Pd. When comparing solution concentration of Pd to sorbed concentration of Pd it is referred to as a sorption isotherm. Three different solid samples were used, bentonite MX-80, Queenston shale and illite. A liquid to solid ratio of 2.0 g/l was used for the bentonite, shale and illite. 50 ml solution of Na-Ca-Cl with I of 0.1 M, 1 M and 4 M were prepared in polypropylene test tubes. The initial concentration of Pd considered was 5×10^{-8} M, 1×10^{-7} M, 5×10^{-7} M and 1×10^{-6}

M. The amount of Pd stock solution added for each concentration is shown in Table 3.3.

Table 3.3: Amount of Pd stock solution added to initial solutions for isotherm experiments. Pd stock solution added replaced an equal volume of Na-Ca-Cl solution. Final volume of Na-Ca-Cl solution, including Pd, was 50 ml.

Target Concentration of Pd (M)	**Volume of Pd Stock Solution Added (μl)**
5×10^{-8}	266
1×10^{-7}	532
5×10^{-7}	2660
1×10^{-6}	5321

After adding Pd, the solutions were placed in an incubator at 20 rpm and 25 °C for 7 days, as determined by the solubility and stability experiment (see Section 5.3.) Pd concentration in solution was measured after 5 and 7 days, according to the procedure outlined in section 3.4.1, to ensure that the initial concentration of Pd was stable and below the solubility limit. If the concentration of Pd in solution after 5 and 7 days was equal it was assumed to be stable and below the solubility limit. After verifying stability and solubility, 0.016g of solid was measured using a mass balance and placed into new polypropylene test tubes and contacted with 8ml of Na-Ca-Cl solution. Before contact, the solutions were centrifuged for 30 minutes at 18,000 rpm. This step of the experiment was completed in duplicate, that is, for each initial solution with I of either 0.1 M, 1 M, or 4 M and initial concentration of either 5×10^{-8} M, 1×10^{-7} M, 5×10^{-7} M or 1×10^{-6} M, two samples of the same solid were contacted. The samples were left in an incubator at 20 rpm and 25 °C for 14 days, as determined by the sorption kinetics experiment (see Section 5.4.) Measurements of Pd concentration in solution were made after the 14 days of sorption time according to the

procedure outline in Section 3.4.1. K_d was calculated using the concentration of Pd in solution 7 days after it was added as the initial concentration, and the concentration in solution after 14 days of contact with the solid as the final concentration.

3.8 Materials

Bentonite used in the experiment was bentonite MX-80, a sodium rich bentonite clay found in Wyoming that is passed through an 80 mesh sieve (Vilks, 2016). The bentonite MX-80 was acquired from the American Colloid Company (ACC). The Ordovician age shale, a sample of Queenston shale, was provided by the NWMO and was crushed to a particle size of 150 to 300 μm. The illite sample was purchased from the Clay Mineral Society (CMS) and was IMt-2 (50 grm/unit) Illite from Silver Hill, Mont. Certified American Chemistry Society (ACS) $CaCl_2$ $2\times H_2O$ and NaCl were acquired from Ficher Scientific and used to control the ionic strengths of the solutions. Palladium came in the form of a 1000 ± 1 $\mu g/ml$ standard solution acquired from Agilent Technologies. The deionized water used during the experiment was produced using a Millipore Milli-Q Direct 8 water system. HNO_3 and NaOH were used for pH adjustment and were also purchased from Fisher Scientific.

The Pd standard solution was diluted down to 1 μg/ml, the concentration of which is 9.397×10^{-6} M. The 1 μg/ml solution was used as a stock solution for spiking Pd into solution and was also used to prepare the ICP-MS calibration solutions. The concentration of the calibration solutions were 1×10^{-8} M, 5×10^{-8} M, 1×10^{-7} M, 2.5×10^{-7} M and 5×10^{-7} M.

3.9 Na-Ca-Cl Stock Solution

The Na-Ca-Cl solutions used in experiment contained a NaCl:$CaCl_2$ mass ratio as defined by the SR-270-PW standard ground water solution (Vilks, 2016). The mass ratio is 50.1 g NaCl to 32.0 g $CaCl_2$. A 4 M I stock solution was made using 79.829 g of NaCl and 129.090 g of $CaCl_2$ $2\times H_2O$ per litre of deionized water. The 4 M solution was diluted using deionized water to make lower I solutions during experiments.

Chapter 4

Modelling Methods

A single layer model developed in PHREEQC was used to model sorption of Pd onto montmorillonite and illite. Surface complexation is the only sorption mechanism being considered in the model as anionic chloride complexes and heutral hydroxide complexes dominant Pd speciation. Therefore it is not necessary to consider the diffuse or electric double layer. The diffuse layer is disabled by default (added with the *-diffuse_layer* flag) however the default sorption model in PHREEQC is the generalized two layer model. The generalized two layer model is an electrostatic model which can be turned off using the *-no_edl* flag, see Section B.

4.1 Thermodynamic Data and Formation Reactions

Table 4.1 shows the initial concentrations of aqueous master species specified in the input file for solution ionic strengths of 0.1 M, 1 M and 4 M. These values were used for both the speciation and sorption models.

The following species are expected to appear in solution based off of the aqueous master species included in the input file (as shown in Table 4.1); H^+, OH^-, H_2O, Ca^{2+}, $CaOH^+$, Cl^-, HClO, $HClO_2$, ClO^-, ClO_2^-, ClO_3^-, ClO_4^-, Na^+, Pd^{2+}, $PdCl^+$, $PdCl_2$, $PdCl_3^-$, $PdCl_4^{2-}$, $PdCl_3OH^{2-}$, $Pd(OH)_2$, $Pd(OH)_3^-$. The formation reactions for these species are shown in Table 4.2, there are no formation reactions for master species (*i.e.* H^+, OH^-, Ca^{2+}, Cl^-, Na^+, Pd^{2+}).

The activity coefficients for the species are calculated using SIT theory, the Extended Debye-Hückel Equation and the Davies Equation. Table 4.3 shows the species which have SIT parameters included in the database, and the respective value of the SIT parameter. The species which do not have SIT parameters in the database are H_2O, $CaOH^+$ HClO, HClO2, ClO^-, ClO_2^-, $PdCl_2$, and $Pd(OH)_2$. Of these only $CaOH^+$ has a_i^0 and b_i values in the database. Therefore the activity coefficient of $CaOH^+$ is calculated using the Extended Debye-Hückel Equation (2.11) with $a_i^0 = 6.0$ and $b_i = 0$, and the rest of the activity coefficients are calculated using the Davies Equation (2.10).

Table 4.1: Aqueous master species included in model solutions.

Concentration of Master Species at I of:	**0.1 M**	**1 M**	**4 M**
Ca^+	0.02195	0.2195	0.8780
Cl^-	0.07805	0.7805	3.1220
Na^+	0.03415	0.3415	1.3660
Pd^{2+}	1×10^{-7}	1×10^{-7}	1×10^{-7}

Table 4.2: JAEA TDB formation reactions of relevant species (Kitamura *et al.*, 2014).

Formation Reaction	**log K**	**Error**
1.0 H^+ + 1.0 OH^- = 1.0 H_2O	-14.00	0.015
4.0 H^+ + + 4.0 e^- - 2.0 H_2O = 1.0 O_2	83.090	0.010
1.0 Ca^{2+} + 1.0 H_2O - 1.0 H^+ = $CaOH^+$	-12.85	0.50
1.0 Cl^- + 1.0 H_2O - 1.0 H^+ - 2.0 e^- = HClO	-50.51	0.109
1.0 Cl^- + 2.0 H_2O - 3.0 H^+ - 4.0 e^- = $HClO_2$	-105.91	0.708
1.0 Cl^- + 1.0 H_2O - 2.0 H^+ - 2.0 e^- = ClO^-	-57.93	0.708
1.0 Cl^- + 2.0 H_2O - 4.0 H^+ - 4.0 e^- = ClO_2^-	-107.87	0.708
1.0 Cl^- + 3.0 H_2O - 6.0 H^+ - 6.0 e^- = ClO_3^-	-146.24	0.236
1.0 Cl^- + 4.0 H_2O - 8.0 H^+ - 8.0 e^- = ClO_4^-	-187.78	0.108
1.0 Pd^{2+} + 1.0 Cl^- = $PdCl^+$	5.00	0.24
1.0 Pd^{2+} + 2.0 Cl^- = $PdCl_2$	8.42	0.24
1.0 Pd^{2+} + 3.0 Cl^- = $PdCl_3^-$	10.93	0.24
1.0 Pd^{2+} + 4.0 Cl^- = $PdCl_4^{-2}$	13.05	0.24
1.0 Pd^{2+} + 3.0 Cl^- + H_2O -1.0 H^+ = $PdCl_3OH^{2-}$	3.77	0.626
1.0 Pd^{2+} + 2.0 H_2O -2.0 H^+ = $Pd(OH)_2$	-3.49	
1.0 Pd^{2+} + 3.0 H_2O -3.0 H^+ = $Pd(OH)_3^-$	-15.48	0.35

Table 4.3: SIT parameters for select species of Pd(II) from the JAEA TDB (Kitamura *et al.*, 2014).

Cation Species	**Anion**	**SIT Parameter**	**Error**
H^+	Cl^-	0.12	0.01
H^+	ClO_4^-	0.14	0.02
OH^-	Na^+	0.04	0.01
Ca^{2+}	Cl^-	0.14	0.01
Ca^{2+}	ClO_4^-	0.27	0.03
$C1^-$	Na^+	0.03	0.01
ClO_3^-	Na^+	-0.01	0.02
ClO_4^-	Na^+	0.01	0.01
Pd^{2+}	ClO_4^-	0.22	
$PdCl^+$	ClO_4^-	0.25	0.02
$PdCl_3^-$	Na^+	0.03	0.01
$PdCl_4^{2-}$	Na^+	-0.044	
$PdCl_3OH^{2-}$	Na^+	-0.044	
$Pd(OH)_3^-$	Na^+	-0.11	

4.2 Surface Definitions

Some parameters of the solids must be defined in the model. PHREEQC uses the number of surface sites and the specific surface area in the calculations run during the surface complexation modeling. Bradbury and Baeyens (2005b) recommends a value of 2×10^{-3} mol/kg for the surface site capacity of both montomorillonite and illite. PHREEQC requires the number of sites, so equation (4.1) is used to determine the number of sites from Bradbury and Beayens recommended value for the site capacities.

$$\text{No. of Sites} = \text{Site Capacity} \times \text{Mass of Solid} \tag{4.1}$$

The liquid to solid ratio used in experiment was 0.5 m^3/kg or 2×10^{-3} kg/l. In the model we assume one liter of water, therefore the mass of solid is 2×10^{-3} kg. Using equation (4.1) we get that there are 4×10^{-6} moles of surface sites. The specific surface area used for montmorillonite was 346.0 m^2/g and the specific surface area used for illite was 83.0 m^2/g (Macht *et al.*, 2011).

4.3 Surface Complexation Reactions

Surface complexation reactions were developed using the following method; started by identifying the possible aqueous Pd species and used them to generate a list of possible surface complexes according to metal binding and ternary surface complex theory. That is, bonding the metal complexes to surface bound oxygens and releasing a proton. These surface complexes and their corresponding aqueous species and hydrolysis constant are shown in Table 4.4. The surface complex corresponding to $PdOH^+$ can immediately be disregarded because the hydrolysis constant for it is zero,

meaning that the aqueous species, and therefore the surface complex, will not form.

Using the pattern of equations (2.17) to (2.19) and (2.21) to (2.23) we were able to develop several possible surface complexation reactions, these are shown in Table 4.5. The log k values for these surface complexation reactions were obtained using Bradbury and Baeyens correlations for montmorillonite (Bradbury and Baeyens, 2005b) and illite (Bradbury and Baeyens, 2009), shown in equations (4.2) and (4.3) respectively.

$$log(K_{Mont.}) = 8.1 \pm 0.3 + (0.90 \pm 0.02)\, log\, ({}^{OH}K) \tag{4.2}$$

$$log(K_{Illite}) = 7.9 \pm 0.4 + (0.83 \pm 0.02)\, log\, ({}^{OH}K) \tag{4.3}$$

The Bradbury and Baeyens correlations are surface specific and relate the hydrolysis constant, formation constant for a hydrolysis reaction, of a aqueous species to the surface complexation constants of species sorbing onto the surface.

Table 4.4: Surface complexes and their corresponding aqueous species and formation constant. The hydrolysis constants (formation constants for hyrdoxide species) is used to determine log k with equations (4.2) for montmorillonite and (4.3) for illite.

Surface Complex	**Aqueous Species**	**Formation Constant**
Metal Binding:		
$S{-}OPd^{+}$	$Pd(OH)^{+}$	0.00
$S{-}OPdOH$	$Pd(OH)_2$	-3.49
$S{-}OPd(OH)_2^{-}$	$Pd(OH)_3^{-}$	-15.48
Ternary:		
$S{-}OPdCl$	$PdCl^{+}$	5.00
$S{-}OPdCl_2^{-}$	$PdCl_2$	8.42
$S{-}OPdCl_3^{2-}$	$PdCl_3^{-}$	10.93
$S{-}OPdCl_4^{3-}$	$PdCl_4^{2-}$	13.05
$S{-}OPdCl_3OH^{3-}$	$PdCl_3OH^{2-}$	3.77

Table 4.5: Possible surface complexation reactions modeled in PHREEQC.

Surface Complexation Reaction	log $K_{Mont.}$	log K_{Illite}
Acid-Base:		
$1.0\ S{-}OH + 1.0\ H^{+} = S{-}OH_2^{+}$	4.0	4.5
$1.0\ S{-}OH - 1.0\ H^{+} = S{-}O^{-}$	-6.2	-7.9
Metal Binding:		
$1.0\ S{-}OH + 1.0\ Pd^{+2} + 1.0\ H_2O - 2.0\ H^{+} = S{-}OPdOH$	4.96	5.00
$1.0\ S{-}OH + 1.0\ Pd^{+2} + 2.0\ H_2O - 3.0\ H^{+} = S{-}OPd(OH)_2^{-}$	-5.83	-4.95
Ternary:		
$1.0\ S{-}OH + 1.0\ Pd^{+2} + 1.0\ Cl^{-} - 1.0\ H^{+} = S{-}OPdCl$	5.00	5.00
$1.0\ S{-}OH + 1.0\ Pd^{+2} + 2.0\ Cl^{-} - 1.0\ H^{+} = S{-}OPdCl_2^{-}$	8.42	8.42
$1.0\ S{-}OH + 1.0\ Pd^{+2} + 3.0\ Cl^{-} - 1.0\ H^{+} = S{-}OPdCl_3^{2-}$	10.93	10.93
$1.0\ S{-}OH + 1.0\ Pd^{+2} + 4.0\ Cl^{-} - 1.0\ H^{+} = S{-}OPdCl_4^{3-}$	13.05	13.05
$1.0\ S{-}OH + 1.0\ Pd^{+2} + 3.0\ Cl^{-} - 1.0\ H^{+} = S{-}OPdCl_3OH^{3-}$	3.77	3.77

They were developed experimentally by comparing measured hydrolysis constants to measured surface complexation constants of species sorbing on the strong sites of montmorillonite and illite. What Bradbury and Baeyens found after comparing several elements is that the logarithm of both values was linearly correlated for a given solid (Bradbury and Baeyens, 2005b).

Bradbury and Beayens recommended that the following metal binding surface complexation reactions be used for Pd sorption. Equations (4.4) and (4.5) correspond to the metal binding formation reactions shown in Table 4.5.

$$\mathrm{S{-}OH + Pd^{2+} + H_2O \Longleftrightarrow S{-}OPdOH + 2H^+} \tag{4.4}$$

$$\mathrm{S{-}OH + Pd^{2+} + H_2O \Longleftrightarrow S{-}OPd(OH)_2^- + 3H^+} \tag{4.5}$$

These surface complexation reactions alone were used at first for the sorption model, however as the fit between model and experiment was not very good additional surface complexation reactions were added in order to improve the fit. Using the speciation and the pH range where the fit between model and experiment needed improvement additional surface complexation reactions were selected and added to the model.

Bradbury and Beayens correlation could not be applied to ternary complex formation, therefore it was necessary to find another method for determining the surface complexation constants for ternary surface complex formation reactions. Fein (2002) determined a correlation for ternary surface complexes and organic ligands. It is possible that his correlation would also apply to inorganic ligands. Fein (2002) proposed that the surface complexation constant of a ternary complex species was correlated

to the sum of the surface complexation constant of the surface ligand complex, S−L, and the metal ligand aqueous species, ML(aq).

$$log\, k\,(\mathrm{S{-}OM{-}L}) = log\, k\,(\mathrm{S{-}L}) + log\,(\mathrm{ML(aq)}) \tag{4.6}$$

Where, $log\, k\,(\mathrm{S{-}L})$ is the formation constant for the reaction shown by equation (4.7) and $log\, k\,(\mathrm{ML(aq)})$ is the formation constant for the reaction (4.8).

$$\mathrm{S{-}OH + L^{l-} + H^{+} \Longleftrightarrow S{-}L + H_2O} \tag{4.7}$$

$$\mathrm{M^{m+} + L^{l-} \Longleftrightarrow ML^{m-l}(aq)} \tag{4.8}$$

When we apply this to Pd surface complexation modeling the reactions become:

$$\mathrm{S{-}OH + Cl^{-} + H^{+} \Longleftrightarrow S{-}Cl + H_2O} \tag{4.9}$$

$$\mathrm{Pd^{2+} + \mathit{a}Cl^{-} \Longleftrightarrow PdCl_{\mathit{a}}^{2-\mathit{a}}(aq)} \tag{4.10}$$

Where a is integer ranging from 1 to 4. Vilks (2016) reported that the sorption of chlorine onto shale and bentonite is zero, therefore the surface complexation constant $log\, k\,(\mathrm{S{-}Cl})$ should be zero. This means that Feins correlation reduces to equation (4.11).

$$log\, k\,(\mathrm{S{-}OPdCl_{\mathit{a}}^{2-\mathit{a}}}) = log\,(\mathrm{PdCl_{\mathit{a}}^{2-\mathit{a}}(aq)}) \tag{4.11}$$

This correlation was applied to the ternary surface complexes in Table 4.4 to yield the surface complexation reaction constants in Table 4.5.

Chapter 5

Results and Analysis

5.1 Detection Limit of Palladium by ICP-MS

The detection limit of Pd by ICP-MS was determine to be 1×10^{-9} M. The results of the experiment are shown in Table 5.1.

Table 5.1: Detection limit of Pd by ICP-MS data.

[Pd] (M)	**CPS ^{105}Pd**	**CPS Bi**	**Ratio**
0	1087.63	36311356	0.00002995
1×10^{-10}	1093.18	36744569	0.00002975
1×10^{-9}	1298.33	36523456	0.00003555
1×10^{-8}	13000.85	36103443	0.00036010
1×10^{-7}	127655.76	36815988	0.00346740

We see that as the concentration of Pd decreases, the CPS of ^{105}Pd also decreases. Bismuth (Bi), is used as an internal standard, it's concentration should be constant. The ratio is the ratio of CPS of ^{105}Pd to CPS of Bi. We also see that as the concentration of Pd decreases, the ratio also decreases. When the concentration of Pd is

1×10^{-9} M the CPS of ^{105}Pd and the ratio are slightly higher than the CPS of ^{105}Pd and the ratio from the blank (zero concentration) solution. When the concentration of Pd is 1×10^{-10} M, although the CPS of ^{105}Pd is slightly higher then the CPS of ^{105}Pd in blank solution, the ratio is below the ratio for the blank solution. Therefore a Pd concentration of 1×10^{-10} M solution is below the detection limit and a Pd concentration of 1×10^{-9} M is slightly above. 1×10^{-9} M was used as a conservative value for the detection limit of Pd by ICP-MS.

5.2 Titrations for pH Probe Calibration

The acid base titration curves generated during experiment are shown in Figure 5.1. pH_c, the actual pH, is calculated from the concentration of H^+ using equation (5.1) or the concentration of OH^- using equation (5.2).

$$pH_c = -log[H^+] \tag{5.1}$$

$$pH_c = 14 + log[OH^-] \tag{5.2}$$

The concentration of H^+ or OH^- was calculated using equation (5.3), where $V_{initial}$ is the initial volume of solution.

$$\frac{[H^+]_{initial} \times V_{initial} + H^+_{added} + OH^-_{added}}{V_{final}} = \begin{cases} [H^+], & \text{if } >0 \\ -[OH^-], & \text{if } <0 \end{cases} \tag{5.3}$$

The titrator records the amount of volume added and the measured pH. Since we know the initial concentration of H^+ and the volume of 0.1 M HCl or NaOH added

we can calculate the amount of H^+ or OH^- added because strong acids, like HCl, and strong bases, like NaOH, completely dissociate into their ions. H^+_{added} and OH^-_{added} can be calculated from the volume of HCl and NaOH added using equations (5.4) and (5.5) respectively, where again V is the volume.

$$H^+_{added} = V_{HCl_{added}} \times [HCl] \tag{5.4}$$

$$OH^-_{added} = V_{NaOH_{added}} \times [NaOH] \tag{5.5}$$

Figure 5.1 shows the relationship between measured pH and actual pH, or pH_c.

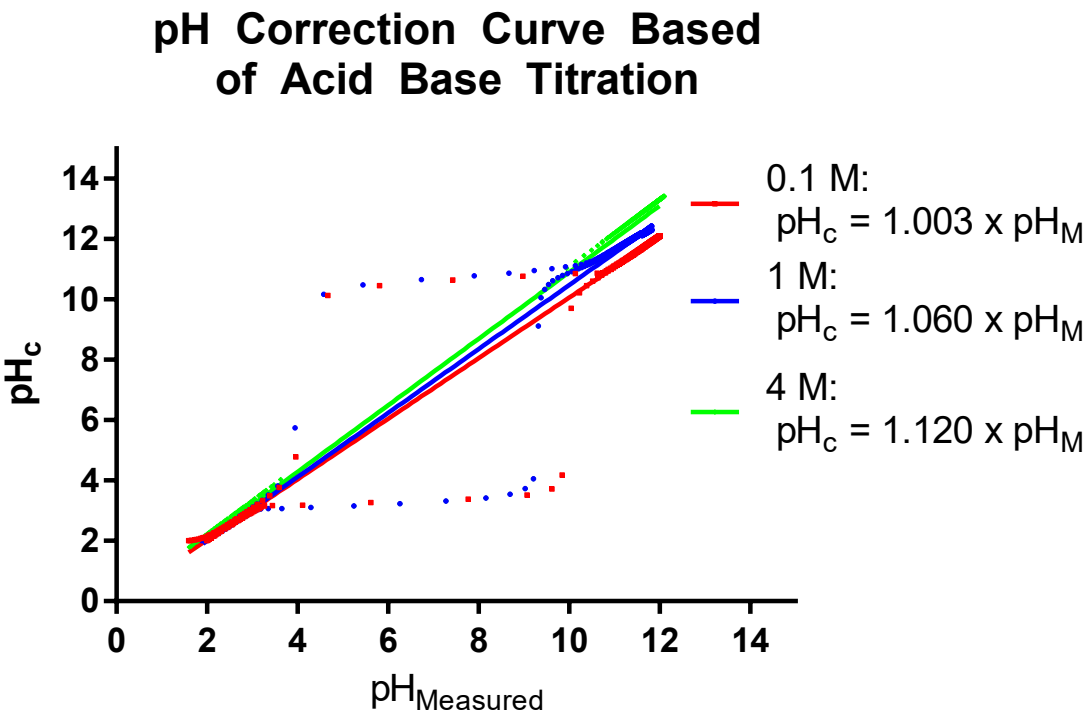

Figure 5.1: Acid base titration curves for I of 0.1 M, 1 M and 4 M.

The line of best fit in Figure 5.1 was calculated using a linear regression and the equation of the line of best fit is shown in the legend. The y-intercepts were omitted

because they were negligible. The line of best fit is the relationship between measured pH and pH_c and can be used to calculate pH_c from measured pH. The equations are summarized in Table 5.2.

Table 5.2: pH adjustment equations for 0.1 M, 1 M and 4 M I solutions.

Ionic Strength	**Adjustment Equation**
0.1 M	$pH_c = 1.003 \times pH_{measured}$
1 M	$pH_c = 1.060 \times pH_{measured}$
4 M	$pH_c = 1.012 \times pH_{measured}$

5.3 Palladium Solubility and Stability

Figure 5.2(a) shows the results of the solubility and stability experiment. Concentration of Pd in solution was plotted against time after Pd was introduced into solution. The concentration of Pd in solution reaches equilibrium after 5 days for all three I solutions. The concentration of Pd in solution should be 1×10^{-4} M, however none of the solutions reached this concentration, meaning that the concentration of Pd solutions is above the solubility limit. The solubility limit for Pd at 0.1 M ranged from 1.9×10^{-5} M to 3.3×10^{-5}, at 1 M it ranged from 6.6×10^{-6} M to 1.5×10^{-5} M and at at 4 M it ranged from 3.8×10^{-5} M to 5.9×10^{-5} M. These results are summarized in Table 5.3. The pH_c of solution ranged between 5.0 and 5.2 in 0.1 M solution, 5.3 and 5.5 in 1 M solution and 5.8 and 6 in 4 M solution. The Eh values were not measured.

Table 5.3: Solubility of Pd in solution for solutions with I of 0.1 M, 1 M and 4 M.

Ionic Strength	**Solubility Limit**
0.1 M	1.9×10^{-6} M − 3.3×10^{-6} M
1 M	6.6×10^{-6} M − 1.5×10^{-5} M
4 M	3.8×10^{-5} M − 5.9×10^{-5} M

5.4 Sorption Kinetics

Figures 5.2(b) to 5.2(d) show the results of the sorption kinetics experiments for betonite, shale and illite respectively. K_d values are plotted against sorption time; the amount of time the solid is in contact with solution before being separated by centrifuge. For all solids, the value of K_d increases quickly over the first 2 days. Between 2 days and 7 days the K_d value continues to increase slowly. After 7 days the value of K_d is no longer increasing. Therefore for the solids bentonite, shale and illite, it takes 7 days to reach sorption equilibrium. For sorption onto bentonite if we consider the K_d values from the region of 7 days to 14 days, the value of K_d ranges between 0.66 m^3/kg and 0.69 m^3/kg in 0.1 M I solutions, between 0.40 m^3/kg and 0.41 m^3/kg in 1 M I solutions and between 0.07 m^3/kg and 0.08 m^3/kg in 4 M I solutions. Similarly for shale it the value of K_d ranges between 8.65 m^3/kg and 9.86 m^3/kg in 0.1 M I solutions, between 6.43 m^3/kg and 7.59 m^3/kg in 1 M I solutions and between 0.96 m^3/kg and 1.11 m^3/kg in 4 M I solutions. Lastly for illite the value of K_d ranges between 0.88 m^3/kg and 1.07 m^3/kg in 0.1 M I solutions, between 0.69 m^3/kg and 0.83 m^3/kg in 1 M I solutions and between 0.1 m^3/kg and 0.11 m^3/kg in 4 M I solutions. The pH_c of solution ranged between 5.8 and 6.6 for bentonite, 6.3 and 7.4 for shale and 5.3 and 5.6 for illite. The Eh values were not measured.

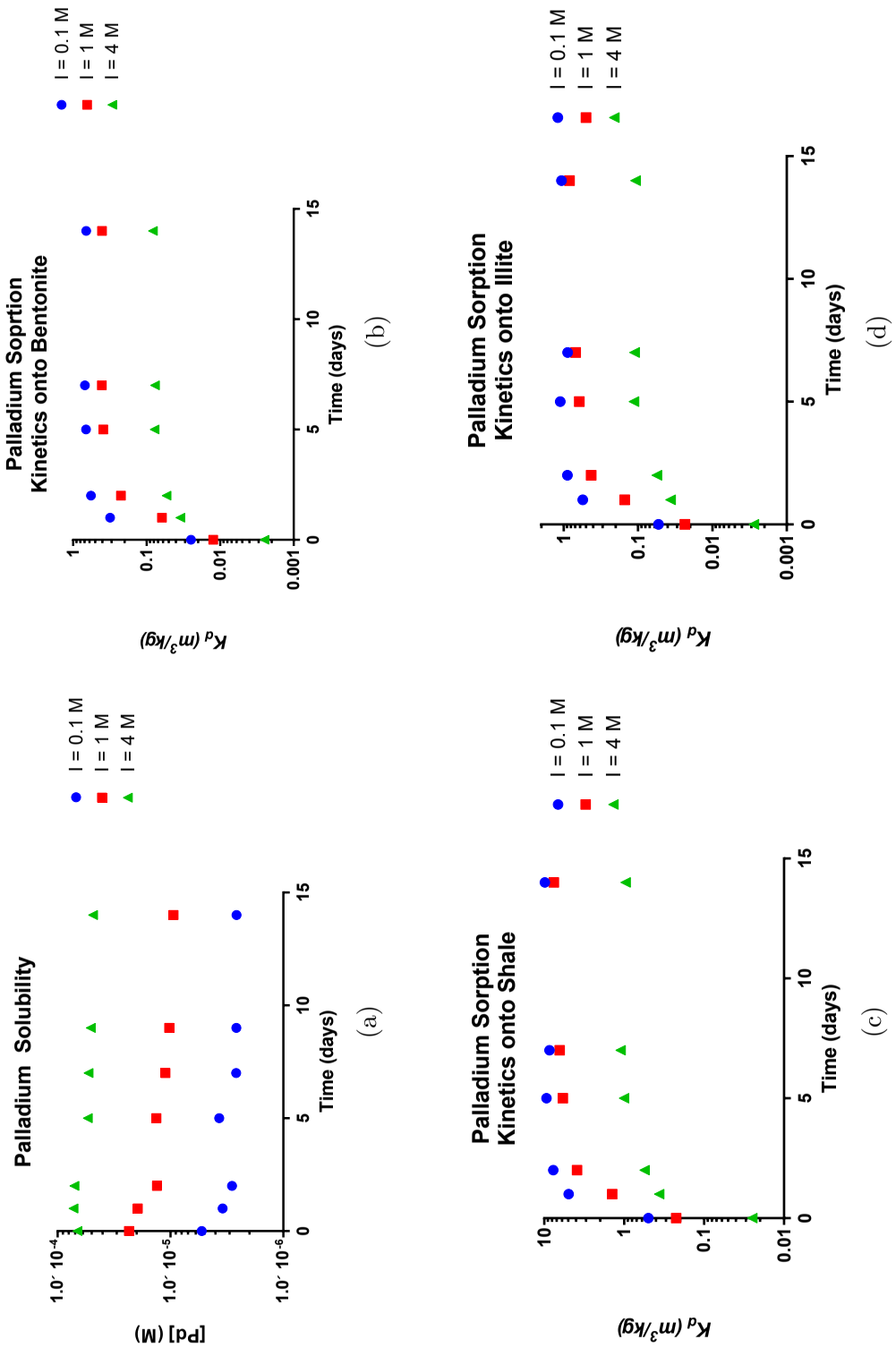

Figure 5.2: Subfigure (a): dissolution kinetics of Pd, Pd reaches a stable concentration after 5 days. Subfigures (b) to (d): sorption kinetics of Pd onto bentonite, shale and illite respectively. For all solids, sorption equilibrium has been reached after 7 days.

5.5 Sorption Experiments

5.5.1 Ionic Strength Dependence of K_d

Figure 5.3 shows the results of the I dependence of K_d experiment. Values of log K_d are plotted against solution ionic strength for sorption of Pd onto bentonite, shale and illite. K_d, pH_c and Eh data for the sorption experiment is summarized in Table 5.4, Eh values are reported versus SHE.

Table 5.4: Recorded data for I dependence sorption experiment.

I (M)	Solid	pH_c	Eh (mV)	K_d (m^3/kg)
0.1	Bentonite	6.83 – 6.91	501 – 506	0.99 – 1.61
0.5	Bentonite	6.55 – 6.65	473 – 506	0.50 – 0.59
1	Bentonite	6.28 – 6.48	484 – 508	0.27 – 0.38
2	Bentonite	6.18 – 6.33	497 – 514	0.17 – 0.20
3	Bentonite	6.06 – 6.31	503 – 513	0.02 – 0.08
4	Bentonite	6.01 – 6.07	513 – 519	0.03 – 0.07
0.1	Shale	7.44 – 7.72	481 – 498	3.90 – 4.42
0.5	Shale	7.20 – 7.36	465 – 476	1.92 – 3.60
1	Shale	7.07 – 7.19	467 – 470	3.02 – 3.89
2	Shale	6.84 – 6.92	485 – 493	1.40 – 1.83
3	Shale	6.71 – 6.74	498 – 501	0.68 – 0.83
4	Shale	6.49 – 6.54	505 – 519	1.29 – 3.11
0.1	Illite	5.34 – 5.83	528 – 542	0.33 – 0.60
0.5	Illite	5.38 – 5.44	550 – 555	0.50 – 0.67
1	Illite	5.40 – 5.50	536 – 546	0.63 – 0.66
2	Illite	5.52 – 5.77	519 – 527	0.32 – 0.35
3	Illite	5.65 – 5.79	517 – 530	0.02 – 0.27
4	Illite	5.53 – 5.73	541 – 545	0.01 – 0.38

For sorption onto bentonite, K_d decreases continuously with increasing I until 3 M. Between 3 M and 4 M K_d becomes constant. Sorption onto shale and illite shows

a slightly different trend, between 0.1 M and 1 M K_d is approximately constant. In the region between 1 M and 3 M K_d decreases with increasing I, and in the region between 3 M and 4 M K_d becomes constant again.

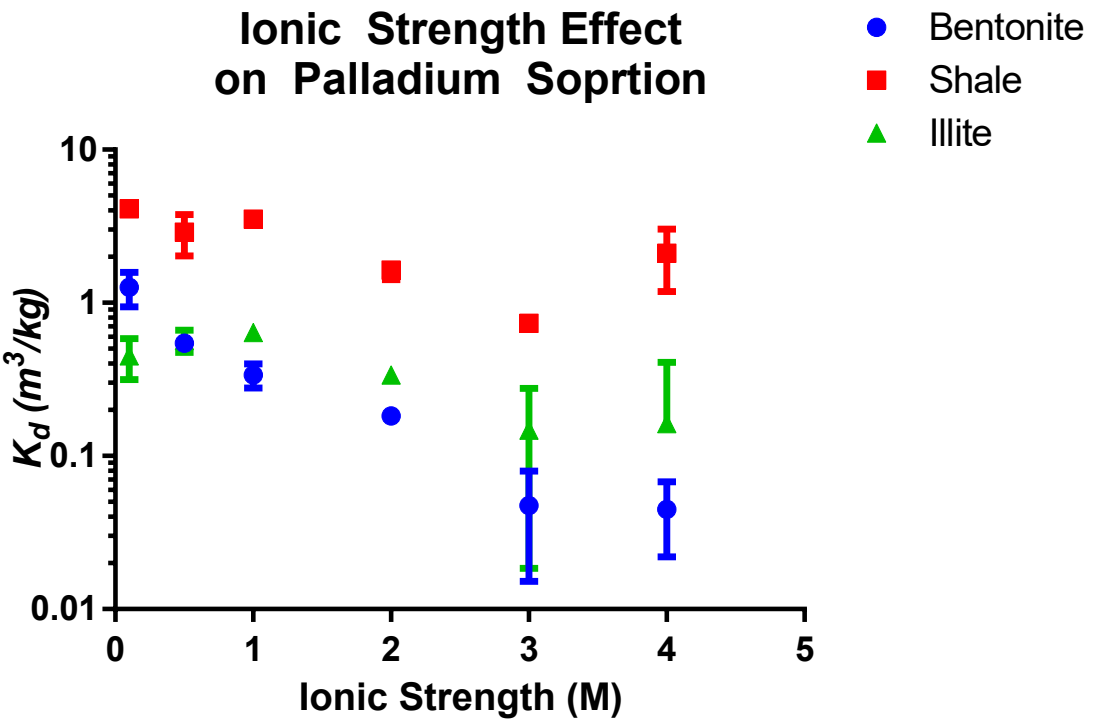

Figure 5.3: Ionic strength dependence of K_d for sorption of Pd onto bentonite, shale and illite.

5.5.2 pH Dependence of K_d

Figures 5.4, 5.5(a) and 5.5(b) show the results of the pH dependence of K_d experiments for the sorption of Pd onto bentonite, shale and illite respectively. The values of K_d are summarized in Table 5.5. Recorded Eh data for the pH dependence sorption experiment is shown in Table 5.6, Eh values are reported versus SHE.

For all solids in 0.1 M I solution we find that K_d decreases with increasing pH. In 1 M and 4 M solutions the relationship is more complicated. For bentonite in 1 M solution, K_d has a local minimum at pH_c 7. Conversely, for bentonite in 4 M solution we find an increase in K_d with increasing pH. For shale in 1 M and 4 M solutions K_d appears to peak around pH_c 7. For illite in 1 M solution, K_d has a local minimum at pH_c 8 and in 4 M solutions it has two peaks, the first around pH_c 6 and the second, smaller, peak around pH_c 8.

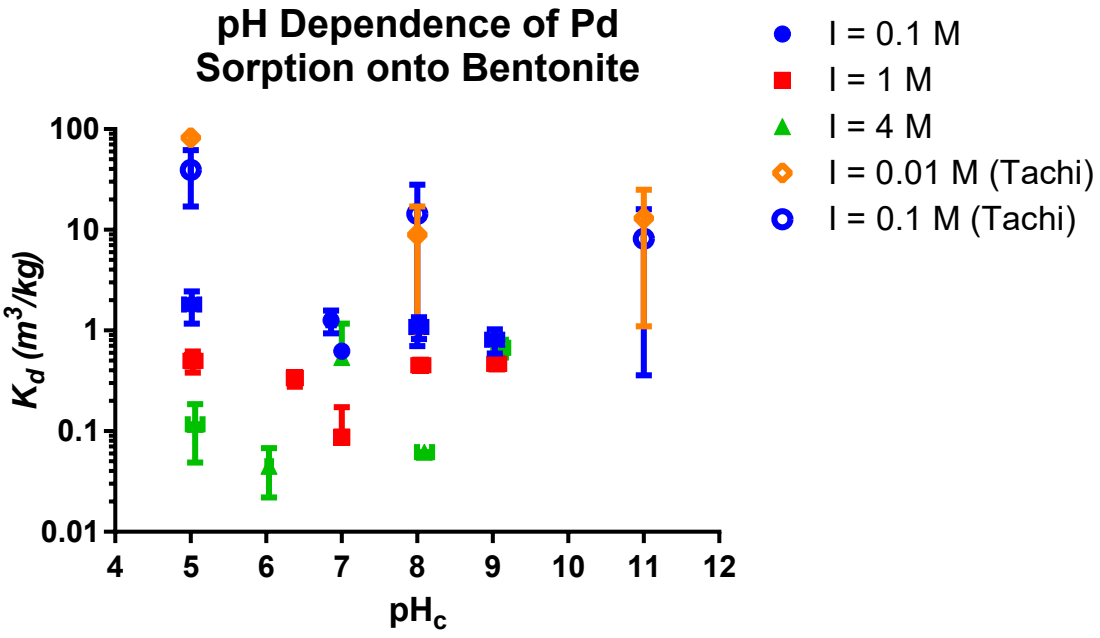

Figure 5.4: pH Dependence of K_d for sorption of Pd onto bentonite. Error bars for data taken from Tachi *et al.* (1999) represent the range of values reported, not the error.

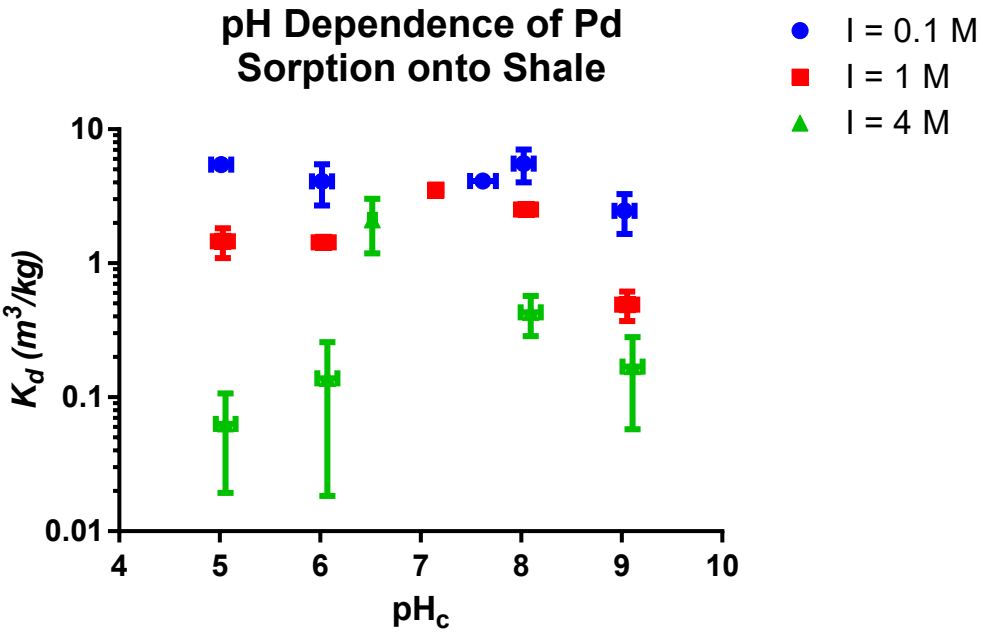

(a)

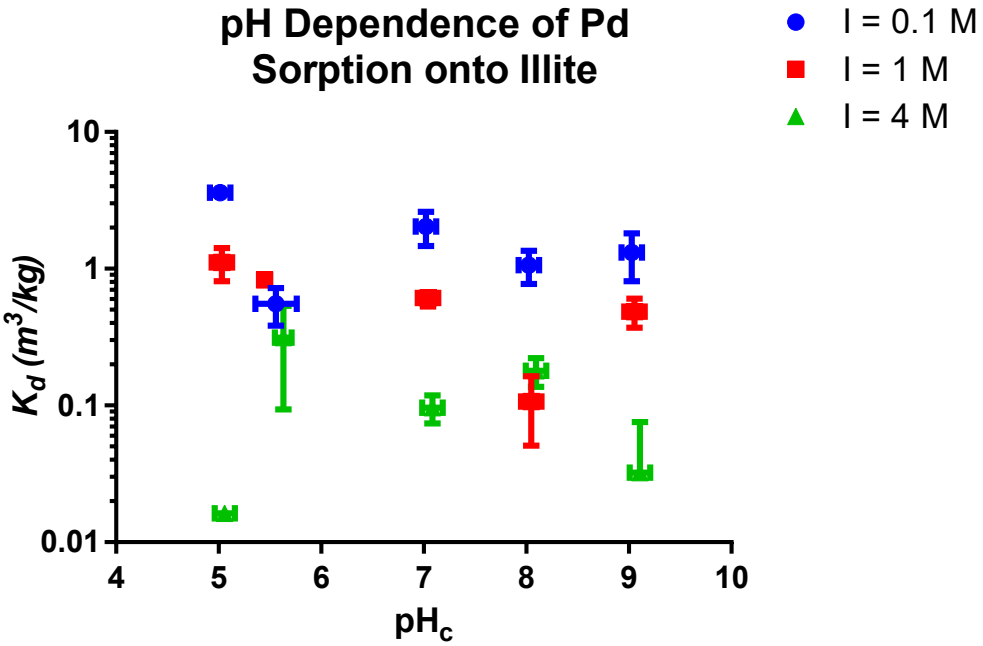

(b)

Figure 5.5: pH Dependence of K_d for sorption of Pd onto (a) shale and (b) illite.

Table 5.5: Recorded K_d data from pH dependence sorption experiment.

I **(M)**	$\mathbf{pH}_c$	K_d **(Bentonite)** $(\mathbf{m^3/kg})$	K_d **(Shale)** $(\mathbf{m^3/kg})$	K_d **(Illite)** $(\mathbf{m^3/kg})$
0.1	5	1.24 – 2.50	5.16 – 5.64	3.40 – 3.73
0.1	6	0.99 – 1.61	3.14 – 5.70	0.41 – 0.74
0.1	7	0.57 – 0.67	3.90 – 4.42	1.60 – 2.68
0.1	8	0.83 – 1.36	4.48 – 7.39	0.73 – 1.24
0.1	9	0.68 – 1.06	1.72 – 3.34	0.87 – 1.86
1	5	0.39 – 0.63	1.15 – 1.87	0.86 – 1.45
1	6	0.27 – 0.38	1.32 – 1.50	0.82 – 0.84
1	7	0.02 – 0.18	3.02 – 3.89	0.52 – 0.68
1	8	0.41 – 0.51	2.34 – 2.64	0.07 – 0.17
1	9	0.42 – 0.54	0.42 – 0.63	0.38 – 0.61
4	5	0.07 – 0.20	0.01 – 0.09	0.01 – 0.02
4	6	0.03 – 0.07	0.05 – 0.27	0.08 – 0.53
4	7	0.06 – 1.25	1.29 – 3.11	0.08 – 0.12
4	8	0.05 – 0.06	0.28 – 0.57	0.13 – 0.21
4	9	0.53 – 0.80	0.04 – 0.25	0.01 – 0.08

Table 5.6: Recorded Eh data from pH dependence sorption experiment.

I **(M)**	$\mathbf{pH}_c$	**Eh (Bentonite)** **(mV)**	**Eh (Shale)** **(mV)**	**Eh (Illite)** **(mV)**
0.1	5	472 – 509	499 – 402	547 – 563
0.1	6	501 – 506	452 – 460	538 – 542
0.1	7	374 – 419	481 – 498	440 – 457
0.1	8	405 – 415	408 – 413	381 – 309
0.1	9	375 – 403	348 – 360	359 – 391
1	5	471 – 491	459 – 473	400 – 435
1	6	484 – 508	431 – 445	536 – 546
1	7	355 – 383	467 – 470	452 – 456
1	8	361 – 363	368 – 380	375 – 382
1	9	365 – 379	350 – 356	361 – 375
4	5	433 – 441	404 – 422	492 – 501
4	6	513 – 519	417 – 427	541 – 545
4	7	353 – 376	405 – 514	436 – 443
4	8	320 – 323	341 – 375	367 – 370
4	9	347 – 357	342 – 373	353 – 361

5.5.3 Sorption Isotherms

Figures 5.6, 5.7(a) and 5.7(b) show the results of the sorption isotherms experiments for the sorption of Pd onto bentonite, shale and illite respectively. The values of K_d are summarized in Table 5.7. Recorded Eh data and pH data are summarized in Tables 5.8 and 5.9 respectively, where Eh values are reported versus SHE.

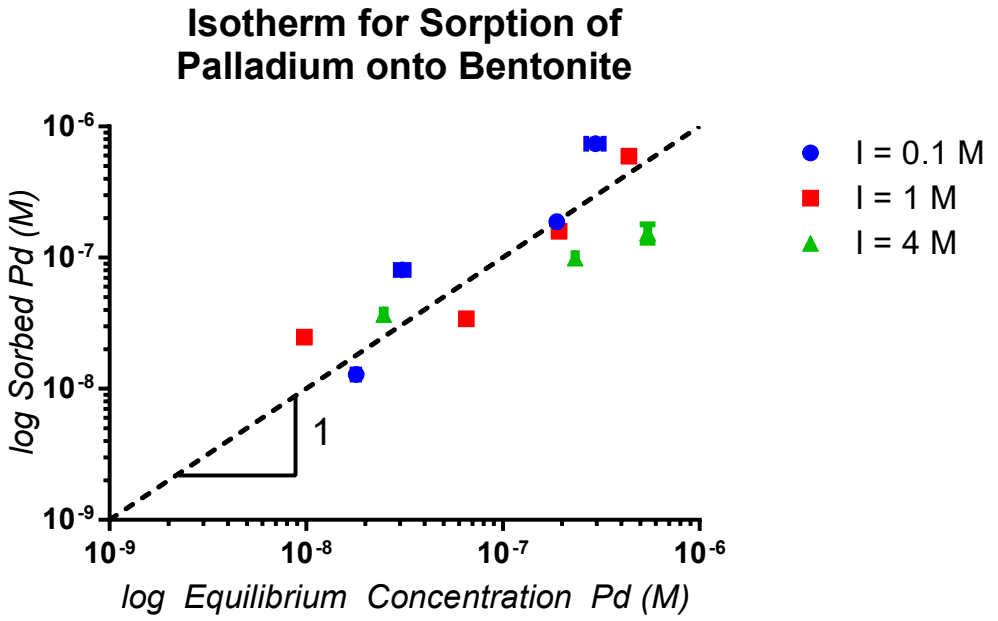

Figure 5.6: Sorption isotherms for Pd sorption onto bentonite.

The sorption isotherm for Pd sorption onto bentonite has a slope of 1. Similarly, the sorption isotherm for Pd sorption onto illite also has a slope of 1. However for the sorption of Pd onto shale, the slope of the isotherm is dependent on ionic strength. For sorption in 0.1 M solutions the slope is 1.3, for sorption in 1 M solutions the slope is 0.85 and for sorption in 4 M solutions the slope is 0.33.

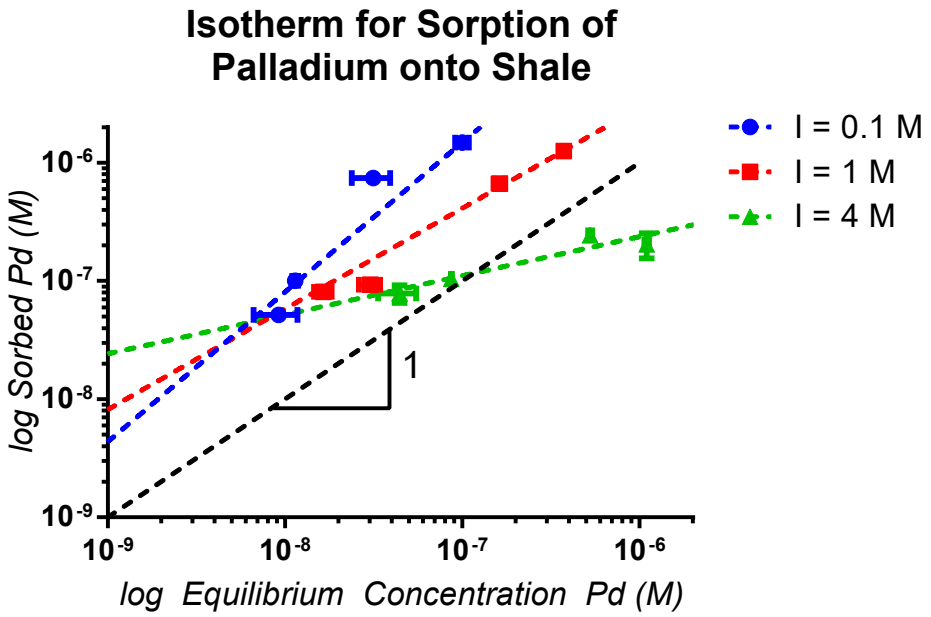

(a)

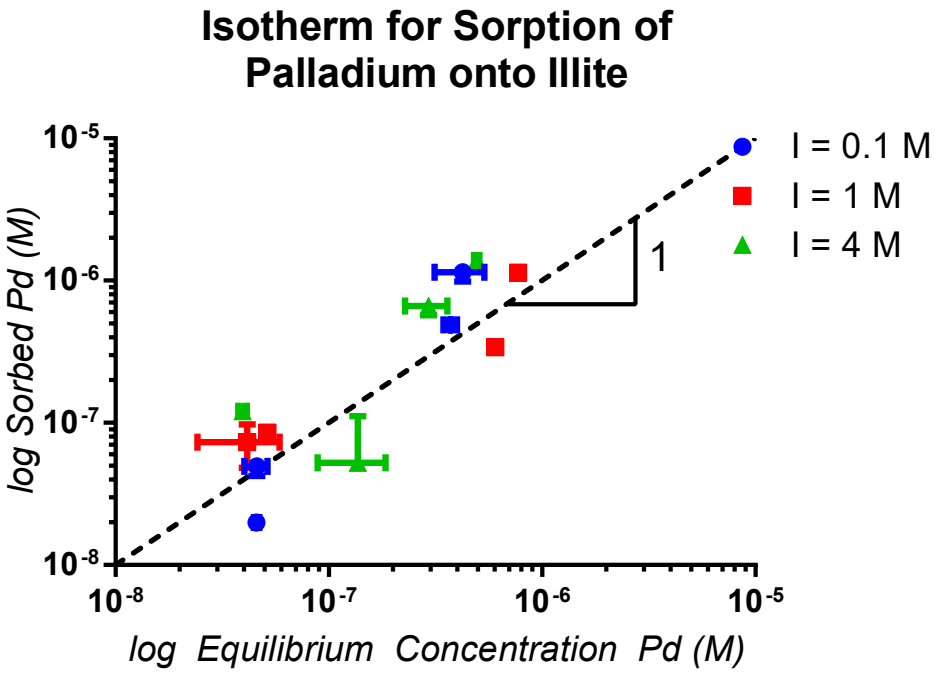

(b)

Figure 5.7: Sorption isotherms for Pd sorption onto (a) shale and (b) illite.

Table 5.7: Recorded Pd concentrations from Pd sorption isotherm experiment.

I (M)	$[Pd]_i$ (M)	$[Pd]_f$ (Bentonite) (M)	$[Pd]_f$ (Shale) (M)	$[Pd]_f$ (Illite) (M)
0.1	5×10^{-8}	1.2×10^{-8}–1.3×10^{-8}	5.4×10^{-8}–4.9×10^{-8}	1.8×10^{-8}–2.1×10^{-8}
0.1	5×10^{-7}	1.9×10^{-7}–1.9×10^{-7}	7.3×10^{-7}–7.5×10^{-7}	5.1×10^{-7}–4.6×10^{-7}
0.1	1×10^{-6}	7.1×10^{-7}–7.7×10^{-7}	1.5×10^{-6}–1.5×10^{-6}	1.0×10^{-6}–1.2×10^{-6}
1	5×10^{-8}	2.3×10^{-8}–2.6×10^{-8}	8.9×10^{-8}–9.7×10^{-8}	9.0×10^{-8}–5.6×10^{-8}
1	5×10^{-7}	1.5×10^{-7}–1.6×10^{-7}	6.6×10^{-7}–6.8×10^{-7}	3.6×10^{-7}–3.2×10^{-7}
1	1×10^{-6}	5.9×10^{-7}–6.0×10^{-7}	1.2×10^{-6}–1.2×10^{-6}	1.1×10^{-6}–1.1×10^{-6}
4	5×10^{-8}	3.5×10^{-8}–3.9×10^{-8}	1.0×10^{-7}–1.0×10^{-7}	1.2×10^{-7}–1.2×10^{-7}
4	5×10^{-7}	9.5×10^{-8}–1.0×10^{-7}	2.6×10^{-7}–2.3×10^{-7}	6.0×10^{-7}–7.3×10^{-7}
4	1×10^{-6}	1.7×10^{-7}–1.4×10^{-7}	1.7×10^{-7}–2.4×10^{-7}	1.4×10^{-6}–1.4×10^{-6}

Table 5.8: Recorded Eh data from Pd sorption isotherm experiment.

I (M)	$[Pd]_i$ (M)	Eh (Bentonite) (mV)	Eh (Shale) (mV)	Eh (Illite) (mV)
0.1	5×10^{-8}	363 – 365	429 – 447	477 – 485
0.1	5×10^{-7}	361 – 385	420 – 421	482 – 489
0.1	1×10^{-6}	372 – 375	424 – 427	543 – 546
1	5×10^{-8}	459 – 472	425 – 430	501 – 518
1	5×10^{-7}	472 – 484	434 – 452	519 – 526
1	1×10^{-6}	475 – 488	445 – 494	540 – 554
4	5×10^{-8}	454 – 461	452 – 458	493 – 500
4	5×10^{-7}	475 – 476	451 – 454	523 – 526
4	1×10^{-6}	502 – 504	456 – 461	546 – 551

Table 5.9: Recorded pH data from Pd sorption isotherm experiment.

I (M)	$[Pd]_i$ (M)	pH_c (Bentonite)	pH_c (Shale)	pH_c (Illite)
0.1	5×10^{-8}	9.57 – 9.64	7.64 – 7.70	5.85 – 6.00
0.1	5×10^{-7}	8.81 – 9.38	7.66 – 7.69	5.45 – 5.54
0.1	1×10^{-6}	9.04 – 9.10	7.60 – 7.65	4.63 – 4.65
1	5×10^{-8}	6.20 – 6.28	7.11 – 7.12	5.53 – 5.54
1	5×10^{-7}	5.97 – 5.99	7.08 – 7.11	4.85 – 5.04
1	1×10^{-6}	5.96 – 5.98	7.06 – 7.07	4.45 – 4.59
4	5×10^{-8}	5.96 – 5.98	6.46 – 6.47	5.37 – 5.58
4	5×10^{-7}	5.46 – 5.65	6.49 – 6.50	4.72 – 4.93
4	1×10^{-6}	4.89 – 5.12	6.51 – 6.52	4.13 – 4.32

5.6 PHREEQC Models

5.6.1 Speciation Models

Surface Site Speciation

Figure 5.8(a) shows the results of modeling the surface site speciation of montmorillonite and illite in PHREEQC with the protonation and deprotonation constants listed in Table 4.5. The speciation of surface sites on both solids is strongly dependent on pH. The dependence on both solids with regard to pH shows the same trends, however they are slightly out of phase. That is, the transition between surface species occurs at lower pH values for montmorillonite then it does for illite. The positive surface site ($S-OH_2^+$) is dominant in the low pH range, the neutral surface site ($S-OH$) is dominant in the intermediate pH range and the negative surface site ($S-O^-$) is dominant in the high pH range. The transition point between $S-OH_2^+$ dominance and $S-OH$ dominance occurs at pH 4 for montmorillonite and pH 4.5 for illite. The transition point between $S-OH$ dominance and $S-O^-$ dominance occurs at pH 6 for montmorillonite and pH 8 for illite.

Aqueous Speciation of Palladium

Figures 5.8(b) to 5.8(d) shows the results of modeling the aqueous speciation of Pd in Na-Ca-Cl solutions with PHREEQC. The thermodynamic data used is listed in Table 4.2. The speciation of Pd in Na-Ca-Cl solutions was strongly dependent on both pH and I. $PdCl_4^{2-}$ is the dominant species in the low pH range, $Pd(OH)_2$ is dominant species in the intermediate pH range and $Pd(OH)_3^-$ is the dominant species in the high pH range. In 0.1 M solution the transition point between $PdCl_4^{2-}$ dominance

and $Pd(OH)_2$ dominance occurs at pH 6 and the transition point between $Pd(OH)_2$ dominance and $Pd(OH)_3^-$ dominance occurs at pH 12. As ionic strength increases the pH value of the transition points changes; the first transition point occurs at higher pH and the second transition point occurs at a slightly lower pH. At 1 M the transition points are at pH 8 and pH 11.7 and at 4 M they are at pH 9.5 and pH 11.5. The size of the region where $PdCl_4^{2-}$ is dominant greatly increases as I increases. Conversely, the size of the region where $Pd(OH)_2$ is dominant greatly decreases as I increases. As I increases the % abundance of $PdCl_3OH^{2-}$ in solution slightly increases. It appears at the transition point between $Pd(OH)_2$ dominance and $Pd(OH)_3^-$ dominance and at 4 M there is a point where all there species are present in almost equal proportions.

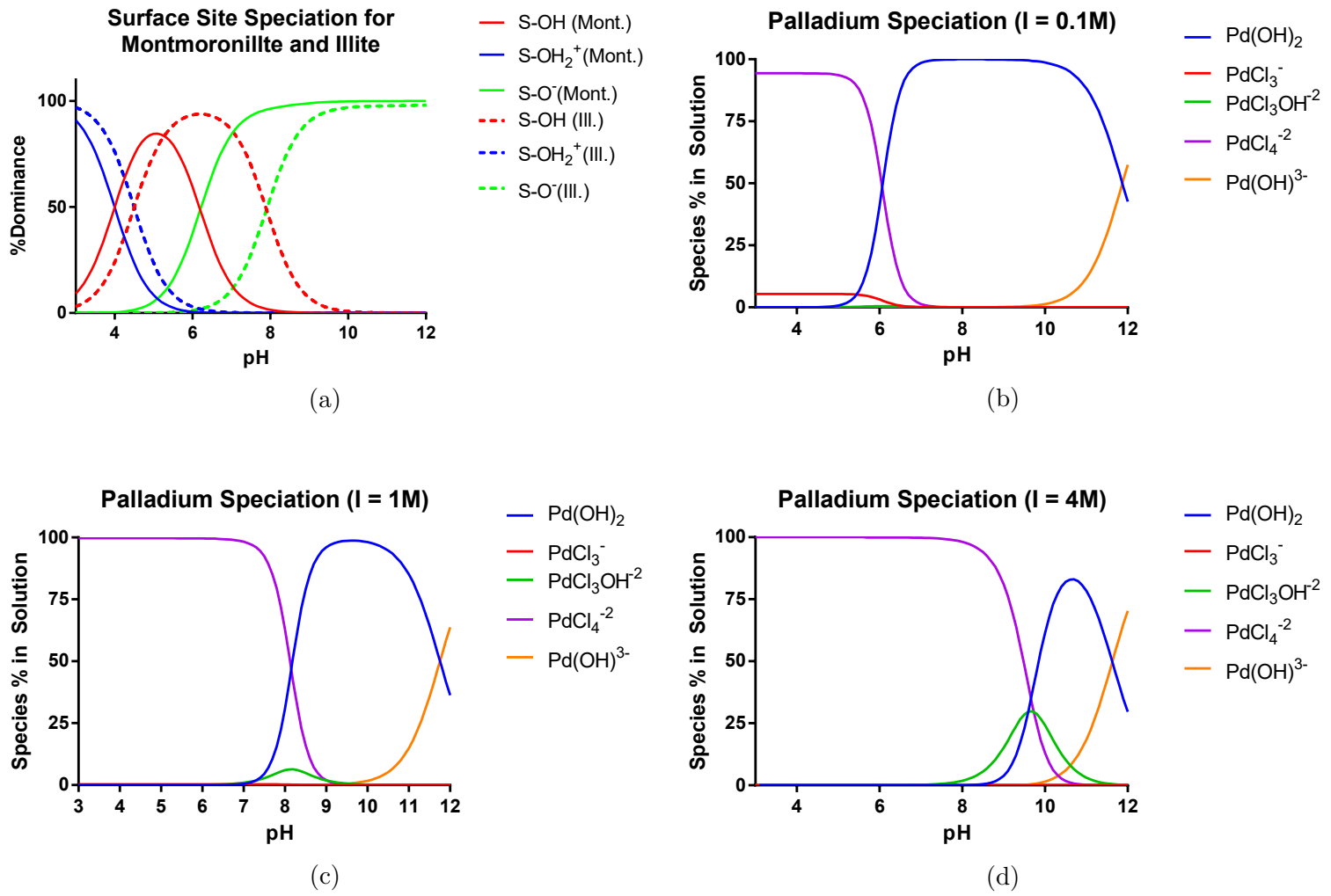

Figure 5.8: Subfigure (a): surface site speciation for montmorillonite and illite. The surface site speciation is independent of ionic strength. Subfigures (b) to (d): aqueous speciation of Pd in 0.1 M, 1 M and 4 M solutions respectively.

5.6.2 Surface Complexation Modeling

Figure 5.9 shows the results of the surface complexation modeling when Bradbury and Baeyens recommended surface complexation reactions were used. The surface complexation constants were calculated using Bradbury and Beayens correlation; (4.2) for sorption onto montmorillonite and (4.3) for sorption onto illite. The median value of the calculated surface complexation constants was applied to the model, see Table 4.5.

Figure 5.10 shows the results of the surface complexation modeling after the first modifications to the model have been made. Bradbury and Baeyens recommended surface complexation reactions were still used and the surface complexation constants were still calculated using Bradbury and Beayens correlation. However, the value of the surface complexation constant was varied within error to improve the fit to the experimental data. The minimum value of the surface complexation reaction constant was used for $S-OPd(OH)$, 4.59 and 4.53 for montmoronillite and illite respectively, and the value of the surface complexation reaction constant used for $S-OPd(OH)_2^-$ were -5.22 and -5.66 for montmoronillite and illite. The range of values for the surface complexation constants is shown in Table 5.10.

Table 5.10: Range of values for surface complexation reaction constants due to error associated with Bradbury and Beayens correlation.

Surface Complexation Reaction	$\log K_{Mont.}$	$\log K_{Illite}$
$S-OH + Pd^{+2} + 2H_2O \leftrightarrow S-OPdOH + 2H^+$	4.59 to 5.33	4.53 to 5.47
$S-OH + Pd^{+2} + 3H_2O \leftrightarrow S-OPd(OH)_2^- + 3H^+$	-6.44 to -5.22	-5.66 to -4.24

Figure 5.11 shows the results of the surface complexation modeling after adding the ternary surface complex formation of $S-OPdCl_4^{3-}$ to the model. Bradbury and Baeyens recommended surface complexation reactions were used with the surface complexation reaction for the formation of the ternary surface complex $S-OPdCl_4^{3-}$. The minimum value of the surface complexation reaction constant produced by the correlation was used for $S-OPd(OH)$, 4.59 and 4.53 for montmoronillite and illite respectively, and the value of the surface complexation reaction constant used for $S-OPd(OH)_2^-$ were -5.22 and -5.66 for montmoronillite and illite respectively. The value of the formation constant for $PdCl_4^{2-}$, 13.5, from the JAEA TDB , adjusted within error to improve fit, was used as the surface complexation constant for $S-OPdCl_4^{3-}$.

Figure 5.12 shows the results of the final surface complexation model. Bradbury and Beayens recommended surface complexation reactions were used with the ternary surface complex formation reaction for $S-OPdCl_4^{3-}$. The values of the surface complexation reaction constants were varied individually to improve the fit. Reducing the value of the surface complexation reaction constant for $S-OPd(OH)$ reduced the value of K_d for the range of pH where $Pd(OH)_2$ was dominant, *i.e.* pH above 6 for 0.1 M solutions, pH above 8 for 1 M solutions and pH above 10 for 4 M solutions. Increasing the value of the surface complexation reaction constant for $S-OPd(OH)_2^-$ increased the K_d for the region of pH above 10, where $Pd(OH)_3^-$ is dominant. Increasing the value of the surface complexation reaction constant for $S-OPdCl_4^{3-}$ increased K_d in the regions where $PdCl_4^{2-}$ is the dominant species, *i.e.* pH below 6 for 0.1 M solutions, pH below 8 for 1 M solutions and pH below 10 for 4 M solutions. Figure

5.13 is a zoomed in version of Figure 5.12 which shows the fit between model and experiment better. The surface complexation reaction constants which best improved the fit are shown in Table 5.11.

Table 5.11: Values of surface complexation reaction constants used to best improve fit between model and experiment.

Surface Complexation Reaction	$\log K_{Mont.}$	$\log K_{Illite}$
$S{-}OH + Pd^{+2} + 2H_2O \leftrightarrow S{-}OPdOH + 2H^+$	3.0	3.0
$S{-}OH + Pd^{+2} + 3H_2O \leftrightarrow S{-}OPd(OH)_2^- + 3H^+$	-4.0	-5.66
$S{-}OH + Pd^{+2} + 4Cl^- \leftrightarrow S{-}OPdCl_4^{3-}$	13.5	12.5

Figure 5.14 shows the fit if the results from the sorption model are shifted left 2 pH units. Figure 5.15 shows a zoomed in version of Figure 5.14 to give at better view of the fit.

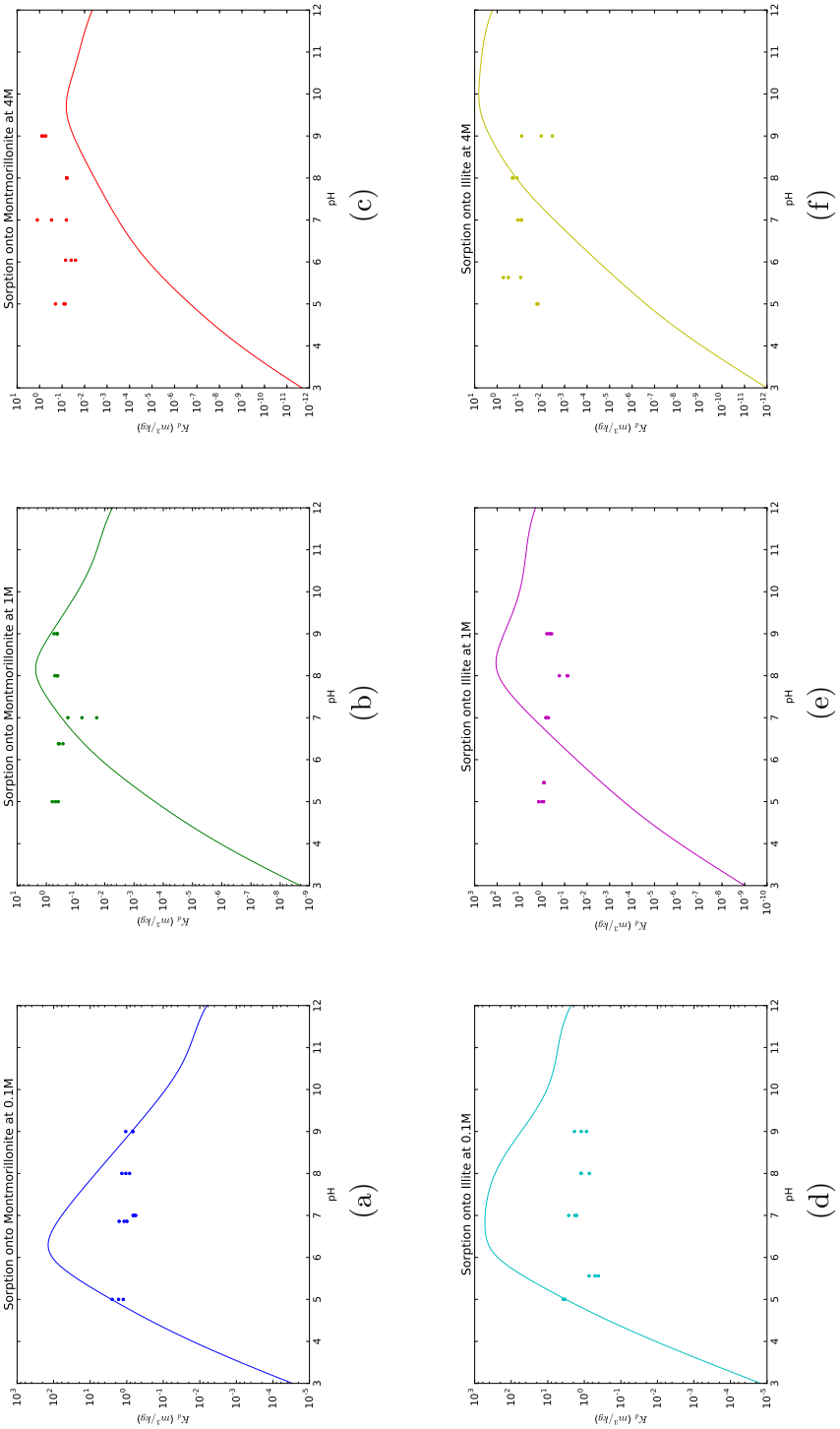

Figure 5.9: Subfigures (a) to (c): surface complexation modeling results for Pd sorption onto montmorillonite at I of 0.1 M, 1 M and 4 M respectively. Subfigures (d) to (f): surface complexation modeling results for Pd sorption onto illite at I of 0.1 M, 1 M and 4 M respectively. Bradbury and Baeyens recommended surface complexation reactions were used. Surface complexation constants were derived using Bradbury and Baeyens correlation

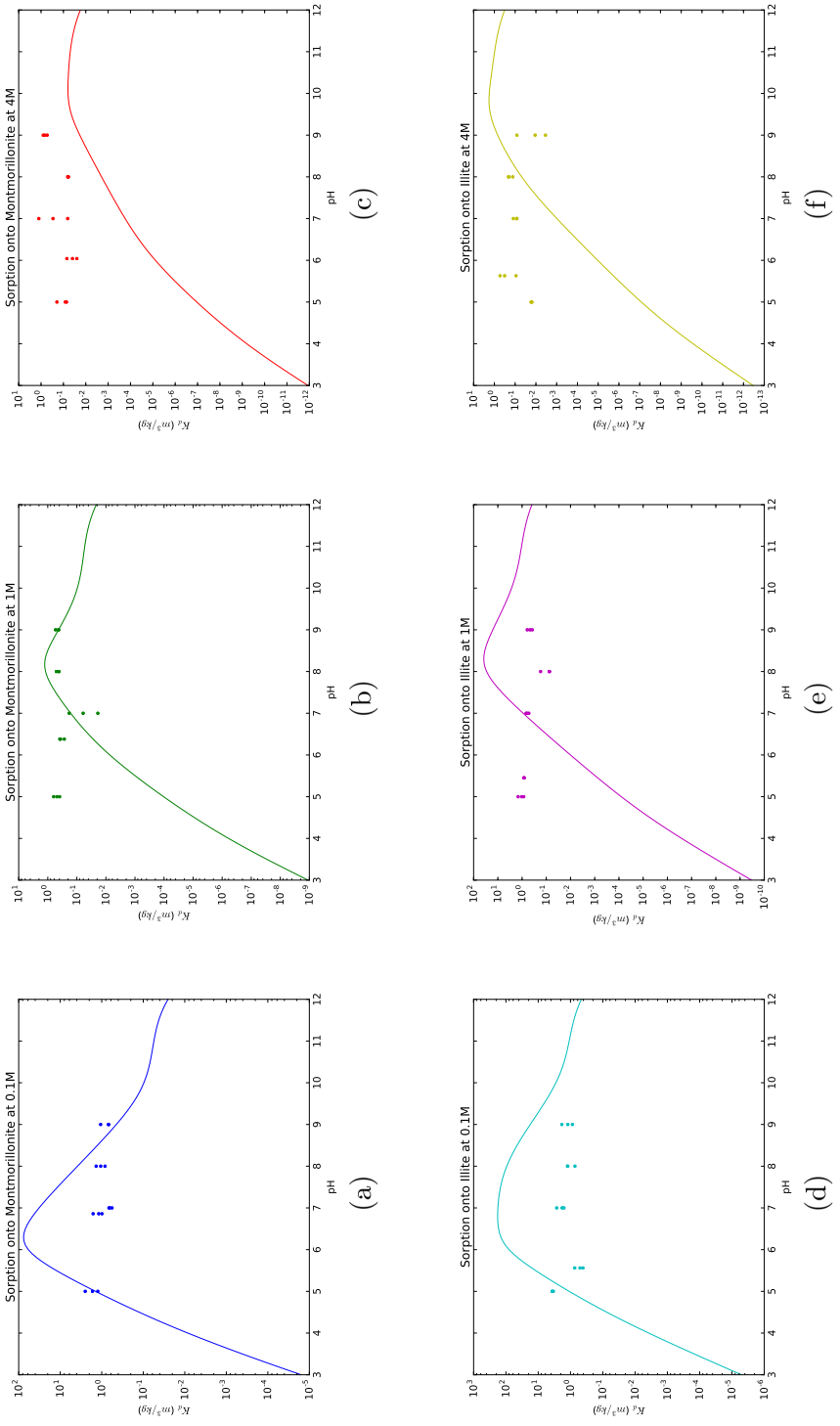

Figure 5.10: Subfigures (a) to (c): surface complexation modeling results for Pd sorption onto montmorillonite at I of 0.1 M, 1 M and 4 M respectively. Subfigures (d) to (f): surface complexation modeling results for Pd sorption onto illite at I of 0.1 M, 1 M and 4 M respectively. Bradbury and Baeyens recommended surface complexation reactions were used. Surface complexation constants were derived using Bradbury and Baeyens but were adjusted within error to imporve fit.

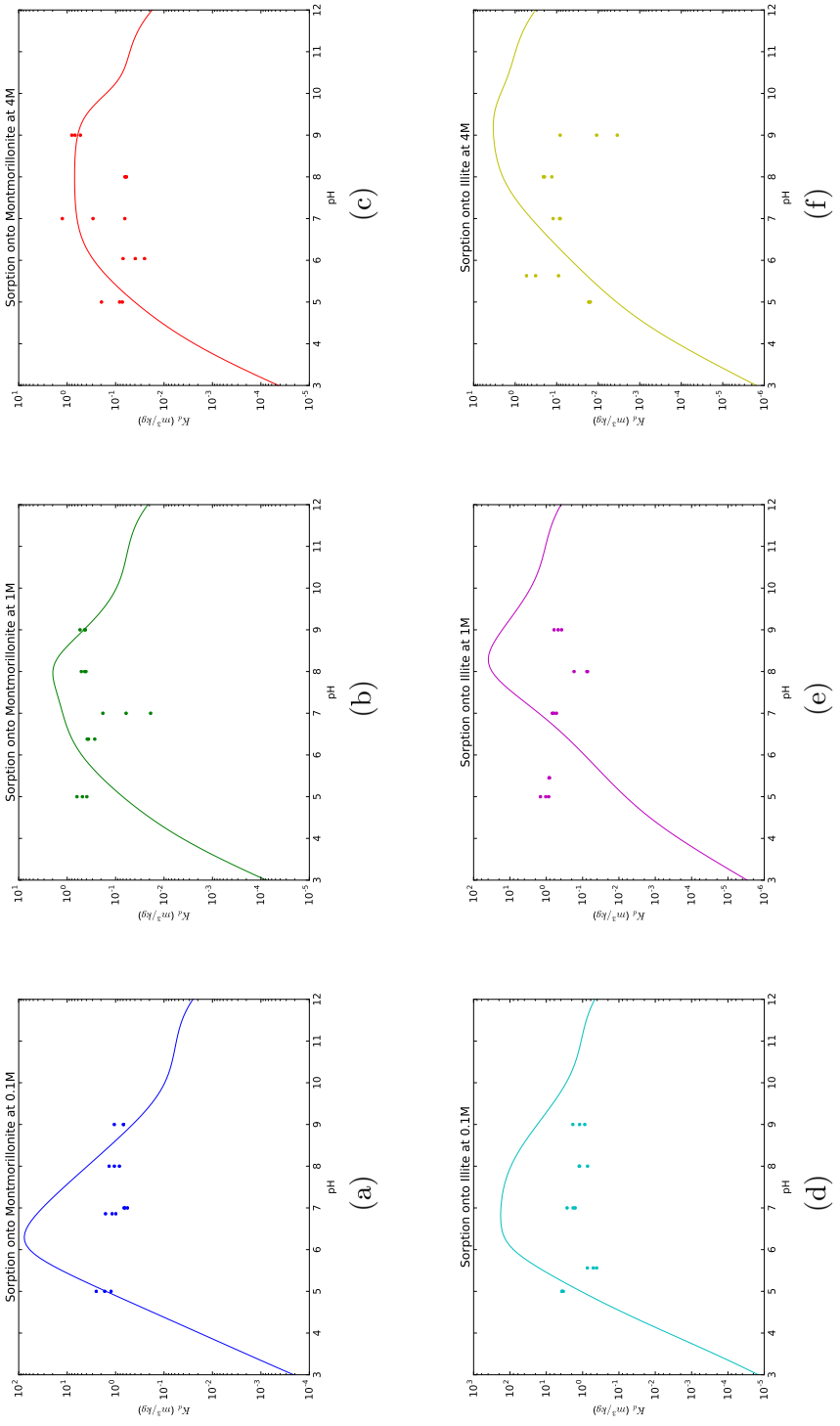

Figure 5.11: Subfigures (a) to (c): surface complexation modeling results for Pd sorption onto montmorillonite at I of 0.1 M, 1 M and 4 M respectively. Subfigures (d) to (f): surface complexation modeling results for Pd sorption onto illite at I of 0.1 M, 1 M and 4 M respectively. Bradbury and Baeyens recommended surface complexation reactions and a ternary surface complex reaction were used. Surface complexation constants were derived using Bradbury and Baeyens correlation, adjusted within error to improve fit, and the Fein correlation.

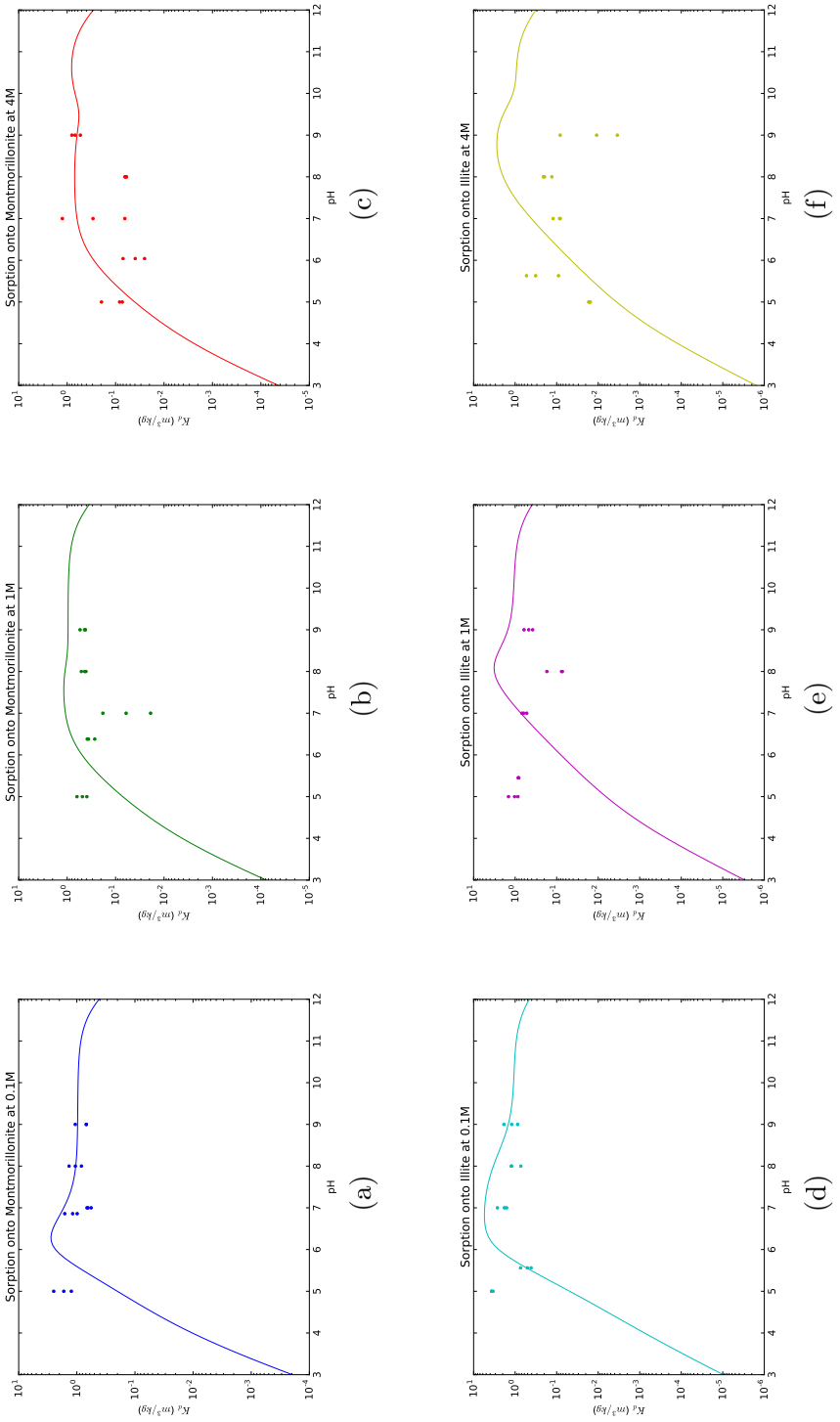

Figure 5.12: Subfigures (a) to (c): surface complexation modeling results for Pd sorption onto montmorillonite at I of 0.1 M, 1 M and 4 M respectively. Subfigures (d) to (f): surface complexation modeling results for Pd sorption onto illite at I of 0.1 M, 1 M and 4 M respectively. Bradbury and Baeyens recommended surface complexation reactions and a ternary surface complex reaction were used. Surface complexation constants were adjusted individually to find the best fit.

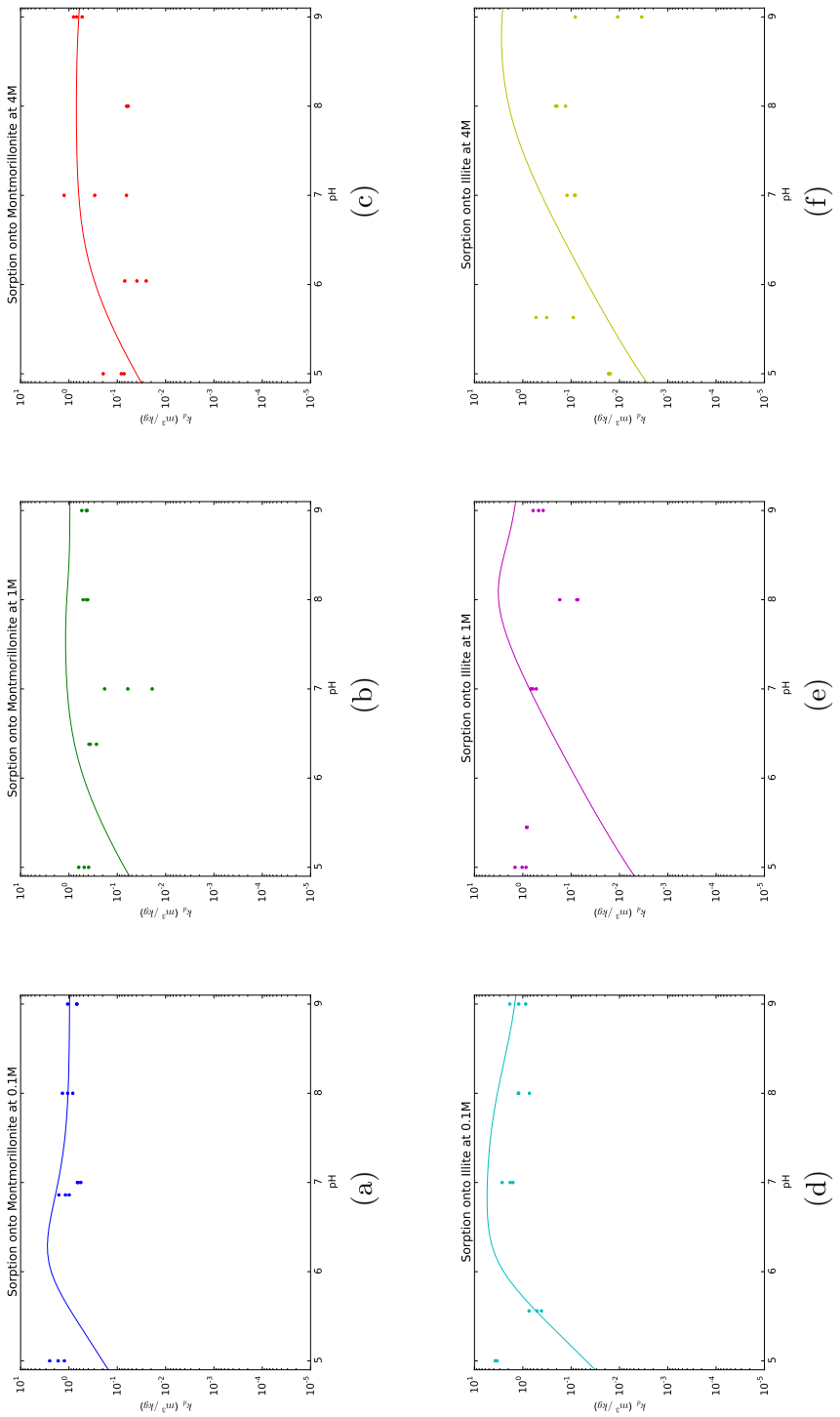

Figure 5.13: Zoomed in version of Figure 5.12. Subfigures (a) to (c): surface complexation modeling results for Pd sorption onto montmorillonite at I of 0.1 M, 1 M and 4 M respectively. Subfigures (d) to (f): surface complexation modeling results for Pd sorption onto illite at I of 0.1 M, 1 M and 4 M respectively. Bradbury and Baeyens recommended surface complexation reactions and a ternary surface complex reaction were used. Surface complexation constants were adjusted individually to find the best fit.

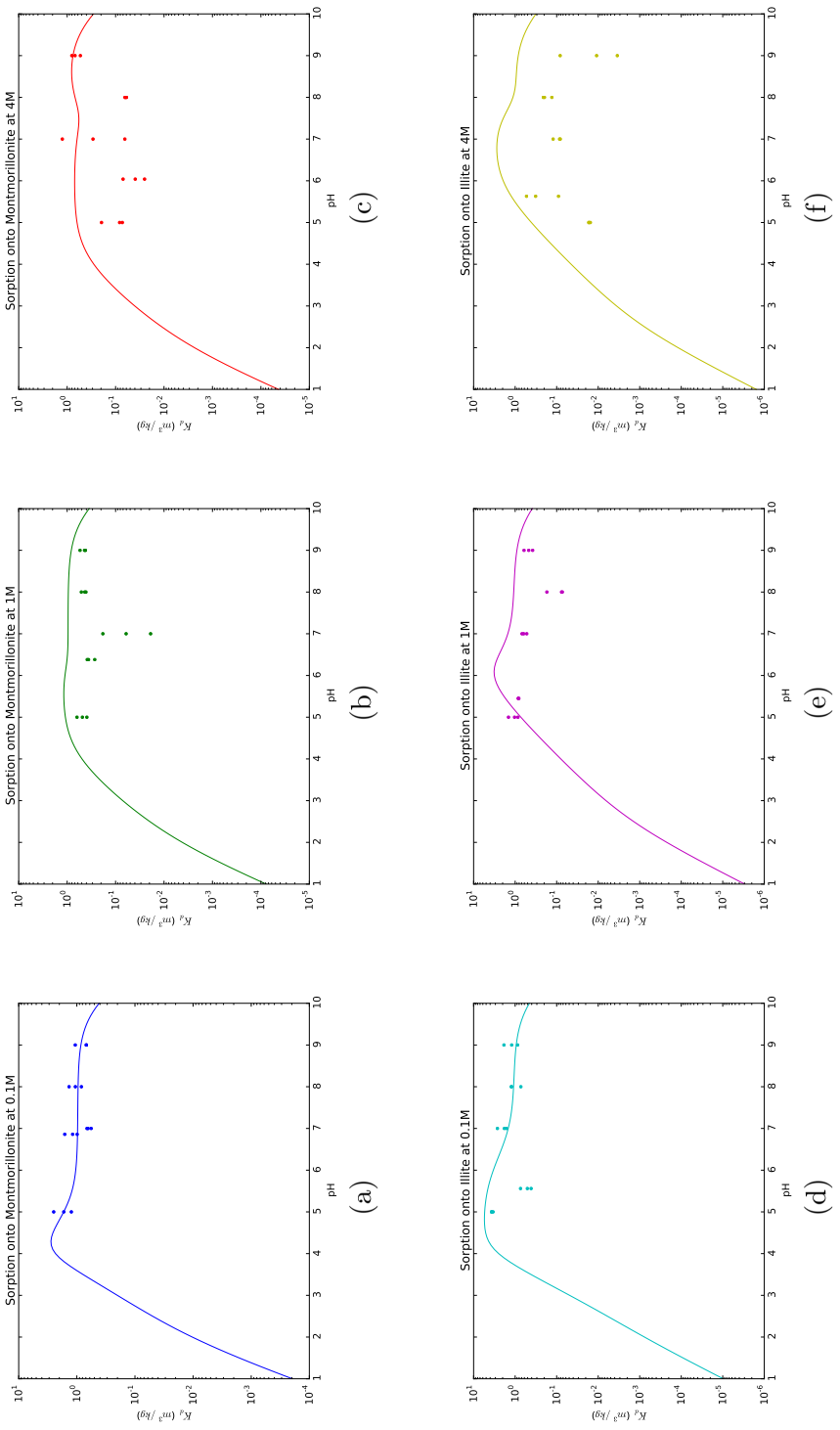

Figure 5.14: Same model as Figure 5.12 but with the model results shifted left by 2 pH units. Subfigures (a) to (c): surface complexation modeling results for Pd sorption onto montmorillonite at I of 0.1 M, 1 M and 4 M respectively. Subfigures (d) to (f): surface complexation modeling results for Pd sorption onto illite at I of 0.1 M, 1 M and 4 M respectively. Bradbury and Baeyens recommended surface complexation reactions and a ternary surface complex reaction were used. Surface complexation constants were adjusted individually to find the best fit.

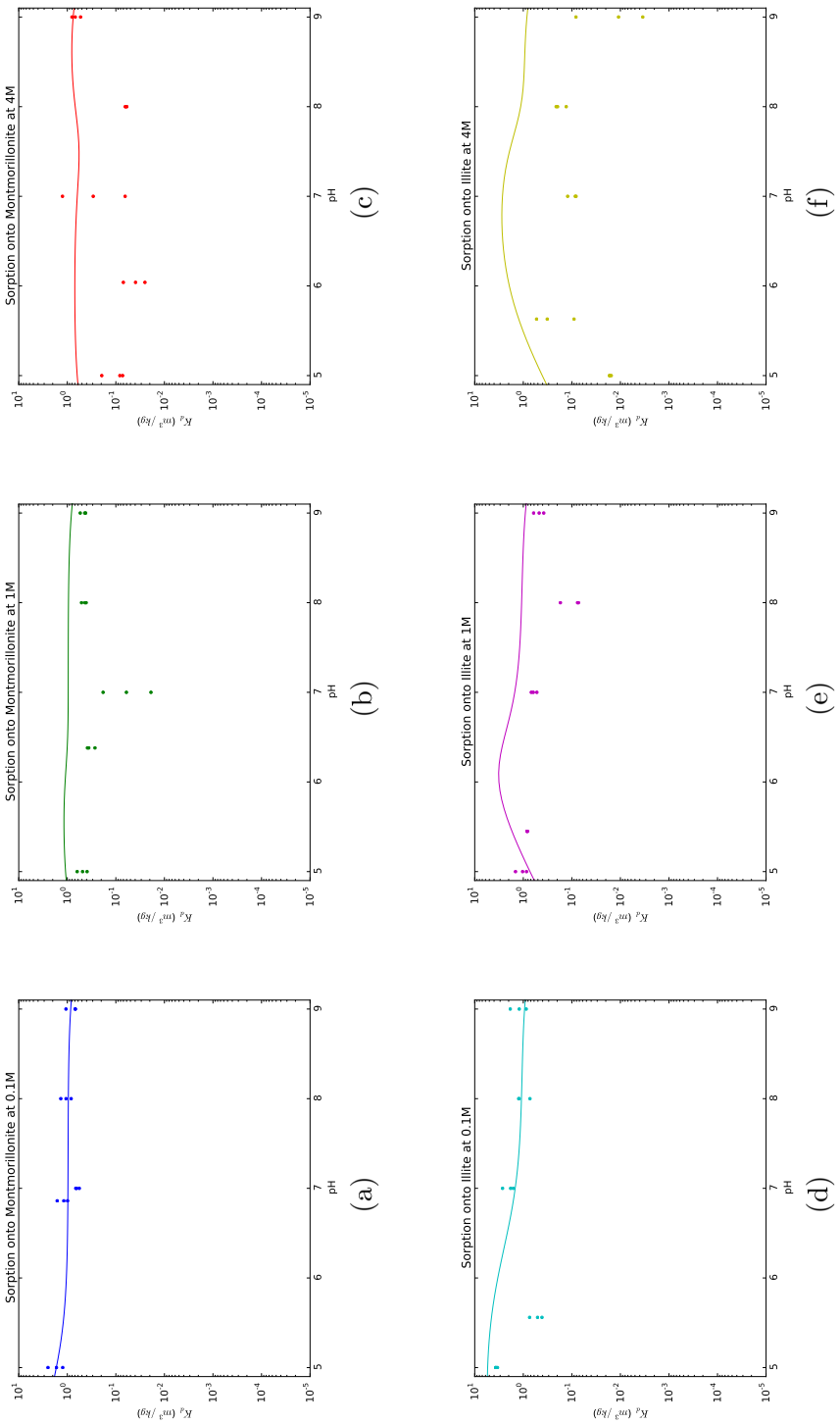

Figure 5.15: Zoomed in version of Figure 5.14, the model results are shifted left by 2 pH units. Subfigures (a) to (c): surface complexation modeling results for Pd sorption onto montmorillonite at I of 0.1 M, 1 M and 4 M respectively. Subfigures (d) to (f): surface complexation modeling results for Pd sorption onto illite at I of 0.1 M, 1 M and 4 M respectively. Bradbury and Baeyens recommended surface complexation reactions and a ternary surface complex reaction were used. Surface complexation constants were adjusted individually to find the best fit.

Chapter 6

Discussion

6.1 Detection Limit of Palladium by ICP-MS

Recall that K_d is calculated using equation (2.5). Since the detection limit of Pd by ICP-MS was 1×10^{-9} M the minimum value of C_{eq} is 1×10^{-9} M. If we substitute this into equation (2.5) and solve for C_i we end up with equation (6.1).

$$C_i = C_{eq}(1 + K_d\frac{S}{L}) \tag{6.1}$$

Therefore we can select the initial concentration of Pd using equation (6.1) and the range of K_d values we want to measure. The range of K_d values reported by Tachi *et al.* (1999) was 3.55 to 61.5 If we substitue 61.5 into equation (6.1) with $\frac{L}{S}$ of 0.5 m^3/kg then we find that the initial concentration of Pd should be 1.24×10^{-7} M. We reduced this value slightly to 1×10^{-7} M for the sorption experiments.

The background level of ^{105}Pd (and ^{106}Pd, data not shown) was quite high during

ICP-MS measurement. If the background levels of Pd could be reduced then the detection limit of Pd could also be reduced. The ICP-MS has several gas modes of operation that are designed to improve detection. Light gases such as hydrogen and helium can be introduced into the detector. When lighter atoms impact the hydrogen or helium they will be deflected, however when heavier atoms impact the hydrogen or helium they will be unaffected. Therefore hydrogen and helium gas modes remove lighter elements from the detector. There is also a reaction cell where Oxygen can be introduced. When ions pass through the reaction cell, some will be bond with oxygen and their mass will be increased. The new mass can be used as the detection mass of the element. The oxygen gas mode is useful when there are two or more isotopes of different elements with the same mass. If the element being studied bonds with oxygen and the other does not then the mass of the element plus the mass of oxygen can be used as the detection mass. All three of these gas modes were applied to Pd, however none of them successfully reduced the background levels of Pd. We decided that there might be the possibility of polyatomic interference. Polyatomic interference is the formation of polyatomic ion from two or more ions in the precursor. The combined mass of the ions which form the polyatomic ion have a combined mass equal to the mass of the isotope being studied. Two polyatomic interference exists for Pd, $ArCu^+$ (May *et al.*, 1998) for ^{105}Pd and $ArZn^+$ (Agilent Technologies, 2013) for ^{106}Pd. Argon (Ar), is used as the carrier gas and various components of the ICP-MS such as the sampling cone are made out of copper (Cu). The zinc (Zn) contamination could be from solutions. Knowing this, it is quite possible that the formation of $ArCu^+$ and $ArZn^+$ inside the detector is causing the high Pd background. The ICP-MS also has a quick scan mode where it measures the CPS at all masses. The CPS is

not very accurate, but the quick scan lets you know what elements are being detected in the solution. When running the quick scan we found high quantities of Ar, Cu and Zn. Therefore since Ar, Cu and Zn are present in high concentrations, it most likely that the polyatomic interference of $ArCu^+$ is causing the high ^{105}Pd background and $ArZn^+$ is causing the high ^{106}Pd. Polyatomic interferences are very hard to remove because it requires removing the source of the ions which form the polyatomic ion. The carrier gas cannot be changed from Ar, and all sources of the Cu and Zn may not be possible to remove.

6.2 Titrations for pH Probe Calibration

As I increased the difference between $pH_{measured}$ and pH_c increased. This is because the pH probe measures the activity of hydrogen ions, not the concentration. As I increases the ion mobility decreases and the hydrogen ion activity differs from the hydrogen ion concentration (Thermo Fisher Scientific, 2014). In order to account of this, all values of $pH_{measured}$ were adjusted using the equations shown in Table 5.2.

6.3 Palladium Solubility and Stability

We have measured the solubility of Pd at 0.1 M I and pH 5.0 to 5.2, 1 M I and pH 5.3 to 5.5 and 4 M I and pH 5.8 to 6. Tachi *et al.* (1999) reported the solubility limit of Pd at 0.1 M I and pH 5 as 5.0×10^{-6} M to 5.1×10^{-6} M. This is two to three times larger that the value we measured at 0.1 M I.

As was shown in section 5.6.1, the speciation of Pd is strongly dependent on pH.

That means that the solubility will also be strongly dependent on pH. In order to fully understand the solubility of Pd in solution and determine whether or not the initial concentration of Pd was below the solubility limit for all the different experimental conditions it is necessary to repeat the experiment at different values of pH. However since we did not repeat the experiment at different values of pH, for each experiment conducted we had to verify that the Pd in solution was in a steady dissolved state and that the concentration of Pd in solution was below the solubility limit.

In the experiment the concentration of Pd in solution reached a steady dissolved state after 5 days. During the sorption experiments, in order to ensure that Pd was in a steady dissolved state, the solutions were left in the incubator for 7 days after Pd was added. We verified that Pd was in a steady dissolved state and that no precipitate was forming, *i.e.* that the concentration of Pd in solution was below the solubility limit, by measuring the concentration of Pd in solution 5 days and 7 days after adding Pd to solution, for all of the sorption experiments. If the concentration in solution after 5 days and 7 days was the same then we assumed that Pd was in a steady dissolved state. Additionally if the concentration of Pd in solution was near the expected value then we assumed that no precipitation was occurring. If the concentration of Pd was lower than expected, then this most likely meant that precipitate was forming. However since before all ICP-MS measurements, and before contacting the solid, the solutions were centrifuged for 30 minutes at 18,000 rpm we can assume that all precipitate was removed from solution before measurements were taken and before the solid was contacted. Therefore since the initial concentration used in the K_d calculation was from the 7 day measurement we can assume that the

sorption results were not effected by precipitation in the initial solution.

6.4 Sorption Kinetics

In the sorption kinetics experiment we see that sorption increases with time. The majority of the sorption occurs quickly over the first 1 to 2 days, after which sorption continues to occur but at a greatly reduced rate. Sorption appears to reach equilibrium after 7 days, however had the samples been left for a much longer amount of time (*e.g.* >100 days), it is likely that sorption would have continued to increase (Vilks, 2016). Having found that sorption reached equilibrium in 7 days it would have sufficient to use a sorption time of 7 days in experiment. However in discussion with Dr. Vilks, the researcher in charge of selecting data for the Canadian SDB, he noted that 7 days was the absolute minimum amount of sorption time he considered acceptable when selecting data for his report. Therefore in order to make the data more credible it was decided to use double the length of time to reach sorption equilibrium as the sorption time during experiment. Therefore a sorption time of 14 days was used. As noted earlier, the sorption would most likely continue to increase if the contact time was longer, therefore the K_d values reported in this thesis can be taken as conservative.

6.5 Ionic Strength Dependence of K_d

We found that there was a strong dependence of K_d on I. This meant that all other sorption experiments had to be conducted using a range of I. For the pH dependence

of K_d and the sorption isotherm experiments 0.1 M, 1 M and 4 M I solutions were used. These were chosen because there were three regions of dependence of K_d on I; 0.1 M to 1 M 1, 1 M to 3 M and 3 M to 4 M. For illite and shale, K_d was constant between 0.1 M and 1 M, however for bentonite it was not. Therefore 0.1 M and 1 M were both selected in order to determine the dependence of K_d on I in this region. For all solids, K_d decreases from 1 M to 3 M and then remained constant. Therefore 1 M and 4 M solutions can be used to determine the I dependence across this entire region.

The results of the speciation modeling in PHREEQC (see Section 5.6.1) showed that surface site speciation is independent of I but dependent on pH and that aqueous speciation was strongly dependent on both I and pH. We also found that as I increased the pH of solution decreased for the sorption experiments involving bentonite and shale. The pH_c values for bentonite were in the range of 6.0 to 6.9. From Figure 5.8(a), in this region both the neutral surface site, S−OH, and the negative surface site, $S-O^-$, are dominant with them being equally dominant at the beginning of the range and the negative site becoming mostly dominant at the end of the range. There is also a dependence of pH_c on I. The lower the I, the higher the pH and as a result in lower I solutions more $S-O^-$ was present. This implies that the I dependence could simply be a pH dependence which arose from the I dependence of pH. We see the same pH dependence on I for shale. pH_c values range from 6.5 to 7.4 with the higher pH corresponding to lower I. Over this range of pH there is a decrease in S−OH dominance and an increase $S-O^-$ dominance with increasing pH. However, for sorption onto illite we do not see a dependence of pH on I, but we do see the same dependence of K_d on I. Since we see the same I dependence when pH dependence

is not present we can conclude that there is a dependence on I. Additionally at first it appeared as if I dependence was correlated to the dominance of $S-O^-$, but the values of pH_c range from 5.3 to 5.8 for the illite sorption experiment, which is a region where $S-O^-$ is not dominant at all. In this region $S-OH_2^+$ dominance is decreasing and S−OH dominance is increasing, with increasing pH.

If we examine the results of the surface site speciation and aqueous speciation of Pd in Section 5.6.1, it may be possible to determine a reason for the I dependence of K_d. From Figure 5.8, as I increased, the region of $Pd(OH)_2$ dominance decreased. At 0.1 M it is dominant in the pH range of 6 to 12, at 1 M it is dominant in the pH range of 8 to 11.8 and at 4 M it is dominant in the pH range of 9.5 to 11.5. As the range $Pd(OH)_2$ dominance decreased, the range of $PdCl_4^{2-}$ dominance increased. In 0.1 M solutions it was dominant up until pH 6, this increases to pH 8 in 1 M solutions and pH 9.5 in 4 M solutions. The range of pH_c in experiment, for all solids and solutions, was 5.3 to 7.8, if we consider the surface site speciation of montmorillonite, over this pH range, both the S−OH and $S-O^-$ surface sites are present. When the I is 0.1 M, both $PdCl_4^{2-}$ and $Pd(OH)_2$ are present in solution and both the S−OH and $S-O^-$ surface sites are present. Sorption can occur between both both $PdCl_4^{2-}$ and S−OH and $Pd(OH)_2$ and $S-O^-$. As I increases to 1 M $Pd(OH)_2$ concentration in solution decreases and $PdCl_4^{2-}$ concentration increases, but the surface site speciation stays the same. Therefore there is reduced sorption, as there is less $Pd(OH)_2$ available to sorb onto the $S-O^-$ surface site. At solution I of 4 M there is even less $Pd(OH)_2$ available to sorb onto the $S-O^-$ surface site and sorption decreases further. However if we consider the surface site speciation of illite over this pH range we find that only

S−OH is dominant. Since the range where $PdCl_4^{2-}$ dominance increases with increasing I we would expect to see increased sorption for sorption onto illite. Therefore there must be some other factor responsible for the I dependence of K_d.

The dependence of sorption on I may be a result of the increase in cations in solution. As the amount of cations in solution increases, there becomes more competition for the limited amount of surface sites. If the sorption affinity between Ca^{2+} or Na^{+} complexes and the surface sites is stronger than that of Pd^{2+} complexes and the surface sites then as I increased and the concentration of Ca^{2+} and Na^{+} in solution increased then the amount of Ca and Na sorption could increase. This would in turn lead to a decrease in sorption of Pd with increasing I as Ca and Na would be taking up more and more of the surface sites.

Another interesting result shown by this experiment is that the K_d values for sorption onto illite were larger than the K_d values for sorption onto shale. We expected sorption onto illite to be large then sorption onto shale, that is $K_{d_{illite}} > K_{d_{shale}}$ as illite is the constituent clay in shale and there is by definition less illite in shale, then in pure illite. Vilks (2016) suggests using 60% of $K_{d_{illite}}$ to represent K_{dshale} when experimental values are not available for shale, where as we have found that $K_{d_{illite}}$ is 5 to 10 times larger then $K_{d_{shale}}$. This suggest that there could be impurities in the Queenston shale sample being used.

6.6 pH Dependence of K_d

We see the same I dependence of K_d from the results of the pH dependence of K_d experiment (see Figures 5.4 and 5.5) as we saw during the I dependence of K_d experiment. For all solids, the K_d values are greatly decreased, across the entire pH range, with increasing I. We also found a strong dependence of K_d on pH for all three solids studied and for all three I solutions used.

For sorption in 0.1 M solutions, all solids showed the same dependence on pH; decreasing K_d with increasing pH. This is the same result found by Tachi *et al.* (1999) for sorption onto bentonite in 0.1 M solutions. When we compare experimental data we find that there is good agreement between the lower range of measured values from Tachi *et al.* (1999) and data measured in this thesis for sorption onto bentonite in 0.1 M solutions. The error bars in Figure 5.4 for data taken from Tachi *et al.* (1999) (unfilled circles) represent the range of measured values, not the error. The decrease in K_d with increasing pH is quite small, over the measured range of pH K_d decreased by about half. Figure 5.8(a) shows the surface site speciation of montmorillonite and illite as a function of pH and Figure 5.8(b) shows the aqueous speciation of Pd as a function of pH. Over the pH range of 5 to 9, $Pd(OH)_2$ is mostly dominant, with the transition from $PdCl_4^{2-}$ to $Pd(OH)_2$ occurring at pH 6. For both montmorillonite and illite the $S-OH$ and $S-O^-$ surface sites are dominant. As pH increases there is a transition from sorption between $PdCl_4^{2-}$ and $S-OH$ to sorption between $Pd(OH)_2$ and $S-O^-$. Since there are sorption options available through out the pH range, it is not clear why the K_d is decreasing. It is possible that it is the result of increasing competition between Ca^{2+} or Na^+ complexes and Pd^{2+} complexes for surface sites at

higher pH.

For sorption in 1 M solutions, we find different dependences on pH for the different solids. Figure 5.8(a) shows the surface site speciation of montmorillonite and illite as a function of pH and Figure 5.8(c) shows the aqueous speciation of Pd as a function of pH. For sorption onto bentonite, there is an initial decrease in K_d from pH 5 to 7, after which K_d begins to increase with increasing pH until pH 9. Over the pH range of 5 to 9, $PdCl_4^{2-}$ is mostly dominant, with the transition from $PdCl_4^{2-}$ to $Pd(OH)_2$ occurring at pH 8. We see a similar transition happening between S−OH dominance and S−O^- dominance occurring at pH 6 for montmorillonite. The concentration on the surface of S−OH sites is decreasing from pH 5 to 7, the same range where $PdCl_4^{2-}$ is dominant and sorption is decreasing. Similarly the concentration on the surface of S−O^- sites is increasing from pH 5 to 9 and $Pd(OH)_2$ concentration is increasing from pH 7 to 9 as is sorption. Therefore for sorption onto bentonite, the pH dependence appears to be a result of the speciation. A similar result is found when examining the sorption onto illite at 1 M. As pH increases from 5 to 8 we find that K_d decreases, and a sharp increase in K_d occurring from pH 8 to 9. Over the pH range of 5 to 9, S−OH is mostly dominant on illite, with the transition between S−OH and S−O^- dominance occurring at pH 8. As pH increases from 6 to 9 the concentration of S−OH surface sites decreases and the concentration of S−O^- surface sites increases. $PdCl_4^{2-}$ is dominant over the range of pH 5 to 8 and therefore as the amount of available S−OH sites for it to sorb on decreases, the sorption decreases. Between pH 8 and 9 the dominance of the S−O^- site and $Pd(OH)_2$ is increasing and as a result we see an increase in sorption. Therefore for sorption onto illite, the pH

dependence appears to also be a result of the speciation. It is more difficult to explain the sorption onto shale using speciation. For sorption onto shale we see the opposite trend as sorption onto bentonite and illite, K_d increases initially, from pH 5 to 7, after which it decreases, from pH 7 to 9. We would expect to see the same trends for sorption onto shale as we saw for sorption onto illite, as illite is the constituent clay in shale. As noted in Section, 6.5, it is possible that there are some impurities in the Queenston shale samples. These impurities could be causing the difference in behavior between illite and shale with respect to pH dependence.

For sorption in 4 M solutions, again we find different dependences on pH for the different solids. Figure 5.8(a) shows the surface site speciation of montmorillonite and illite as a function of pH and Figure 5.8(d) shows the aqueous speciation of Pd as a function of pH. For sorption onto bentonite, the overall trend appears to be an increase in K_d from pH 5 to 7, and then K_d remains constant from pH 7 to 9. Over the pH range of 5 to 9, $PdCl_4^{2-}$ is always dominant. Again, both the S$-$OH and S$-$O$^-$ surface sites are dominant in the pH range of 5 to 9 with a transition between S$-$OH dominance and S$-$O$^-$ dominance occurring at pH 6 for montmorillonite. From this we would expect to see a decrease in K_d with increasing pH as the concentration of S$-$OH sites for which $PdCl_4^{2-}$ can sorb decrease. However, if we consider the possible explanation for I dependence mentioned in Section 6.5, namely that an increase in I leads to an increase in cations in solution which compete against Pd for sorption sites, then it is possible that the pH dependence observed for bentonite in 4 M solutions is a result of the speciation of competitive complexes. For sorption onto illite, the dependence on pH is quite complex. K_d increases from pH 5 to 6, after which K_d

decrease from pH 6 to 7. K_d then peaks a second time at pH 8. The first peak in K_d can be explained using the speciation. $PdCl_4^{2-}$ is the dominant species over the entire pH range. The S−OH surface site concentration peaks at pH 6, therefore the sorption peaks as the amount of available surface sites peaks. However the second peak can not be explained using speciation, as new aqueous species which can sorb onto the negative surface site do not start forming until after pH of 8. As with bentonite, it is possible that the pH dependence between pH 7 and 9 for sorption onto illite can be result of the speciation of competitive complexes. For the sorption onto shale, K_d shows the same dominance on pH as exhibited in 1 M solutions, that is a peak at pH 7, but now the peak is more defined.

6.7 Sorption Isotherms

The sorption isotherms for sorption onto bentonite and illite have slopes of one for all I considered. This means that K_d for the sorption of Pd onto bentonite and illite is independent of initial concentration of Pd. Additionally it means that Pd sorption is the result of forming Pd inner- and outer- sphere complexes inside of the Stern layer. Sorption can be modeled using a single layer, *i.e.* no diffuse or electric double layer, model. The sorption mechanism is most likely specific chemical sorption through surface complexation.

The sorption isotherms for sorption onto shale are much different. Once again, we would have expected that the sorption isotherms for illite and shale would have been the same. Therefore we have even more evidence to the fact that the Queenston

shale samples contain impurities. The slope of the Freundlich isotherms for sorption onto shale was dependent on I and decreased with increasing I. Since the slope is not equal to one, it means that K_d for sorption of Pd onto shale is dependent on initial concentration of Pd. Additionally it means that cooperative sorption is occurring and that there are interactions between sorbates or between sorbates and sorbents in solution. The sorption of Pd onto shale was not modeled as it was originally assumed that sorption onto shale could be modeled by the sorption onto illite (with the values slightly reduced). After it was discovered that the sorption of Pd onto illite and shale exhibited different behavior, we did not model the sorption onto shale as surface complexation constants were not available for shale. However, if we were to model the sorption of Pd onto shale it would be necessary to use a multi layer model such as the generalized two layer (electric double layer in PHREEQC) model or by adding a unique diffuse layer to the single layer model.

6.8 Speciation

6.8.1 Surface Site Speciation

The surface site speciation, see Figure 5.8(a), was plotted for many different I; 0.1 M, 0.5M, 1 M, 2M, 3 M, and 4 M, but only one was included in this thesis because they were all identical. Therefore the surface site speciation was heavily dependent on pH, but was not dependent on I. The dependence of surface site speciation on pH was expected. If we consider the protonation and deprotonation reactions, equations (2.2) and (2.3) respectively, we see that one of the terms is H^+. The equilibrium

constant for protonation and deprotonation reactions is given by equations (6.2) and (6.3) respectively.

$$K_{protonation} = \frac{[\mathrm{S{-}OH_2^+}]}{[\mathrm{S{-}OH}][\mathrm{H^+}]} \tag{6.2}$$

$$K_{deprotonation} = \frac{[\mathrm{S{-}O^-}][\mathrm{H^+}]}{[\mathrm{S{-}OH}]} \tag{6.3}$$

Recall that pH $= -log([H^+])$ and since $K_{protonation}$ and $K_{deprotonation}$ are constant, when the pH changes, the concentration of H^+ changes and as a result the concentration of S$-$OH, S$-O^-$, S$-OH_2^+$ must change to maintain the constant values of $K_{protonation}$ and $K_{deprotonation}$. Therefore we have a dependence of surface site speciation on pH.

As discussed in Section 5.6.1, S$-OH_2^+$ is dominant at low pH, S$-O^-$ is dominant at high pH and S$-$OH is dominant in the intermediate pH region in between for both montmorillonite and illite. This result was also expected, and was discussed in Section 2.1.1. Montomorillonite and illite differ in the location of the transition points between dominant surface species. Transitions between surface species occur at lower pH values for montmorillonite then illite. This is a result of the protolysis constants used to describe the protonation and deprotonation reactions. The protolysis constant for protonation was larger for illite then it was for montmorillonite and the protolyis constant for deprotonation was larger for montmorillonite then it was for illite. The values of protolysis constants used are shown in Table 4.5 under the heading *Acid-Base*.

6.8.2 Aqueous Speciation of Palladium

The aqueous speciation was both heavily dependent on I and pH. The region of interest, with regard to the experiments conducted is the pH range of 5 to 9. In this region $PdCl_4^{2-}$ and $Pd(OH)_2$ are dominant. The transition point between $PdCl_4^{2-}$ dominance and $Pd(OH)_2$ dominance occurs at pH 6 in 0.1 M solutions and at pH 8 in 1 M solutions. In 4 M solutions $PdCl_4^{2-}$ is always dominant in the range of pH 5 to 9. Focus was placed on these two species when trying to improve the fit of the surface complexation model to the data.

The aqueous speciation is heavily dependent on pH for much the same reason as it was for surface site speciation; the formation reaction of multiple aqueous species, *e.g.* $Pd(OH)_2$ and $Pd(OH)_3^-$, contain H^+. The hydroxide aqueous species such as $Pd(OH)_2$ and $Pd(OH)_3^-$ are dominant at high pH because their formation is dependent on concentration of $[OH^-]$ in solutions. If we consider the formation reaction for $Pd(OH)_2$, shown in Table 4.2, the equation for the formation constant is given by equation (6.4).

$$K_{Pd(OH)_2} = \frac{[Pd(OH)_2]}{[Pd^{2+}][OH^-]^2} \tag{6.4}$$

Since $K_{Pd(OH)_2}$ and $[Pd^{2+}]$ are constant if the concentration of OH^- increases then the concentration of $Pd(OH)_2$ must increase to compensate for this. Conversely chloride complexes such as $PdCl_4^{2-}$ appear at lower pH because they do not require either free H^+ or free OH^- to form. $Pd(OH)_2$ is the preferred species at intermediate pH because less OH^- is required in the formation. As OH^- concentration increases, the increase in $Pd(OH)_2$ concentration is proportional to the increase in OH^- concentration to the power of two, where as the increase in $Pd(OH)_3^-$ concentration is proportional to the

increase in OH^- concentration to the power of three. Therefore when OH^- is readily available in solution, such as at high pH, $Pd(OH)_3^-$ becomes the more dominant species.

A similar explanation can be used to explain why the aqueous speciation is heavenly dependent on I. Ionic strength is the measure of the concentration of free ions in solution . If we consider the formation reaction for $PdCl_4^{2-}$, shown in Table 4.2, the equation for the formation constant is given by equation (6.5).

$$K_{PdCl_4^{2-}} = \frac{[PdCl_4^{2-}]}{[Pd^{2+}][Cl^-]^4} \tag{6.5}$$

The Pd^{2+} and Cl^- are free ions in solutions. We increase the I of solution by adding NaCl and $CaCl_2$ so that there are more free ions, such as, Cl^-, Ca^{2+} and N^+ in solution. Therefore when the I of the solution increases the concentration of Cl^- increases and as a result the concentration of $PdCl_4^{2-}$ in solution must increase to maintain equilibrium. The formation of $PdCl_4^{2-}$ increases more with increasing I, compared to other chloride complexes, because the increase in concentration of $PdCl_4^{2-}$ is proportional to the concentration of Cl^- to the power of four.

6.9 Surface Complexation Modeling

The initial surface complexation model was based off of the surface complexation reactions recommended by Bradbury and Baeyens and the surface complexation reaction constants were derived using the correlations they developed. For sorption onto montmorillonite in 0.1 M solutions, the model over predicted K_d through out

the range of pH used in experiment, that is pH 5 to pH 9. The same is true for sorption onto illite in 0.1 M solutions. For sorption onto montmorillonite the model under predicted K_d in the pH range of pH < 7 and pH < 9 in 1 M and 4 M solutions respectively. For sorption onto illite in 1 M and 4 M solutions, the model both over predicts and under predicts the value of K_d. In 1 M solutions, it under predicts K_d for pH < 7 and over predicts K_d for pH > 7. In 4 M solutions, it under predicts K_d for pH < 8 and over predicts K_d for pH > 8.

Since the Bradbury and Baeyens correlation were developed from a fit to experimental data, there is an error associated with it. The error involved with the correlation means that there is a range of values applicable for each surface complexation reaction constant. The range of values for each surface complexation constant is shown in Table 5.10. We were able to slightly improve the fit by adjusting the surface complexation reaction constants used in the model. For sorption onto montmorillonite it reduced the range in which the model was over predicting K_d in 0.1 M solutions from pH 5 to 9 down to pH 5 to 8.5. The amount the model over predicted K_d for sorption onto montomorillonite in 1 M solution was reduced in the range of pH 8 to 9. There was little effect on the model for sorption onto montmorillonite in 4 M solutions. For sorption onto illite in 0.1 M solutions, it reduced the over prediction of K_d by an order of magnitude. For sorption onto illite in 1 M and 4 M solutions, the amount by which the model both over predicted and under predicted the value of K_d was also reduced.

The region where sorption is being drastically under predicted; low pH and high

I, corresponds to the region where $PdCl_4^{2-}$ is the dominant species. Therefore in order to improve the fit in this region the surface complexation reaction for $PdCl_4^{2-}$ was added to the model. $PdCl_4^{2-}$ forms a ternary surface complex, the surface complexation reaction constant for which was derived using the Fein correlation. The addition of the surface complexation reaction for $PdCl_4^{2-}$ to the model had little effect on K_d values predicted for sorption in 0.1 M solutions. It did however have a large effect on the K_d values predicted for sorption in 1 M and 4 M solutions. For sorption onto montmorillonite in 1 M and 4 M solutions the fit was greatly improved as the model no longer under predicts K_d. For sorption in 1 M solutions we do not see the same trends as we same in experiment, namely the local minimum at pH 7, however the K_d values being predicted are much closer to the K_d values measured in experiment. For sorption in 4 M the model does predict the trends we saw in experiment, namely an increase in K_d from pH 5 to 7 and then constant K_d from pH 7 to 9. For sorption onto illite in 1 M and 4 M solutions the fit was only slightly improved. For sorption in 1 M solutions, the model is no longer under predicting K_d but it is however over predicting K_d, which is not necessarily an improvement. For sorption in 4 M solutions, the predicted K_d values fit well to experimental data over the pH range of 5 to 6, but over the range of pH 6 to 9 the K_d values are being over predicted.

The Fein correlation was developed for the formation of ternary surface complexes with organic ligands. It is unclear whether the Fein correlation was successfully applied to inorganic ligands, as the fit was only improved for the sorption onto montmorillonite. In order to further improve the fit, we decided to adjust the values of the surface complexation constants manually. Bradbury and Baeyens correlation was

developed using data collected from experiments which were conducted under different experimental conditions. The major difference being that Bradbury and Baeyens used low, < 0.1 M, I solutions (Bradbury and Baeyens, 2005a). It is possible that Bradbury and Baeyens correlation can not be applied to Pd surface complexation reactions in high I conditions. The surface complexation reactions were adjusted one at a time, in increments of 0.5, until the best fit was achieved. The best fit was determined graphically. The values of the surface complexation constants chosen are shown in Table 5.11. By manually adjusting the values of the surface complexation constants we were able to greatly improve the fit between model and experiment. The fit was best for sorption in 0.1 M solutions. The fit in 1 M and 4 M solutions was good for sorption onto montmorillonite, but there is still some under prediction from the model for sorption onto illite in 1 M solutions and some over prediction from the model for sorption onto illite in 4 M solutions. The value the surface complexation constant used for the ternary surface complex was not adjusted outside of error, therefore the Fein correlation might be suitable for determining surface complexation constants for the formation of ternary surface complexes with inorganic ligands.

For sorption onto montmorillonite, because the model was able to accurately predict sorption, we can conclude that the sorption mechanisms for sorption of Pd onto montomorillonite were those used in the model; specific chemical sorption through surface complexation. The surface complexes forming are $S-OPdOH$, $S-OPd(OH)_2^-$ and $S-OPdCl_4^{3-}$. For sorption onto illite, the model was only able to accurately predict sorption in 0.1 M solutions, therefore we can not conclude that we modeled the sorption mechanism successfully. The isotherms shown that Pd is forming inner- and

outer- sphere complexes inside the Stern layer as the slope of the Freundlich isotherm was one, so we believe that using a single layer model was the correct decision. From Figures 5.12 it appears that if the model results were shifted 2 pH units to left, it may imporve the fit. The results of performing this operation are shown in Figure 5.14 and Figure 5.15. Shifting the model results left by 2 pH units did not effect the results for sorption onto bentonite, it did however greatly improve the results for sorption onto illite. $S-OPdCl_4^{3-}$ is a surface complex involving S−OH, the S−OH surface site is dominant over a wide pH range, and by shifting the sorption model results left 2 pH units we effectively reduced the range where S−OH is dominant. Since this improved the fit between model and experiment it is possible the protonation and deprotonation constants being used for sorption onto illite may not be accurate, at least with regard to the illite sample we are using.

Chapter 7

Conclusions

The detection limit of Pd was successfully determined to be 1×10^{-9} M. The detection limit is higher then expected due to the high background of Pd found during measurements. The high background is due to polyatomic interference from the polyatomic ions $ArCu^{+}$ and $ArZn^{+}$. Removing the source of the polyatomic ions would reduce or remove the polyatomic interference.

The solubility limit of Pd was determined experimentally at pH 5. We found that the solubility of Pd at pH 5 was strongly dependent on ionic strength. In 0.1 M I solutions the solubility limit of Pd was in the range of 1.9×10^{-6} M and 3.3×10^{-6} M. Tachi *et al.* (1999) reported a solubility limit for Pd in 0.1 M I solutions as 5.0×10^{-6} M to 5.1×10^{-6} M at pH 5. The value reported by Tachi *et al.* (1999) is two to three times larger than the value measured experimentally. In 1 M I solutions the solubility limit of Pd was in the range of 6.6×10^{-6} M and 1.5×10^{-5} M. In 4 M I solutions the solubility limit of Pd was in the range of 3.8×10^{-5} M and 5.9×10^{-5} M. The solubility of Pd increased with increasing I at pH 5. The stability of Pd in

solution was measured in parallel with solubility. We found that Pd reached a steady dissolved state after 5 days. Since the stability and solubility of Pd was only measured at pH 5, we were unable to conclude that for all experimental conditions that Pd would be in a steady dissolved state and below the solubility limit. As a result it was necessary to verify the solubility and stability for all experiments independently. We found that for all experiments, the concentration of Pd in solution 5 days and 7 days after being added to solution was constant, and the concentration was near to the expected value and therefore we can conclude that for all experiments Pd was in a steady dissolved state and that Pd was below the solubility limit for all experiments.

The time taken to reach sorption equilibrium was also measured experimentally. For all solids, sorption equilibrium was reached within 7 days. In order to make the sorption results more credible, the amount of time taken to reach equilibrium was double for experiments, that is, 14 days was used for the sorption time in experiments.

The pH dependence and ionic strength dependence of K_d for sorption of Pd onto bentonite, illite and shale was successfully determined from experiments. When comparing the results of the sorption experiments we found that K_d for shale was always the largest, and bentonite and illite were comparable. That is $K_{d_{shale}} > K_{d_{illite}} \approx K_{d_{bentonite}}$. We expected $K_{d_{illite}} > K_{d_{shale}}$ as illite is the constituent clay component in shale. There was a strong dependence of K_d on both I and pH. For sorption onto bentonite, the K_d decreased from solution I of 0.1 M to 3 M after which it became constant. For sorption onto illite and shale the K_d was constant between I of 0.1 M and 1 M, as well as between 3 M and 4 M. K_d decreased with increasing I over

the range of 1 M to the 3 M. There was also a strong dependence of K_d on pH. For sorption in 0.1 M solutions, all solids exhibited a slight decrease in K_d with increasing pH. As I increased, the relationship between K_d became more complicated. For sorption onto bentonite and illite in 1 M solutions, both solids experienced a local minimum due to the reduced concentration of S−OH surface sites and the increase in concentration of S−O^-surface sites. For sorption onto shale the opposite trend was observed; a local maximum. We expected to see the same pH dependence for shale as we saw for illite, and as a result we were unable to explain the results using speciation. In 4 M solutions the pH dependence of K_d was visible, but the trends were not clear. In cases where the pH and I dependence of K_d could not be described using the aqueous speciation of Pd and the surface site speciation, it is possible that the dependencies being observed are a result of competitive sorption. That is, Pd is competing with other elements or species in solution for the limited amount of sorption sites.

The dependence of sorption on initial concentration of Pd, also known as the sorption isotherms of Pd, were also successfully measured experimentally for the sorption of Pd onto bentonite, illite and shale. Fruendlich isotherms were fitted to the data. We found that for sorption onto bentonite and illite, the slope of the isotherm was one in solutions of 0.1 M, 1 M and 4 M I meaning that Pd was forming inner- and outer- sphere complexes inside the Stern layer. For sorption onto shale the slope of the isotherm was dependent on I. At 0.1 M I the slope was 1.3, as I increased to 1 M and 4 M the slope decreased to 0.85 and 0.33 respectively. Since the slope was not one for sorption onto shale it is most likely that cooperative sorption is occurring

and interactions between sorbates or sorbates and sorbents is occurring.

Both the surface site speciation and the aqueous speciation of Pd were modeled successfully in PHREEQC. We saw a strong dependence on I for aqueous speciation of Pd. As I increased, the pH region where the aqueous species $PdCl_4^{2-}$ is dominant increased, and as a result the pH region where the aqueous species $Pd(OH)_2$ is dominant decreased. The surface site speciation had no dependence on I. Both the surface site speciation and the aqueous speciation of Pd has a strong dependence on pH. At low pH the $S-OH_2^+$ surface site is dominant, as pH increases the $S-OH$ surface site becomes dominant, as pH increases further the $S-O^-$ surface site becomes dominant. Similarly, at low pH the aqueous species $PdCl_4^{2-}$ is dominant, as pH increases aqueous species $Pd(OH)_2$ becomes dominant, as pH increases further the aqueous species $Pd(OH)_3^-$ becomes dominant.

Since the isotherms for sorption onto montomorillonite and illite had a slope of one, meaning that Pd was forming inner- and outer- sphere complexes inside the Stern layer, our choice of sorption model (single layer model) was justified. As further justification, surface complexation was modeled successfully in PHREEQC using a single layer model for sorption of Pd onto montmorillonite in 0.1 M, 1 M and 4 M solutions and for sorption of Pd onto illite in 0.1 M solutions. We were only able to establish a good fit between the model and experiment for sorption of Pd onto illite in 1 M and 4 M solutions after shifting the results from the sorption model left 2 pH units. For sorption onto montmorillonite and illite we can conclude that the sorption mechanism is specific chemical sorption, in the form of surface complexation. The surface

complexes forming are $S-OPd(OH)$, $S-OPd(OH)_2^-$ and $S-OPdCl_4^{3-}$. For sorption of Pd onto illite it is possible that the protonation and deprotonation constants are not appropriate for the illite sample being used in experiment because we were able to improve the fit between model and experiment by reducing the region where $S-OH$ is dominant. Sorption onto shale was not modeled as surface complexation reaction constants, or a correlation to determine surface complexation reaction constants, are not available for shale. However if they were, it would have been necessary to develop multi layer model as the slope of the sorption isotherms showed that cooperative sorption was most likely occurring.

Previously Pb was used as a chemical analog for Pd for sorption onto shale. The K_d values for Pb ranged from 0.59 to 3.38 m^3/kg over a pH between 6.0 and 6.5 and I of 0.25 M (Vilks, 2011). We found that the K_d values for Pd for sorption onto shale at the same pH and I of 0.1 M ranged from 3.1 to 5.7 m^3/kg. At similar I the K_d we measured are significantly higher, and therefore when the safety assessment is conducted we can take credit for the improved sorption properties of palladium over lead due to the research we conducted.

Bibliography

Agilent Technologies (2013). Agilent 8800 ICP-QQQ Application Handbook. Technical report.

Allan, C. J. and Dormuth, K. W. (2001). The Back End of the Fuel Cycle and CANDU. Technical report, International Atomic Energy Agency.

Allison, J. D., Brown, D. S., and Novo-Gradac, K. J. (1991). MINTEQA2/PRODEFA2, a Geochemical Assessment Model for Environmental Systems: Version 3.0 User's Manual. Technical report, U. S. Environmental Protection Agenc.

Ball, J. W., Jenne, E. A., and Cantrell, M. W. (1981). WATEQ3: A Geochemical Model with Uranium Added. Technical report, U. S. Geological Survey.

Bradbury, M. H. and Baeyens, B. (1997). A mechanistic description of Ni and Zn sorption on Part II: modelling. *Journal of Contaminant Hydrology*, **27**, 223–248.

Bradbury, M. H. and Baeyens, B. (2005a). Experimental measurements and modeling of sorption competition on montmorillonite. *Geochimica et Cosmochimica Acta*, **69**(17), 4187–4197.

Bradbury, M. H. and Baeyens, B. (2005b). Modelling the sorption of Mn(II), Co(II), Ni(II), Zn(II), Cd(II), Eu(III), Am(III), Sn(IV), Th(IV), Np(V) and U(VI) on montmorillonite: Linear free energy relationships and estimates of surface binding constants for some selected heavy metals and actinide. *Geochimica et Cosmochimica Acta*, **69**(4), 875–892.

Bradbury, M. H. and Baeyens, B. (2009). Sorption modelling on illite. Part II: Actinide sorption and linear free energy relationships. *Geochimica et Cosmochimica Acta*, **73**(4), 1004–1013.

Candu Energy Inc. (2014). Brochure: MACSTOR Modular Air-Cooled Storage.

Coplen, T., Bohlke, J., De Bievre, P., Ding, T., Holden, N., Hopple, J., Krouse, H., Lamberty, a., Peiser, H., Revesz, K., Rieder, S., Rosman, K., Roth, E., Taylor, P., Vocke, R., and Xiao, Y. (2002). Isotope-abundance variations of selected elements (IUPAC Technical Report). *Pure and Applied Chemistry*, **74**(10), 1987–2017.

Crowe, R., Birch, K., Freire-Canosa, J., Chen, J., Doyle, D., Garisto, F., Giersewski, P., Gobien, M., Hatton, C., Hunt, N., Hirchorn, S., Hobbs, M., Jensen, M., Keech, P., Kennell, L., Kremer, E., Maak, P., Mckelvie, J., Medri, C., Mielcarek, M., Murchison, A., Parmenter, A., Ross, R., Sykes, E., and Yang, T. (2015). Technical Program for Long-Term Management of Canada' s Used Nuclear Fuel Annual Report 2013. Technical report, Nuclear Waste Mangement Organization.

Dada, A., Olalekan, A., Olatunya, A., and Dada, O. (2012). Langmuir, Freundlich, Temkin and Dubinin-Radushkevich Isotherms Studies of Equilibrium Sorption of Zn2+ Unto Phosphoric Acid Modified Rice Husk. *IOSR Journal of Applied Chemistry*, **3**(1), 38–45.

Davies, C. W. (1962). *Ion Association*. Butterwoths Pub., Washington, DC.

Debye, P. and Huckel, E. (1923). Zur Theorie der Elektrolyte. I. Gefrierpunktserniedrigung und verwandte Erscheinungen [The theory of electrolytes. I. Lowering of freezing point and related phenomena]. *Physikalische Zeitschrift*, **24**, 185–206.

Dzombak, D. A. and Morel, F. M. M. (1990). *Surface Complexation Modeling: Hydrous Ferric Oxide*. John Wiley & Sons, Inc.

Fein, J. B. (2002). The effects of ternary surface complexes on the adsorption of metal cations and organic acids onto mineral surfaces. *Water Rock Interactions, Ore Deposits, and Environmental Geochemistry*, (7).

Felmy, A. R., Girvin, D. C., and Jenne, E. A. (1984). MINTEQ – A Computer Program for Calculating Aqueous Geochemical Equilibria.PDF. Technical report, U.S. Enviornmental Protection Agency.

Garamszeghy, M. (2015). Nuclear Fuel Waste Projections in Canada – 2015 Update. Technical report, Nuclear Waste Mangement Organization.

Grenthe, I. and Plyasunov, A. (1997). On the use of semiempirical electrolyte theories for modeling of solution chemical data. *Pure and Applied Chemistry*, **69**(5), 951–958.

Gustafsson, J. (2009). Visual MINTEQ. Technical report, KTH Royal Institute of Technology.

IUPAC (1987). *IUPAC Compendium of Analytical Nomenclature*. Blackwell Scientific Publications.

Kitamura, A., Doi, R., and Yoshida, Y. (2014). Update of JAEA-TDB: Update of Thermodynamic Data for Palladium and Tin , Refinement of Thermodynamic Data for Protactinium , and Preparation of PHREEQC Database for Use of the Brønsted-Guggenheim-Scatchard Model. Technical report, Japan Atomic Energy Agency.

Liu, S. (2015). Cooperative adsorption on solid surfaces. *Journal of Colloid and Interface Science*, **450**, 224–238.

Lothenbach, B., Ochs, M., Wanner, H., and Yui, M. (1999). Thermodynamic data for the speciation and solubility of Pd, Pb, Sn, Sb, Nb and Bi in aqueous solution. Technical report, Japan Nuclear Cycle Development Institute.

Macht, F., Eusterhues, K., Pronk, G. J., and Totsche, K. U. (2011). Specific surface area of clay minerals: Comparison between atomic force microscopy measurements and bulk-gas (N2) and -liquid (EGME) adsorption methods. *Applied Clay Science*, **53**(1), 20–26.

May, T. W., Wiedmeyer, R. H., Chaudhary-webb, M., Paschal, D. C., Elliott, W. C., Hopkins, H. P., Ghazi, a. M., Ting, B. C., Romieu, I., Vicente, O., Pelfort, E., Martinez, L., Olsina, R., Marchevsky, E., Chen, H. P., Miller, D. T., and Morrow, J. C. (1998). A table of polyatimic interferences in ICP-MS. *Atomic Spectroscopy*, **19**(5), 150–155.

McMurry, J. and Fay, R. (2003). *Chemistry*. Pearson, 4th edition.

Michalke, B. (2003). Element speciation definitions, analytical methodology, and some examples. *Ecotoxicology and Environmental Safety*, **56**(1), 122–139.

Navibantes, B. I. and Kalabina, L. V. (1970). State of palladium(II) in perchlorate solutions. *Russian Journal of Inorganic Chemistry*, **15**, 818–821.

Nordberg, M., Duffus, J. H., and Templeton, D. M. (2004). Glossary of terms used in toxicokinetics (IUPAC Recommendations 2003). *Pure and Applied Chemistry*, **76**(5), 1033–1082.

Ontario Power Generation (2011). Environmental Impact Statement. Technical report, Ontario Power Generation.

Parkhurst, D. L. and Appelo, C. (2013). Description of Input and Examples for PHREEQC Version 3 – A Computer Program for Speciation, Batch-Reaction, One-Dimensional Transport, and Inverse Geochemical Calculations. In *U.S. Geological Survey Techniques and Methods*, chapter A43.

Parkhurst, D. L. and Appelo, C. A. J. (1999). User's Guide to PHREEQC (Version 2) (Equations on which the program is based). Technical report, U.S. Geological Survey.

Rai, D., Yui, M., and Kitamura, A. (2012). Thermodynamic Model for Amorphous Pd(OH)2 Solubility in the Aqueous Na+–K+–H+–OH–Cl- –ClO4 –H2O System at 25 C: A Critical Review. *Journal of Solution Chemistry*, **41**(11), 1965–1985.

Remani, C. (2013). *Methods for Solving Systems of Nonlinear Equations*. Ph.D. thesis, Lakehead University.

Shannon, R. D. (1976). Revised effective ionic radii and systematic studies of interatomic distances in halides and chalcogenides. *Acta Crystallographica Section A*, **32**(5), 751–767.

Stern, O. (1924). Zur theorie der electrolytischen doppelschict. *Zeitschrift für Elektrochemie und angewandte physikalische Chemie*, **30**, 508–516.

Stumm, W. and Morgan, J. J. (1996). *Aquatic Chemistry: Chemical Equilibria and Rates in Natural Waters*. John Wiley & Sons, Inc., New York, 3rd edition.

Suyama, T. and Tachi, Y. (2012). Development of Sorption Database (JAEA-SDB): Update of Sorption Data Including Soil and Cement Systems. Technical report, Japan Atomic Energy Agency.

Tachi, Y., Shibutani, T., Sato, H., and Shibata, M. (1999). Sorption and Diffusion Behavior of Palladium in Bentonite, Granodiorite and Tuff. Technical report, Japan Nuclear Cycle Development Institute.

Tait, J., Gauld, I., and Wilkin, G. (1989). Derivation of Initial Radionuclide Inventories for the Safety Assessment of the Disposal of Used CANDU Fuel. Technical report, Atomic Energy of Canada Ltd.

Thermo Fisher Scientific (2014). Measuring pH of Concentrated Samples. Technical report, Thermo Fisher Scientific.

Tinsley, I. J. (2004). *Chemical Concepts in Pollutant Behavior*. John Wiley & Sons, Inc.

Truesdell, A. and Jones, B. F. (1974). WATEQ, A Computer Program for Calculating Chemical Equilibria in Natural Waters. *U. S. Geological Survey Journal of Research*, **2**, 233–248.

Vilks, P. (2011). Sorption of Selected Radionuclides on Sedimentary Rocks in Saline

Conditions – Literature Review. Technical report, Nuclear Waste Mangement Organization.

Vilks, P. (2016). Sorption of Selected Radionuclides on Sedimentary Rocks in Saline Conditions - Updated Sorption Values. Technical report, Nuclear Waste Mangement Organiation.

Wasywich, K. (1993). Characteristics of Used CANDU Fuel Relevant to the Canadian Nuclear Fuel Waste Management Program. Technical report, Atomic Energy of Canada Ltd.

Westall, J. C., Zachary, J. L., and Morel, F. M. M. (1976). MINEQL, A Computer Program for the Calculation of Chemical Equilibrium Composition of Aqueous Systems. Technical report, Massachusetts Institue of Technology.

Appendix A

Data

Data from the sorption kinetics experiments is shown in Tables A.1 to A.3. Data from the pH and I dependence experiments is shown in Tables A.4 to A.10. Data from the sorption isotherm experiments is shown in Tables A.11 to A.14.

Table A.1: Data for Sorption Kinetics Experiments

Sample ID	Solid	Sorption Time (days)	I (M)	pH_c	Eh (mV)	$[Pd]_i$ (M)	K_d (m^3/kg)
KIN-MX-I0.1-s0d	Bentonite	0	0.1	6.60	–	1.00E-07	0.025
KIN-MX-I0.1-s1d	Bentonite	1	0.1	6.45	–	1.00E-07	0.315
KIN-MX-I0.1-s2d	Bentonite	2	0.1	6.53	–	1.00E-07	0.574
KIN-MX-I0.1-s5d	Bentonite	5	0.1	6.24	–	1.00E-07	0.672
KIN-MX-I0.1-s7d	Bentonite	7	0.1	6.34	–	1.00E-07	0.693
KIN-MX-I0.1-s14d	Bentonite	14	0.1	6.28	–	1.00E-07	0.665
KIN-MX-I1-s0d	Bentonite	0	1	6.10	–	1.00E-07	0.013
KIN-MX-I1-s1d	Bentonite	1	1	6.05	–	1.00E-07	0.062
KIN-MX-I1-s2d	Bentonite	2	1	5.99	–	1.00E-07	0.224
KIN-MX-I1-s5d	Bentonite	5	1	6.03	–	1.00E-07	0.390
KIN-MX-I1-s7d	Bentonite	7	1	5.87	–	1.00E-07	0.409
KIN-MX-I1-s14d	Bentonite	14	1	6.11	–	1.00E-07	0.406
KIN-MX-I4-s0d	Bentonite	0	4	5.81	–	1.00E-07	0.003
KIN-MX-I4-s1d	Bentonite	1	4	5.92	–	1.00E-07	0.035
KIN-MX-I4-s2d	Bentonite	2	4	5.83	–	1.00E-07	0.054
KIN-MX-I4-s5d	Bentonite	5	4	6.14	–	1.00E-07	0.079
KIN-MX-I4-s7d	Bentonite	7	4	6.13	–	1.00E-07	0.078
KIN-MX-I4-s14d	Bentonite	14	4	5.88	–	1.00E-07	0.082
KIN-SH-I0.1-s0d	Shale	0	0.1	7.23	–	1.00E-07	0.500
KIN-SH-I0.1-s1d	Shale	1	0.1	7.35	–	1.00E-07	4.970
KIN-SH-I0.1-s2d	Shale	2	0.1	7.42	–	1.00E-07	7.730
KIN-SH-I0.1-s5d	Shale	5	0.1	7.11	–	1.00E-07	9.400
KIN-SH-I0.1-s7d	Shale	7	0.1	7.24	–	1.00E-07	8.650
KIN-SH-I0.1-s14d	Shale	14	0.1	7.36	–	1.00E-07	9.860

Table A.2: Data for Sorption Kinetics Experiments

Sample ID	Solid	Sorption Time (days)	I (M)	pH_c	Eh (mV)	$[Pd]_i$ (M)	K_d (m^3/kg)
KIN-SH-I1-s0d	Shale	0	1	6.57	–	1.00E-07	0.225
KIN-SH-I1-s1d	Shale	1	1	6.88	–	1.00E-07	1.420
KIN-SH-I1-s2d	Shale	2	1	6.45	–	1.00E-07	3.900
KIN-SH-I1-s5d	Shale	5	1	6.76	–	1.00E-07	5.870
KIN-SH-I1-s7d	Shale	7	1	6.77	–	1.00E-07	6.430
KIN-SH-I1-s14d	Shale	14	1	6.65	–	1.00E-07	7.590
KIN-SH-I4-s0d	Shale	0	4	6.43	–	1.00E-07	0.025
KIN-SH-I4-s1d	Shale	1	4	6.32	–	1.00E-07	0.366
KIN-SH-I4-s2d	Shale	2	4	6.37	–	1.00E-07	0.558
KIN-SH-I4-s5d	Shale	5	4	6.44	–	1.00E-07	1.010
KIN-SH-I4-s7d	Shale	7	4	6.46	–	1.00E-07	1.110
KIN-SH-I4-s14d	Shale	14	4	6.39	–	1.00E-07	0.961
KIN-IL-I0.1-s0d	Illite	0	0.1	5.34	–	1.00E-07	0.053
KIN-IL-I0.1-s1d	Illite	1	0.1	5.43	–	1.00E-07	0.553
KIN-IL-I0.1-s2d	Illite	2	0.1	5.44	–	1.00E-07	0.894
KIN-IL-I0.1-s5d	Illite	5	0.1	5.37	–	1.00E-07	1.110
KIN-IL-I0.1-s7d	Illite	7	0.1	5.52	–	1.00E-07	0.884
KIN-IL-I0.1-s14d	Illite	14	0.1	5.58	–	1.00E-07	1.070
KIN-IL-I1-s0d	Illite	0	1	5.29	–	1.00E-07	0.024
KIN-IL-I1-s1d	Illite	1	1	5.45	–	1.00E-07	0.151
KIN-IL-I1-s2d	Illite	2	1	5.52	–	1.00E-07	0.428
KIN-IL-I1-s5d	Illite	5	1	5.53	–	1.00E-07	0.618
KIN-IL-I1-s7d	Illite	7	1	5.53	–	1.00E-07	0.691
KIN-IL-I1-s14d	Illite	14	1	5.44	–	1.00E-07	0.835

Table A.3: Data for Sorption Kinetics Experiments

Sample ID	Solid	Sorption Time (days)	I (M)	pH_c	Eh (mV)	$[Pd]_i$ (M)	K_d (m^3/kg)
KIN-IL-I4-s0d	Illite	0	4	5.33	–	1.00E-07	0.003
KIN-IL-I4-s1d	Illite	1	4	5.43	–	1.00E-07	0.037
KIN-IL-I4-s2d	Illite	2	4	5.34	–	1.00E-07	0.056
KIN-IL-I4-s5d	Illite	5	4	5.58	–	1.00E-07	0.114
KIN-IL-I4-s7d	Illite	7	4	5.39	–	1.00E-07	0.112
KIN-IL-I4-s14d	Illite	14	4	5.49	–	1.00E-07	0.108

Table A.4: Data for pH and I Dependence Sorption Experiments

Sample ID	Solid	Sorption Time (days)	I (M)	pH_c	Eh (mV)	$[Pd]_i$ (M)	K_d (m^3/kg)
SRP-MX-I0.1-1	Bentonite	14	0.1	6.91	506	1.00E-07	1.614
SRP-MX-I0.1-2	Bentonite	14	0.1	6.83	508	1.00E-07	1.181
SRP-MX-I0.1-3	Bentonite	14	0.1	6.83	501	1.00E-07	0.987
SRP-MX-I0.5-1	Bentonite	14	0.5	6.55	502	1.00E-07	0.505
SRP-MX-I0.5-2	Bentonite	14	0.5	6.60	495	1.00E-07	0.589
SRP-MX-I0.5-3	Bentonite	14	0.5	6.65	473	1.00E-07	0.544
SRP-MX-I1-1	Bentonite	14	1	6.48	484	1.00E-07	0.362
SRP-MX-I1-2	Bentonite	14	1	6.38	494	1.00E-07	0.385
SRP-MX-I1-3	Bentonite	14	1	6.28	508	1.00E-07	0.269
SRP-MX-I2-1	Bentonite	14	2	6.33	497	1.00E-07	0.167
SRP-MX-I2-2	Bentonite	14	2	6.18	502	1.00E-07	0.197
SRP-MX-I2-3	Bentonite	14	2	6.18	514	1.00E-07	0.184
SRP-MX-I3-1	Bentonite	14	3	6.17	505	1.00E-07	0.023
SRP-MX-I3-2	Bentonite	14	3	6.31	503	1.00E-07	0.084
SRP-MX-I3-3	Bentonite	14	3	6.06	513	1.00E-07	0.036
SRP-MX-I4-1	Bentonite	14	4	6.03	517	1.00E-07	0.025
SRP-MX-I4-2	Bentonite	14	4	6.07	513	1.00E-07	0.039
SRP-MX-I4-3	Bentonite	14	4	6.01	519	1.00E-07	0.070
SRP-SH-I0.1-1	Shale	14	0.1	7.44	498	1.00E-07	3.999
SRP-SH-I0.1-2	Shale	14	0.1	7.72	492	1.00E-07	3.895
SRP-SH-I0.1-3	Shale	14	0.1	7.70	481	1.00E-07	4.419
SRP-SH-I0.5-1	Shale	14	0.5	7.20	476	1.00E-07	3.164
SRP-SH-I0.5-2	Shale	14	0.5	7.36	465	1.00E-07	3.604
SRP-SH-I0.5-3	Shale	14	0.5	7.29	468	1.00E-07	1.916

Table A.5: Data for pH and I Dependence Sorption Experiments

Sample ID	Solid	Sorption Time (days)	I (M)	pH_c	Eh (mV)	$[Pd]_i$ (M)	K_d (m^3/kg)
SRP-SH-I1-1	Shale	14	1	7.18	467	1.00E-07	3.026
SRP-SH-I1-2	Shale	14	1	7.07	469	1.00E-07	3.641
SRP-SH-I1-3	Shale	14	1	7.19	470	1.00E-07	3.894
SRP-SH-I2-1	Shale	14	2	6.84	493	1.00E-07	1.403
SRP-SH-I2-2	Shale	14	2	6.92	485	1.00E-07	1.673
SRP-SH-I2-3	Shale	14	2	6.85	493	1.00E-07	1.830
SRP-SH-I3-1	Shale	14	3	6.73	501	1.00E-07	0.692
SRP-SH-I3-2	Shale	14	3	6.71	500	1.00E-07	0.829
SRP-SH-I3-3	Shale	14	3	6.74	498	1.00E-07	0.683
SRP-SH-I4-1	Shale	14	4	6.54	507	1.00E-07	1.293
SRP-SH-I4-2	Shale	14	4	6.54	505	1.00E-07	1.927
SRP-SH-I4-3	Shale	14	4	6.49	519	1.00E-07	3.111
SRP-IL-I0.1-1	Illite	14	0.1	5.34	538	1.00E-07	0.596
SRP-IL-I0.1-2	Illite	14	0.1	5.52	542	1.00E-07	0.421
SRP-IL-I0.1-3	Illite	14	0.1	5.83	542	1.00E-07	0.333
SRP-IL-I0.5-1	Illite	14	0.5	5.44	553	1.00E-07	0.499
SRP-IL-I0.5-2	Illite	14	0.5	5.44	550	1.00E-07	0.675
SRP-IL-I0.5-3	Illite	14	0.5	5.38	555	1.00E-07	0.531
SRP-IL-I1-1	Illite	14	1	5.50	552	1.00E-07	0.639
SRP-IL-I1-2	Illite	14	1	5.44	546	1.00E-07	0.625
SRP-IL-I1-3	Illite	14	1	5.41	536	1.00E-07	0.657
SRP-IL-I2-1	Illite	14	2	5.77	527	1.00E-07	0.325
SRP-IL-I2-2	Illite	14	2	5.73	519	1.00E-07	0.340
SRP-IL-I2-3	Illite	14	2	5.52	525	1.00E-07	0.352

Table A.6: Data for pH and I Dependence Sorption Experiments

Sample ID	Solid	Sorption Time (days)	I (M)	pH_c	Eh (mV)	$[Pd]_i$ (M)	K_d (m^3/kg)
SRP-IL-I3-1	Illite	14	3	5.79	517	1.00E-07	0.275
SRP-IL-I3-2	Illite	14	3	5.65	526	1.00E-07	0.017
SRP-IL-I3-3	Illite	14	3	5.70	530	1.00E-07	0.151
SRP-IL-I4-1	Illite	14	4	5.53	541	1.00E-07	0.212
SRP-IL-I4-2	Illite	14	4	5.73	541	1.00E-07	0.381
SRP-IL-I4-3	Illite	14	4	5.62	541	1.00E-07	0.010
SRP-MX-I0.1-PH5-1	Bentonite	14	0.1	5.02	485	1.00E-07	1.243
SRP-MX-I0.1-PH5-2	Bentonite	14	0.1	5.02	472	1.00E-07	1.677
SRP-MX-I0.1-PH5-3	Bentonite	14	0.1	5.02	509	1.00E-07	2.500
SRP-MX-I1-PH5-1	Bentonite	14	1	5.03	492	1.00E-07	0.626
SRP-MX-I1-PH5-2	Bentonite	14	1	5.03	471	1.00E-07	0.484
SRP-MX-I1-PH5-3	Bentonite	14	1	5.03	475	1.00E-07	0.392
SRP-MX-I4-PH5-1	Bentonite	14	4	5.06	439	1.00E-07	0.195
SRP-MX-I4-PH5-2	Bentonite	14	4	5.06	433	1.00E-07	0.073
SRP-MX-I4-PH5-3	Bentonite	14	4	5.06	441	1.00E-07	0.083
SRP-MX-I0.1-PH6-1	Bentonite	14	0.1	6.91	506	1.00E-07	1.614
SRP-MX-I0.1-PH6-2	Bentonite	14	0.1	6.83	508	1.00E-07	1.181
SRP-MX-I0.1-PH6-3	Bentonite	14	0.1	6.83	501	1.00E-07	0.987
SRP-MX-I1-PH6-1	Bentonite	14	1	6.48	484	1.00E-07	0.362
SRP-MX-I1-PH6-2	Bentonite	14	1	6.38	494	1.00E-07	0.385
SRP-MX-I1-PH6-3	Bentonite	14	1	6.28	508	1.00E-07	0.269
SRP-MX-I4-PH6-1	Bentonite	14	4	6.03	517	1.00E-07	0.025
SRP-MX-I4-PH6-2	Bentonite	14	4	6.07	513	1.00E-07	0.039
SRP-MX-I4-PH6-3	Bentonite	14	4	6.01	519	1.00E-07	0.070

Table A.7: Data for pH and I Dependence Sorption Experiments

Sample ID	Solid	Sorption Time (days)	I (M)	pH_c	Eh (mV)	$[Pd]_i$ (M)	K_d (m^3/kg)
SRP-MX-I0.1-PH7-1	Bentonite	14	0.1	7.02	420	1.00E-07	0.642
SRP-MX-I0.1-PH7-2	Bentonite	14	0.1	7.02	419	1.00E-07	0.669
SRP-MX-I0.1-PH7-3	Bentonite	14	0.1	7.02	419	1.00E-07	0.567
SRP-MX-I1-PH7-1	Bentonite	14	1	7.04	374	1.00E-07	0.019
SRP-MX-I1-PH7-2	Bentonite	14	1	7.04	383	1.00E-07	0.183
SRP-MX-I1-PH7-3	Bentonite	14	1	7.04	382	1.00E-07	0.061
SRP-MX-I4-PH7-1	Bentonite	14	4	7.08	352	1.00E-07	1.257
SRP-MX-I4-PH7-2	Bentonite	14	4	7.08	301	1.00E-07	0.292
SRP-MX-I4-PH7-3	Bentonite	14	4	7.08	376	1.00E-07	0.064
SRP-MX-I0.1-PH8-1	Bentonite	14	0.1	8.02	415	1.00E-07	1.060
SRP-MX-I0.1-PH8-2	Bentonite	14	0.1	8.02	407	1.00E-07	1.361
SRP-MX-I0.1-PH8-3	Bentonite	14	0.1	8.02	405	1.00E-07	0.834
SRP-MX-I1-PH8-1	Bentonite	14	1	8.05	361	1.00E-07	0.433
SRP-MX-I1-PH8-2	Bentonite	14	1	8.05	363	1.00E-07	0.409
SRP-MX-I1-PH8-3	Bentonite	14	1	8.05	362	1.00E-07	0.509
SRP-MX-I4-PH8-1	Bentonite	14	4	8.10	323	1.00E-07	0.064
SRP-MX-I4-PH8-2	Bentonite	14	4	8.10	322	1.00E-07	0.059
SRP-MX-I4-PH8-3	Bentonite	14	4	8.10	320	1.00E-07	0.062
SRP-MX-I0.1-PH9-1	Bentonite	14	0.1	9.03	403	1.00E-07	0.690
SRP-MX-I0.1-PH9-2	Bentonite	14	0.1	9.03	375	1.00E-07	0.682
SRP-MX-I0.1-PH9-3	Bentonite	14	0.1	9.03	376	1.00E-07	1.064
SRP-MX-I1-PH9-1	Bentonite	14	1	9.05	379	1.00E-07	0.418
SRP-MX-I1-PH9-2	Bentonite	14	1	9.05	366	1.00E-07	0.437
SRP-MX-I1-PH9-3	Bentonite	14	1	9.05	365	1.00E-07	0.542

Table A.8: Data for pH and I Dependence Sorption Experiments

Sample ID	Solid	Sorption Time (days)	I (M)	pH_c	Eh (mV)	$[Pd]_i$ (M)	K_d (m^3/kg)
SRP-SH-I1-PH7-1	Shale	14	1	7.18	467	1.00E-07	3.026
SRP-SH-I1-PH7-2	Shale	14	1	7.07	469	1.00E-07	3.641
SRP-SH-I1-PH7-3	Shale	14	1	7.19	470	1.00E-07	3.894
SRP-SH-I4-PH7-1	Shale	14	4	6.54	507	1.00E-07	1.293
SRP-SH-I4-PH7-2	Shale	14	4	6.54	425	1.00E-07	1.927
SRP-SH-I4-PH7-3	Shale	14	4	6.49	519	1.00E-07	3.111
SRP-SH-I0.1-PH8-1	Shale	14	0.1	8.02	413	1.00E-07	4.482
SRP-SH-I0.1-PH8-2	Shale	14	0.1	8.02	408	1.00E-07	4.838
SRP-SH-I0.1-PH8-3	Shale	14	0.1	8.02	409	1.00E-07	7.292
SRP-SH-I1-PH8-1	Shale	14	1	8.05	379	1.00E-07	2.636
SRP-SH-I1-PH8-2	Shale	14	1	8.05	368	1.00E-07	2.559
SRP-SH-I1-PH8-3	Shale	14	1	8.05	370	1.00E-07	2.344
SRP-SH-I4-PH8-1	Shale	14	4	8.10	344	1.00E-07	0.570
SRP-SH-I4-PH8-2	Shale	14	4	8.10	344	1.00E-07	0.433
SRP-SH-I4-PH8-3	Shale	14	4	8.10	344	1.00E-07	0.285
SRP-SH-I0.1-PH9-1	Shale	14	0.1	9.03	358	1.00E-07	3.335
SRP-SH-I0.1-PH9-2	Shale	14	0.1	9.03	360	1.00E-07	2.335
SRP-SH-I0.1-PH9-3	Shale	14	0.1	9.03	348	1.00E-07	1.725
SRP-SH-I1-PH9-1	Shale	14	1	9.05	354	1.00E-07	0.421
SRP-SH-I1-PH9-2	Shale	14	1	9.05	356	1.00E-07	0.424
SRP-SH-I1-PH9-3	Shale	14	1	9.05	350	1.00E-07	0.632
SRP-SH-I4-PH9-1	Shale	14	4	9.11	351	1.00E-07	0.251
SRP-SH-I4-PH9-2	Shale	14	4	9.11	342	1.00E-07	0.216
SRP-SH-I4-PH9-3	Shale	14	4	9.11	344	1.00E-07	0.042

Table A.9: Data for pH and I Dependence Sorption Experiments

Sample ID	Solid	Sorption Time (days)	I (M)	pH_c	Eh (mV)	$[Pd]_i$ (M)	K_d (m^3/kg)
SRP-IL-I0.1-PH5-1	Illite	14	0.1	5.02	549	1.00E-07	3.733
SRP-IL-I0.1-PH5-2	Illite	14	0.1	5.02	547	1.00E-07	3.402
SRP-IL-I0.1-PH5-3	Illite	14	0.1	5.02	563	1.00E-07	3.643
SRP-IL-I1-PH5-1	Illite	14	1	5.03	535	1.00E-07	1.032
SRP-IL-I1-PH5-2	Illite	14	1	5.03	532	1.00E-07	1.446
SRP-IL-I1-PH5-3	Illite	14	1	5.03	500	1.00E-07	0.857
SRP-IL-I4-PH5-1	Illite	14	4	5.06	493	1.00E-07	0.015
SRP-IL-I4-PH5-2	Illite	14	4	5.06	501	1.00E-07	0.017
SRP-IL-I4-PH5-3	Illite	14	4	5.06	495	1.00E-07	0.017
SRP-IL-I0.1-PH6-1	Illite	14	0.1	5.34	538	1.00E-07	0.740
SRP-IL-I0.1-PH6-2	Illite	14	0.1	5.52	542	1.00E-07	0.507
SRP-IL-I0.1-PH6-3	Illite	14	0.1	5.83	542	1.00E-07	0.412
SRP-IL-I1-PH6-1	Illite	14	1	5.50	552	1.00E-07	0.839
SRP-IL-I1-PH6-2	Illite	14	1	5.44	546	1.00E-07	0.817
SRP-IL-I1-PH6-3	Illite	14	1	5.41	536	1.00E-07	0.836
SRP-IL-I4-PH6-1	Illite	14	4	5.53	541	1.00E-07	0.321
SRP-IL-I4-PH6-2	Illite	14	4	5.73	541	1.00E-07	0.531
SRP-IL-I4-PH6-3	Illite	14	4	5.62	541	1.00E-07	0.090
SRP-IL-I0.1-PH7-1	Illite	14	0.1	7.02	441	1.00E-07	2.676
SRP-IL-I0.1-PH7-2	Illite	14	0.1	7.02	453	1.00E-07	1.605
SRP-IL-I0.1-PH7-3	Illite	14	0.1	7.02	458	1.00E-07	1.822
SRP-IL-I1-PH7-1	Illite	14	1	7.04	453	1.00E-07	0.622
SRP-IL-I1-PH7-2	Illite	14	1	7.04	452	1.00E-07	0.526
SRP-IL-I1-PH7-3	Illite	14	1	7.04	456	1.00E-07	0.684

Table A.10: Data for pH and I Dependence Sorption Experiments

Sample ID	Solid	Sorption Time (days)	I (M)	pH_c	Eh (mV)	$[Pd]_i$ (M)	K_d (m^3/kg)
SRP-IL-I4-PH7-1	Illite	14	4	7.08	443	1.00E-07	0.122
SRP-IL-I4-PH7-2	Illite	14	4	7.08	437	1.00E-07	0.082
SRP-IL-I4-PH7-3	Illite	14	4	7.08	436	1.00E-07	0.085
SRP-IL-I0.1-PH8-1	Illite	14	0.1	8.02	381	1.00E-07	1.243
SRP-IL-I0.1-PH8-2	Illite	14	0.1	8.02	396	1.00E-07	0.730
SRP-IL-I0.1-PH8-3	Illite	14	0.1	8.02	409	1.00E-07	1.214
SRP-IL-I1-PH8-1	Illite	14	1	8.05	376	1.00E-07	0.076
SRP-IL-I1-PH8-2	Illite	14	1	8.05	375	1.00E-07	0.073
SRP-IL-I1-PH8-3	Illite	14	1	8.05	382	1.00E-07	0.172
SRP-IL-I4-PH8-1	Illite	14	4	8.10	374	1.00E-07	0.210
SRP-IL-I4-PH8-2	Illite	14	4	8.10	368	1.00E-07	0.197
SRP-IL-I4-PH8-3	Illite	14	4	8.10	367	1.00E-07	0.131
SRP-IL-I0.1-PH9-1	Illite	14	0.1	9.03	357	1.00E-07	0.871
SRP-IL-I0.1-PH9-2	Illite	14	0.1	9.03	359	1.00E-07	1.212
SRP-IL-I0.1-PH9-3	Illite	14	0.1	9.03	361	1.00E-07	1.860
SRP-IL-I1-PH9-1	Illite	14	1	9.05	391	1.00E-07	0.611
SRP-IL-I1-PH9-2	Illite	14	1	9.05	375	1.00E-07	0.471
SRP-IL-I1-PH9-3	Illite	14	1	9.05	369	1.00E-07	0.379
SRP-IL-I4-PH9-1	Illite	14	4	9.11	360	1.00E-07	0.011
SRP-IL-I4-PH9-2	Illite	14	4	9.11	354	1.00E-07	0.082
SRP-IL-I4-PH9-3	Illite	14	4	9.11	354	1.00E-07	0.003

Table A.11: Data for Isotherm Experiments

Sample ID	Solid	Sorption Time (days)	I (M)	pH_c	Eh (mV)	$[Pd]_i$ (M)	$[Pd]_{eq}$ (M)	$[Pd]_s$ (M)
ISO-MX-I0.1-5E-8-1	Bentonite	14	0.1	9.64	365	5.00E-08	1.86E-08	1.22E-08
ISO-MX-I0.1-5E-8-2	Bentonite	14	0.1	9.57	363	5.00E-08	1.72E-08	1.34E-08
ISO-MX-I0.1-1E-7-1	Bentonite	14	0.1	6.91	506	1.00E-07	1.86E-07	2.20E-07
ISO-MX-I0.1-1E-7-2	Bentonite	14	0.1	6.83	508	1.00E-07	1.90E-07	2.09E-07
ISO-MX-I0.1-1E-7-3	Bentonite	14	0.1	6.83	501	1.00E-07	3.24E-07	2.08E-07
ISO-MX-I0.1-5E-7-1	Bentonite	14	0.1	9.38	361	5.00E-07	2.65E-07	7.69E-07
ISO-MX-I0.1-5E-7-2	Bentonite	14	0.1	8.81	395	5.00E-07	9.78E-09	2.34E-08
ISO-MX-I0.1-1E-6-1	Bentonite	14	0.1	9.10	372	1.00E-06	9.83E-09	2.59E-08
ISO-MX-I0.1-1E-6-2	Bentonite	14	0.1	9.04	374	1.00E-06	2.77E-08	8.36E-08
ISO-MX-I1-5E-8-1	Bentonite	14	1	6.20	469	5.00E-08	3.16E-08	7.98E-08
ISO-MX-I1-5E-8-2	Bentonite	14	1	6.28	458	5.00E-08	3.32E-08	7.82E-08
ISO-MX-I1-1E-7-1	Bentonite	14	1	6.48	484	1.00E-07	1.92E-07	1.52E-07
ISO-MX-I1-1E-7-2	Bentonite	14	1	6.38	494	1.00E-07	1.93E-07	1.64E-07
ISO-MX-I1-1E-7-3	Bentonite	14	1	6.28	508	1.00E-07	4.56E-07	5.89E-07
ISO-MX-I1-5E-7-1	Bentonite	14	1	5.99	472	5.00E-07	4.17E-07	6.01E-07
ISO-MX-I1-5E-7-2	Bentonite	14	1	5.77	484	5.00E-07	2.42E-08	3.52E-08
ISO-MX-I1-1E-6-1	Bentonite	14	1	5.98	475	1.00E-06	2.53E-08	3.86E-08
ISO-MX-I1-1E-6-2	Bentonite	14	1	5.98	482	1.00E-06	6.29E-08	3.65E-08
ISO-MX-I4-5E-8-1	Bentonite	14	4	5.96	461	5.00E-08	6.37E-08	3.57E-08
ISO-MX-I4-5E-8-2	Bentonite	14	4	5.98	454	5.00E-08	6.90E-08	3.04E-08
ISO-MX-I4-1E-7-1	Bentonite	14	4	6.03	517	1.00E-07	2.37E-07	9.48E-08
ISO-MX-I4-1E-7-2	Bentonite	14	4	6.07	513	1.00E-07	2.28E-07	1.04E-07
ISO-MX-I4-1E-7-3	Bentonite	14	4	6.01	519	1.00E-07	5.35E-07	1.71E-07
ISO-MX-I4-5E-7-1	Bentonite	14	4	5.65	476	5.00E-07	5.54E-07	1.37E-07

Table A.12: Data for Isotherm Experiments

Sample ID	Solid	Sorption Time (days)	I (M)	pH_c	Eh (mV)	$[Pd]_i$ (M)	$[Pd]_{eq}$ (M)	$[Pd]_s$ (M)
ISO-MX-I4-5E-7-2	Bentonite	14	4	5.46	476	5.00E-07	1.27E-07	2.64E-09
ISO-MX-I4-1E-6-1	Bentonite	14	4	4.89	504	1.00E-06	1.16E-07	1.32E-08
ISO-MX-I4-1E-6-2	Bentonite	14	4	5.12	502	1.00E-06	1.28E-07	9.66E-10
ISO-SH-I0.1-5E-8-1	Shale	14	0.1	7.70	447	5.00E-08	6.64E-09	5.42E-08
ISO-SH-I0.1-5E-8-2	Shale	14	0.1	7.64	429	5.00E-08	1.17E-08	4.91E-08
ISO-SH-I0.1-1E-7-1	Shale	14	0.1	7.44	498	1.00E-07	1.08E-08	1.00E-07
ISO-SH-I0.1-1E-7-2	Shale	14	0.1	7.72	492	1.00E-07	1.14E-08	1.00E-07
ISO-SH-I0.1-1E-7-3	Shale	14	0.1	7.70	481	1.00E-07	1.19E-08	9.98E-08
ISO-SH-I0.1-5E-7-1	Shale	14	0.1	7.66	200	5.00E-07	3.91E-08	7.33E-07
ISO-SH-I0.1-5E-7-2	Shale	14	0.1	7.69	200	5.00E-07	2.37E-08	7.48E-07
ISO-SH-I0.1-1E-6-1	Shale	14	0.1	7.65	204	1.00E-06	1.08E-07	1.47E-06
ISO-SH-I0.1-1E-6-2	Shale	14	0.1	7.60	207	1.00E-06	9.10E-08	1.49E-06
ISO-SH-I1-5E-8-1	Shale	14	1	7.11	205	5.00E-08	3.43E-08	8.87E-08
ISO-SH-I1-5E-8-2	Shale	14	1	7.12	207	5.00E-08	2.60E-08	9.70E-08
ISO-SH-I1-1E-7-1	Shale	14	1	7.18	467	1.00E-07	1.90E-08	7.83E-08
ISO-SH-I1-1E-7-2	Shale	14	1	7.07	469	1.00E-07	1.56E-08	8.17E-08
ISO-SH-I1-1E-7-3	Shale	14	1	7.19	470	1.00E-07	1.47E-08	8.27E-08
ISO-SH-I1-5E-7-1	Shale	14	1	7.08	434	5.00E-07	1.74E-07	6.55E-07
ISO-SH-I1-5E-7-2	Shale	14	1	7.11	438	5.00E-07	1.50E-07	6.80E-07
ISO-SH-I1-1E-6-1	Shale	14	1	7.07	452	1.00E-06	3.69E-07	1.25E-06
ISO-SH-I1-1E-6-2	Shale	14	1	7.07	445	1.00E-06	3.75E-07	1.25E-06
ISO-SH-I4-5E-8-1	Shale	14	4	6.46	452	5.00E-08	8.72E-08	1.03E-07
ISO-SH-I4-5E-8-2	Shale	14	4	6.47	458	5.00E-08	8.62E-08	1.04E-07
ISO-SH-I4-1E-7-1	Shale	14	4	6.54	507	1.00E-07	5.74E-08	6.51E-08

Table A.13: Data for Isotherm Experiments

Sample ID	Solid	Sorption Time (days)	I (M)	pH_c	Eh (mV)	$[Pd]_i$ (M)	$[Pd]_{eq}$ (M)	$[Pd]_s$ (M)
ISO-SH-I4-1E-7-2	Shale	14	4	6.54	505	1.00E-07	4.38E-08	7.87E-08
ISO-SH-I4-1E-7-3	Shale	14	4	6.49	519	1.00E-07	3.12E-08	9.13E-08
ISO-SH-I4-5E-7-1	Shale	14	4	6.50	451	5.00E-07	5.12E-07	2.56E-07
ISO-SH-I4-5E-7-2	Shale	14	4	6.50	454	5.00E-07	5.38E-07	2.30E-07
ISO-SH-I4-1E-6-1	Shale	14	4	6.51	456	1.00E-06	1.13E-06	1.69E-07
ISO-SH-I4-1E-6-2	Shale	14	4	6.52	461	1.00E-06	1.06E-06	2.38E-07
ISO-IL-I0.1-5E-8-1	Illite	14	0.1	6.00	485	5.00E-08	4.71E-08	1.85E-08
ISO-IL-I0.1-5E-8-2	Illite	14	0.1	5.85	477	5.00E-08	4.46E-08	2.11E-08
ISO-IL-I0.1-1E-7-1	Illite	14	0.1	5.34	538	1.00E-07	3.83E-08	5.68E-08
ISO-IL-I0.1-1E-7-2	Illite	14	0.1	5.52	542	1.00E-07	4.72E-08	4.79E-08
ISO-IL-I0.1-1E-7-3	Illite	14	0.1	5.83	542	1.00E-07	5.22E-08	4.30E-08
ISO-IL-I0.1-5E-7-1	Illite	14	0.1	5.54	482	5.00E-07	3.44E-07	5.14E-07
ISO-IL-I0.1-5E-7-2	Illite	14	0.1	5.45	489	5.00E-07	3.98E-07	4.61E-07
ISO-IL-I0.1-1E-6-1	Illite	14	0.1	4.63	543	1.00E-06	5.36E-07	1.03E-06
ISO-IL-I0.1-1E-6-2	Illite	14	0.1	4.65	546	1.00E-06	3.13E-07	1.25E-06
ISO-IL-I1-5E-8-1	Illite	14	1	5.54	518	5.00E-08	2.41E-08	9.02E-08
ISO-IL-I1-5E-8-2	Illite	14	1	5.54	501	5.00E-08	5.88E-08	5.55E-08
ISO-IL-I1-1E-7-1	Illite	14	1	5.50	552	1.00E-07	5.11E-08	8.58E-08
ISO-IL-I1-1E-7-2	Illite	14	1	5.44	546	1.00E-07	5.20E-08	8.50E-08
ISO-IL-I1-1E-7-3	Illite	14	1	5.41	536	1.00E-07	5.13E-08	8.57E-08
ISO-IL-I1-5E-7-1	Illite	14	1	4.85	526	5.00E-07	5.80E-07	3.63E-07
ISO-IL-I1-5E-7-2	Illite	14	1	5.04	519	5.00E-07	6.26E-07	3.18E-07
ISO-IL-I1-1E-6-1	Illite	14	1	4.59	540	1.00E-06	7.64E-07	1.14E-06
ISO-IL-I1-1E-6-2	Illite	14	1	4.45	554	1.00E-06	7.81E-07	1.13E-06

Table A.14: Data for Isotherm Experiments

Sample ID	Solid	Sorption Time (days)	I (M)	pH_c	Eh (mV)	$[Pd]_i$ (M)	$[Pd]_{eq}$ (M)	$[Pd]_s$ (M)
ISO-IL-I4-5E-8-1	Illite	14	4	5.58	493	5.00E-08	3.77E-08	1.22E-07
ISO-IL-I4-5E-8-2	Illite	14	4	5.37	500	5.00E-08	4.12E-08	1.18E-07
ISO-IL-I4-1E-7-1	Illite	14	4	5.53	541	1.00E-07	1.15E-07	7.37E-08
ISO-IL-I4-1E-7-2	Illite	14	4	5.73	541	1.00E-07	9.15E-08	9.72E-08
ISO-IL-I4-1E-7-3	Illite	14	4	5.62	541	1.00E-07	2.02E-07	1.40E-08
ISO-IL-I4-5E-7-1	Illite	14	4	4.72	522	5.00E-07	3.59E-07	5.96E-07
ISO-IL-I4-5E-7-2	Illite	14	4	4.83	526	5.00E-07	2.27E-07	7.27E-07
ISO-IL-I4-1E-6-1	Illite	14	4	4.37	546	1.00E-06	5.08E-07	1.36E-06
ISO-IL-I4-1E-6-2	Illite	14	4	4.13	553	1.00E-06	4.79E-07	1.39E-06

Appendix B

Example Input File for PHREEEQC

At the beginning of the file you specify the database to be used and the title of the work.

```
DATABASE C:\phreeqc\database\140331s0.tdb
TITLE Sorption of Palladium onto Montmorillonite and Illite
```

The master surface species are not included in the JAEA TDB so they must be defined separately using the `SURFACE_MASTER_SPECIES` command. The code block below shows the initialization of the master species for montmorillonite, `Mon_sOH`, and illite, `Ill_sOH`. `Mon_s` and `Ill_s` are keywords used in the model to denote species bound to the surface, such as `Mon_sOPd(OH)` and `Ill_sOPd(OH)`.

```
SURFACE_MASTER_SPECIES
 Mon_s Mon_sOH
 Ill_s Ill_sOH
```

Surface species are defined using the `SURFACE_SPECIES` command. The surface species are the surface complexes, defined using surface complexation reactions. They

are written as formation reactions, where the components in the formation reactions are either master surface species or master aqueous species. `log_k` is the surface complexation reaction constant. Note that all surface complexes have the prefix `Mon_s` or `Ill_s`. The surface complexation reactions are the same for both montmorillonite and illite, however since the surface complexation reactions are different for the two solids two sets surface complexation reactions must be included.

```
SURFACE_SPECIES
# Montmorillonite Surface Complexation Reactions

    # Surface Sites
     Mon_sOH = Mon_sOH
     log_k  0.0
     Mon_sOH  + H+ = Mon_sOH2+
     log_k  4.0
     Mon_sOH = Mon_sO- + H+
     log_k -6.2

    # Inner/Outer Sphere Complexes
     Mon_sOH + Pd+2 + H2O = Mon_sOPd(OH) +2H+
     log_k  3
     Mon_sOH + Pd+2 + 2H2O = Mon_sOPd(OH)2- + 3H+
     log_k  -4

    # Ternary Complexes (Type A)
     Mon_sOH + Pd+2 + 4Cl- = Mon_sOPdCl4-3 + H+
     log_k =  13.5

 # Illite Surface Complexation Reactions

     # Surface Sites
     Ill_sOH = Ill_sOH
     log_k  0.0
     Ill_sOH  + H+ = Ill_sOH2+
     log_k  4.5
     Ill_sOH = Ill_sO- + H+
     log_k -7.9
```

```
# Inner/Outer Sphere Complexes
 Ill_sOH + Pd+2 + H2O = Ill_sOPd(OH) +2H+
 log_k  3
 Ill_sOH + Pd+2 + 2H2O = Ill_sOPd(OH)2- + 3H+
 log_k  -5.6580

# Ternary Complexes (Type A)
 Ill_sOH + Pd+2 + 4Cl- = Ill_sOPdCl4-3 + H+
 log_k =  12.5
```

Solutions are defined using the `SOLUTION` command. This is an example of a 0.1 M solution. For solutions of different I all parameters would stay the same, however the amounts of each of Na, Ca and Cl would change, according to the amounts shown in Table 4.1, in order to increase the I.

```
SOLUTION 1 I = 0.1M
     temp      25
     -units     mol/kgw
     -density   1
     -water     1 # kg
    pe         7.5
    redox      pe
     pH         3
     Ca         0.02195
     Na         0.03415
     Cl         0.07805
     Pd         1E-07
```

The code below is a for loop related to the definition of solution 1 above. Each defined solution would have a similar for loop. The loop is used for varying the pH. It generates a loop file where the definition of the solution is repeated but with the amount of base in solution increasing incrementally such that pH ranges from 3 to 12. The `USER_GRAPH` command reads the loop file and runs the calculation for each

solution defined. The PHASES code block defines the master species Fix_H+. Fix_H+ is part of the loop file command and defines a fixed amount of hydrogen ions to set the initial pH to the desired value.

```
SELECTED_OUTPUT
     -file PdSCM_Mon_0.1
     -reset false
USER_PUNCH
  10 FOR i = 3.0 to 12 STEP 0.1
  20 a$ = EOL$ + "USE solution 1" + CHR$(59) + " USE surface 1" + EOL$
  30 a$ = a$ + "EQUILIBRIUM_PHASES 1" + EOL$
  40 a$ = a$ + "   Fix_H+ " + STR$(-i) + " NaOH 10.0" + EOL$
  50 a$ = a$ + "END" + EOL$
  60 PUNCH a$
  70 NEXT i
END

PHASES
     Fix_H+
     H+ = H+
     log_k  0.0
END
```

Below is an example of the first three iterations of the generated loop file. This block of code is not included in the input file, but is generated by the input file and saved in a separate loop file.

```
USE solution 1; USE surface 1
EQUILIBRIUM_PHASES 1
   Fix_H+           -3 NaOH 10.0
END

USE solution 1; USE surface 1
EQUILIBRIUM_PHASES 1
   Fix_H+  -3.1000e+00 NaOH 10.0
END

USE solution 1; USE surface 1
```

```
EQUILIBRIUM_PHASES 1
   Fix_H+  -3.2000e+00 NaOH 10.0
END
```

The surface characteristics for montomorillonite and illite are defined using the SURFACE command. The three numbers to the right of the name of the surface site are the number of sites in moles, the specific surface area in m^2/g and the mass of solid in g.

```
SURFACE 1
     Mon_sOH        4e-6        346.0     2
     -no_edl

SURFACE 2
     Ill_sOH        4e-6        83.0      2
     -no_edl
```

In order to specify the values to be included in the input file the SELECTED_OUTPUT command must be used. The ionic strength, pH, and redox potential are included by default. May other values are included by default, but are not wanted, these are turned of using the '-' flag and the false keyword as shown below. Values that are not included by default are included using '-' flag followed by a keyword. The molalities keyword saves the number of moles of all the species in the list which follows the command.

```
SELECTED_OUTPUT
     -file PdSCM.out
     -reset true
     -simulation false
     -state false
     -solution true
     -distance false
     -time false
     -reaction false
     -temperature false
```

```
    -alkalinity false
    -charge false
    -percent_error false
    -water false
    -step false
    -molalities Pd+2
                Mon_sOH Mon_sOH2+ Mon_sO- Mon_sOPd(OH)
                Mon_sOPd(OH)2- Mon_sOPdCl Mon_sOPdCl2-
                Mon_sOPdCl4-3 Mon_sOPdCl3-2
                Ill_sOH Ill_sOH2+ Ill_sO- Ill_sOPd(OH)
                Ill_sOPd(OH)2- Ill_sOPdCl Ill_sOPdCl2-
                Ill_sOPdCl4-3 Ill_sOPdCl3-2
```

This final block of code shows how the plots are created. If the `USER_GRAPH` commands are not included in the input file then the calculations are not completed and no data is included in the output file. `-LA("H+")` represent the pH, as `-LA(" ")` is the negative of the log of the species inside the quotations. The SURF command calculates the total amount of Pd on surface which include the phrase `Mon` and `TOT` calculates the total amount of all species (aqueous and surface) that include Pd. The `INCLUDE` command specifies the name of the loop file created earlier for varying the pH.

```
USER_PUNCH
 10
USER_GRAPH 1 Palladium Sorption onto Montmoronillite (I = 0.1M)
     -headings mu kd
     -chart_title "Palladium Sorption onto Montmoronillite (I = 0.1M)"
     -axis_titles "pH" "Kd [m3/kg]"
  -start
  10 GRAPH_X -LA("H+")
  20 GRAPH_Y (SURF("Pd","Mon")/TOT("Pd")*(1/2))
  -end
INCLUDE$ PdSCM_Mon_0.1
END
```

Appendix C

ICP-MS Quick Scan Results

The following is the results of a quick scan run using a blank (deionized water) solution. There should be very low CPS of Pd, however as we can see from the spectrum, Figure C.1, the detector is detecting "Pd" (shown by the green bars). The red bars are isotopes of Cu and Zn with masses ranging from 63 to 68. Ar has a mass of 40, it is not shown in the spectrum as it is not ionizing on its own and therefore the detector cannot detect it. The polyatomics of ArCu and ArZn are however forming and ionizing, the ions of which have masses in the range of 103 to 108, the same range of masses as isotopes of Pd. Table C.1 shows the CPS for the key masses identified in the spectrum.

Table C.1: CPS for masses of interest in ICP-MS quick scan of blank solution. Isotope masses correspond to red bars in Figure C.1 and polyatomic masses correspond to green bars in Figure C.1.

Isotope Mass	**Isotope CPS**	**Isotope**	**Polyatomic Mass**	**Polyatomic CPS**	**Polyatomic**
63	2290.00	Cu	103	0.00	$^{40}Ar^{63}Cu$
64	3860.00	Zn	104	143.00	$^{40}Ar^{64}Zn$, ^{104}Pd
65	714.00	Cu	105	571.00	$^{40}Ar^{65}Cu$, ^{105}Pd
66	2710.00	Zn	106	1140.00	$^{40}Ar^{66}Zn$, ^{106}Pd
67	1290.00	Zn	107	0.00	$^{40}Ar^{67}Zn$
68	2140.00	Zn	108	2430.00	$^{40}Ar^{68}Zn$, ^{108}Pd

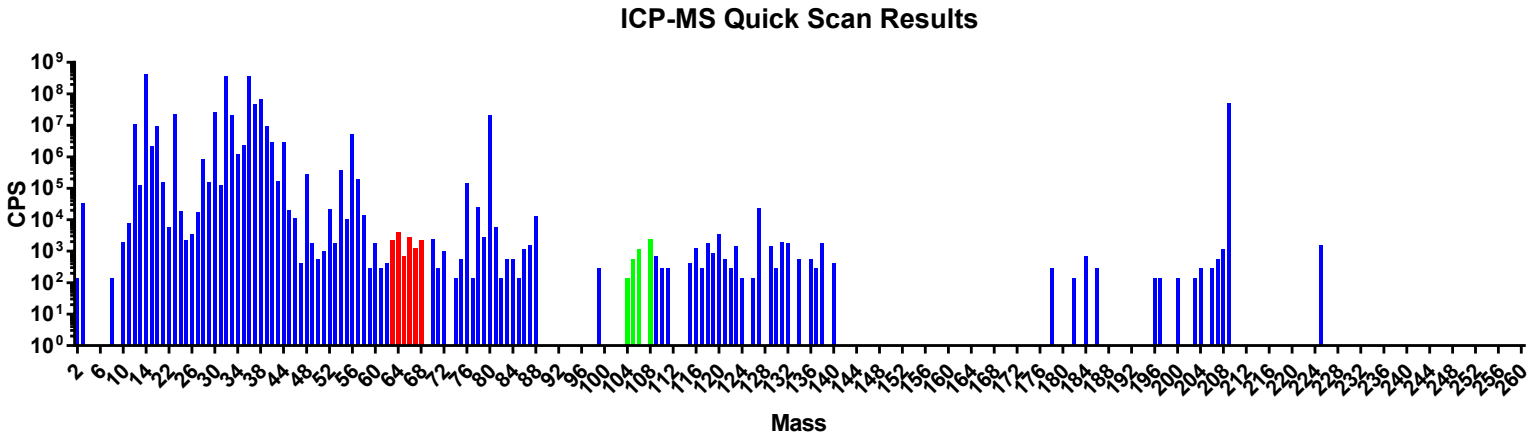

Figure C.1: Results from ICP-MS quick over full mass range. Red bars represent the CPS for isotopes of Cu and Zr. Green bars represent polyatomic ions of ArZn and ArCu.